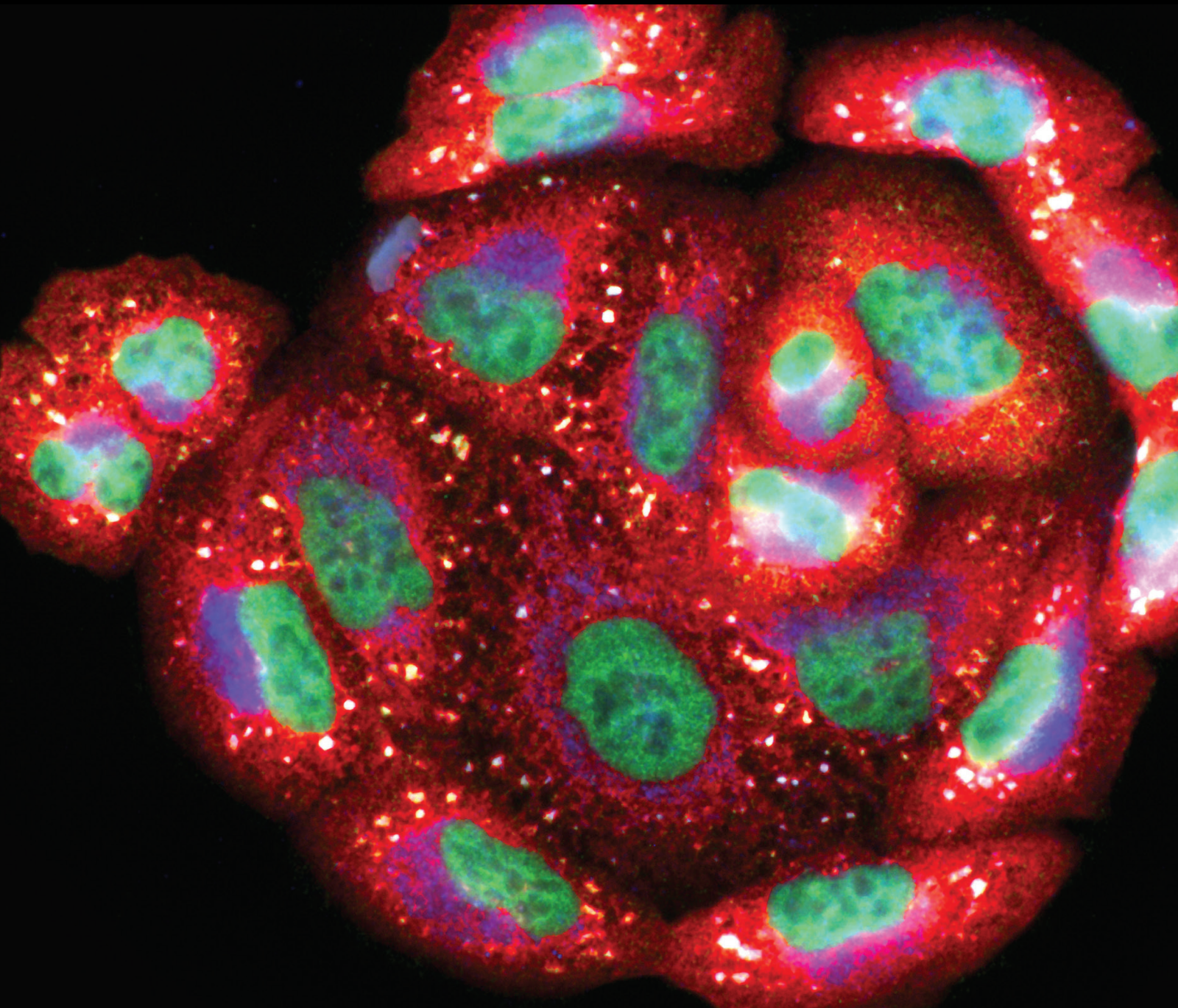# Nutraceuticals as Anti-aging Medicine

Lead Guest Editor: Muhammad Akhlaq
Guest Editors: Shah Hussain and Aamir Jalil

Nutraceuticals as Anti-aging Medicine

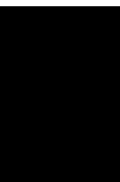# Nutraceuticals as Anti-aging Medicine

Lead Guest Editor: Muhammad Akhlaq
Guest Editors: Shah Hussain and Aamir Jalil

Anwen Shao, China
Iman Sherif, Egypt
Salah A Sheweita, Saudi Arabia
Xiaolei Shi, China
Manjari Singh, India
Giulia Sita, Italy
Ramachandran Srinivasan, India
Adrian Sturza, Romania
Kuo-hui Su, United Kingdom
Eisa Tahmasbpour Marzouni, Iran
Hailiang Tang, China
Carla Tatone, Italy
Shane Thomas, Australia
Carlo Gabriele Tocchetti, Italy
Angela Trovato Salinaro, Italy
Rosa Tundis, Italy
Kai Wang, China
Min-qi Wang, China
Natalie Ward, Australia
Grzegorz Wegrzyn, Poland
Philip Wenzel, Germany
Guangzhen Wu, China
Jianbo Xiao, Spain
Qiongming Xu, China
Liang-Jun Yan, USA
Guillermo Zalba, Spain
Jia Zhang, China
Junmin Zhang, China
Junli Zhao, USA
Chen-he Zhou, China
Yong Zhou, China
Mario Zoratti, Italy

Contents

Retraction

Retracted: si-PDGFR*β*-Loaded Exosomes Suppress the Progression of Glioma by Inhibiting the Oxidative Associated PI3K/Akt/EZH2 Signaling Pathway

Oxidative Medicine and Cellular Longevity

This article has been retracted by Hindawi following an investigation undertaken by the publisher [1]. This investigation has uncovered evidence of one or more of the following indicators of systematic manipulation of the publication process:

(1) Discrepancies in scope

(2) Discrepancies in the description of the research reported

(3) Discrepancies between the availability of data and the research described

(4) Inappropriate citations

(5) Incoherent, meaningless and/or irrelevant content included in the article

(6) Manipulated or compromised peer review

The presence of these indicators undermines our confidence in the integrity of the article's content and we cannot, therefore, vouch for its reliability. Please note that this notice is intended solely to alert readers that the content of this article is unreliable. We have not investigated whether authors were aware of or involved in the systematic manipulation of the publication process.

Wiley and Hindawi regrets that the usual quality checks did not identify these issues before publication and have since put additional measures in place to safeguard research integrity.

We wish to credit our own Research Integrity and Research Publishing teams and anonymous and named external researchers and research integrity experts for contributing to this investigation.

The corresponding author, as the representative of all authors, has been given the opportunity to register their agreement or disagreement to this retraction. We have kept a record of any response received.

References

[1] Y. Li, H. Yu, Q. Ma et al., "si-PDGFR*β*-Loaded Exosomes Suppress the Progression of Glioma by Inhibiting the Oxidative Associated PI3K/Akt/EZH2 Signaling Pathway," *Oxidative Medicine and Cellular Longevity*, vol. 2022, Article ID 5081439, 15 pages, 2022.

Retraction

Retracted: Composite Dietary Antioxidant Index and Plasma Levels of Soluble Klotho: Insights from NHANES

Oxidative Medicine and Cellular Longevity

This article has been retracted by Hindawi, as publisher, following an investigation undertaken by the publisher [1]. This investigation has uncovered evidence of systematic manipulation of the publication and peer-review process. We cannot, therefore, vouch for the reliability or integrity of this article.

Please note that this notice is intended solely to alert readers that the peer-review process of this article has been compromised.

Wiley and Hindawi regret that the usual quality checks did not identify these issues before publication and have since put additional measures in place to safeguard research integrity.

We wish to credit our Research Integrity and Research Publishing teams and anonymous and named external researchers and research integrity experts for contributing to this investigation.

The corresponding author, as the representative of all authors, has been given the opportunity to register their agreement or disagreement to this retraction. We have kept a record of any response received.

References

[1] H. He, X. Chen, D. Miao et al., "Composite Dietary Antioxidant Index and Plasma Levels of Soluble Klotho: Insights from NHANES," *Oxidative Medicine and Cellular Longevity*, vol. 2023, Article ID 3524611, 8 pages, 2023.

Retraction

Retracted: Antioxidant Indexes and Immune Function of the Intestinal Flora of Compound Microecological Preparations

Oxidative Medicine and Cellular Longevity

This article has been retracted by Hindawi following an investigation undertaken by the publisher [1]. This investigation has uncovered evidence of one or more of the following indicators of systematic manipulation of the publication process:

(1) Discrepancies in scope

(2) Discrepancies in the description of the research reported

(3) Discrepancies between the availability of data and the research described

(4) Inappropriate citations

(5) Incoherent, meaningless and/or irrelevant content included in the article

(6) Manipulated or compromised peer review

The presence of these indicators undermines our confidence in the integrity of the article's content and we cannot, therefore, vouch for its reliability. Please note that this notice is intended solely to alert readers that the content of this article is unreliable. We have not investigated whether authors were aware of or involved in the systematic manipulation of the publication process.

Wiley and Hindawi regrets that the usual quality checks did not identify these issues before publication and have since put additional measures in place to safeguard research integrity.

We wish to credit our own Research Integrity and Research Publishing teams and anonymous and named external researchers and research integrity experts for contributing to this investigation.

The corresponding author, as the representative of all authors, has been given the opportunity to register their agreement or disagreement to this retraction. We have kept a record of any response received.

References

[1] W. Sun and L. Zhang, "Antioxidant Indexes and Immune Function of the Intestinal Flora of Compound Microecological Preparations," *Oxidative Medicine and Cellular Longevity*, vol. 2022, Article ID 5498514, 13 pages, 2022.

Hindawi

Retraction

Retracted: Metoprolol Mitigates Ischemic Heart Remodeling and Fibrosis by Increasing the Expression of AKAP5 in Ischemic Heart

Oxidative Medicine and Cellular Longevity

This article has been retracted by Hindawi following an investigation undertaken by the publisher [1]. This investigation has uncovered evidence of one or more of the following indicators of systematic manipulation of the publication process:

(1) Discrepancies in scope

(2) Discrepancies in the description of the research reported

(3) Discrepancies between the availability of data and the research described

(4) Inappropriate citations

(5) Incoherent, meaningless and/or irrelevant content included in the article

(6) Peer-review manipulation

The presence of these indicators undermines our confidence in the integrity of the article's content and we cannot, therefore, vouch for its reliability. Please note that this notice is intended solely to alert readers that the content of this article is unreliable. We have not investigated whether authors were aware of or involved in the systematic manipulation of the publication process.

Wiley and Hindawi regrets that the usual quality checks did not identify these issues before publication and have since put additional measures in place to safeguard research integrity.

We wish to credit our own Research Integrity and Research Publishing teams and anonymous and named external researchers and research integrity experts for contributing to this investigation.

The corresponding author, as the representative of all authors, has been given the opportunity to register their agreement or disagreement to this retraction. We have kept a record of any response received.

References

[1] F. Zhu, Q. Wang, Z. Wang, X. Zhang, B. Zhang, and H. Wang, "Metoprolol Mitigates Ischemic Heart Remodeling and Fibrosis by Increasing the Expression of AKAP5 in Ischemic Heart," *Oxidative Medicine and Cellular Longevity*, vol. 2022, Article ID 5993459, 8 pages, 2022.

Retraction

Retracted: Composite Dietary Antioxidant Index and Plasma Levels of Soluble Klotho: Insights from NHANES

Oxidative Medicine and Cellular Longevity

This article has been retracted by Hindawi, as publisher, following an investigation undertaken by the publisher [1]. This investigation has uncovered evidence of systematic manipulation of the publication and peer-review process. We cannot, therefore, vouch for the reliability or integrity of this article.

Please note that this notice is intended solely to alert readers that the peer-review process of this article has been compromised.

Wiley and Hindawi regret that the usual quality checks did not identify these issues before publication and have since put additional measures in place to safeguard research integrity.

We wish to credit our Research Integrity and Research Publishing teams and anonymous and named external researchers and research integrity experts for contributing to this investigation.

The corresponding author, as the representative of all authors, has been given the opportunity to register their agreement or disagreement to this retraction. We have kept a record of any response received.

References

[1] H. He, X. Chen, D. Miao et al., "Composite Dietary Antioxidant Index and Plasma Levels of Soluble Klotho: Insights from NHANES," *Oxidative Medicine and Cellular Longevity*, vol. 2023, Article ID 3524611, 8 pages, 2023.

Research Article

Composite Dietary Antioxidant Index and Plasma Levels of Soluble Klotho: Insights from NHANES

Huiqin He [ID],[1] **Xin Chen** [ID],[1] **Da Miao** [ID],[2] **Hongxia Zhang** [ID],[1] **Yu Wang** [ID],[1] **Xingkang He** [ID],[1] **Xiaoli Chen** [ID],[1] **and Ning Dai** [ID][1]

[1]*Department of Gastroenterology, Sir Run Run Shaw Hospital, Zhejiang University Medical School, Hangzhou 310016, China*
[2]*Department of Endoscopy Center, Sir Run Run Shaw Hospital, Zhejiang University Medical School, Hangzhou 310016, China*

Correspondence should be addressed to Xingkang He; hexingkang@zju.edu.cn, Xiaoli Chen; dr_chenxl@zju.edu.cn, and Ning Dai; ndaicn@zju.edu.cn

Objectives. The association between dietary antioxidants and soluble Klotho (S-Klotho) levels remains unknown. We investigated to explore whether the composite dietary antioxidant index (CDAI) was associated with serum levels of S-Klotho in the middle-aged population. *Methods*. Eligible participants were identified from the National Health and Nutrition Examination Surveys (NHANES) from 2007 until 2016. The CDAI was calculated from the intake of six dietary antioxidants. The serum levels of S-Klotho were measured via enzyme-linked immunosorbent assay (ELISA). Generalized linear and nonlinear models were established to analyze the relationship between CDAI and S-Klotho levels. *Results*. Based on the S-Klotho quartiles, S-Klotho levels were higher in young women, Blacks, higher education, never smokers, lower waistlines, no medication use, and those with higher CDAI. Univariate analysis revealed that age, gender, race, smoking status, body mass index, waistline, and medication use were associated with serum levels of S-Klotho. When potential confounders were controlled, CDAI was significantly associated with S-Klotho levels. Subgroup analysis also revealed that this association remained significant in individuals who had the highest quartiles of CDAI, aged population (>60 years), male, and never smoker. A nonlinear relationship was observed between the CDAI and S-Klotho plasma concentrations. *Conclusion*. CDAI was positively correlated with plasma levels of S-Klotho after controlling for covariates. Further studies are needed to validate the current findings and explore the fundamental mechanisms.

1. Introduction

Oxidative stress is caused by the imbalance between oxidant generation and elimination, which contributes to multiple chronic diseases, such as cancer, aging, neurodegenerative, and cardiovascular diseases [1–3]. Overwhelming release of reactive oxygen and nitrogen species (RONS) [4] by endogenous and exogenous mechanisms can lead to deleterious effects, impaired immune defense, and signaling events [5, 6]. It is believed that accumulation of oxidative damage caused by RONS leads to impaired macromolecule synthesis (lipids, DNA, and proteins) and aging [7, 8]. For example, oxidative stress damages telomere attrition and impairs their capacity for repair, which accelerates aging and increases the risk of age-related diseases due to oxidative stress [9–11].

Conceptually, antioxidants have been postulated to protect biological systems from free radical toxicity, acting as scavengers of oxidants [12, 13]. Whether antioxidants improve adverse health consequences remains a hotly debated topic [14].

As an age-suppressor gene, Klotho is considered to originally extend life expectancy [15]. Mutations in Klotho resulted in shortened life spans in addition to multiple disorders resembling premature aging in humans [16–18]. In contrast, overexpression of Klotho in mice slowed down the aging process and increased life expectancy by 20% to 30% [17]. In humans, serum levels of Klotho were also decreased with age [19, 20]. Espuch-Oliver et al. demonstrated that soluble levels of Klotho were decreased in healthy-aged individuals duo to aging-related physiological

TABLE 1: Characteristics of population based on S-Klotho plasma levels quartiles ($N = 10,393$).

Characteristic	S-Klotho level quartiles				P value
	Quartile 1	Quartile 2	Quartile 3	Quartile 4	
Age (years)	57.40	56.28	55.99	55.03	<0.01
Gender					<0.01
Female (%)	24.13	24.36	25.55	25.96	
Male (%)	25.40	28.04	25.60	20.96	
Race					<0.01
White (%)	25.09	27.01	25.76	22.14	
Mexican (%)	23.59	25.84	27.49	23.08	
Black (%)	24.50	20.59	20.87	34.03	
Other (%)	22.72	23.87	27.22	26.18	
Marital status					0.31
No married (%)	25.69	24.78	25.18	24.35	
Married (%)	24.26	26.73	25.77	23.25	
Education					0.01
Grade or less (%)	25.17	26.52	24.40	23.91	
High school (%)	27.40	25.03	26.37	21.19	
Some college (%)	25.12	26.62	26.32	21.94	
College or more (%)	22.34	26.11	24.86	26.69	
Poverty	3.26	3.32	3.36	3.33	0.58
Smoke					<0.01
Never (%)	22.36	25.44	25.94	26.26	
Former (%)	26.67	26.03	25.84	21.45	
Now (%)	28.30	28.08	24.04	19.58	
Energy intake (kcal/day)	1970.11	2013.07	2023.08	1989.21	0.23
BMI	29.73	29.50	29.51	29.28	0.30
Waist circumference (cm)	102.85	102.26	101.76	100.37	<0.01
Use of medication (%)					<0.01
Yes	25.73	26.71	24.87	22.69	
No	22.29	24.55	27.31	25.85	
CDAI	0.78	1.31	1.44	1.38	<0.01

CDAI: composite dietary antioxidant index; BMI: body mass index.

declines [21]. They proposed that the soluble Klotho (S-Klotho) level through ELISA measurement could be considered a simple and meaningful marker of aging that can improve quality of life for the elderly [21]. Actually, the Klotho gene encoded several forms of Klotho protein, including membrane bound form and secreted form Klotho [22]. The membrane bound Klotho was primarily expressed in the renal distal convolution distal convoluted tubules of the kidney as well as in the brain [17]. The extracellular region of membrane bound Klotho could be released into the blood and urine by cleavage of α- and β-secretases [23]. The cleaved Klotho had pleiotropic properties and functioned as a humoral factor, known as the soluble Klotho (S-Klotho) [23]. Further, Klotho deficiency was related to multiple aging-related conditions, such as kidney disease, hypertension, and cancer [24]. Nakanishi et al. suggested that low-serum Klotho concentrations were associated with multiple preclinical disorders, such as overweight, abdominal obesity, hypertension, and hyperlipidemia [25]. Qiao et al. observed an inverse association between serum levels

of S-Klotho and risk of pan-cancer [26]. Besides, serum levels of S-Klotho were also related to inflammatory cytokines and showed several protective effects. Martín-Núñez et al. found that reduced levels of S-Klotho were associated with the proinflammatory status, such as higher ratio of tumor necrosis factor-alpha/interleukin-10 and the C-reactive protein level [27]. Wu et al. also demonstrated that the serum levels of S-Klotho were significantly and inversely associated with four well-recognized inflammation-related biomarkers (white blood cell count, mean platelet volume, C-reactive protein, and uric acid) in the cohort [28]. Several experimental models demonstrated that upregulation of endogenous Klotho or exogenous administration of Klotho both could suppress renal fibrosis and maintain kidney function in chronic kidney disease [29]. Considering the protective effects of S-Klotho, we were curious about the association between S-Klotho levels and oxidative stress. Previously, Klotho was reported to downregulate oxidative stress [30]. However, whether antioxidants could influence S-Klotho levels has yet to be studied.

Table 2: Univariate analysis for S-Klotho plasma levels.

Characteristic	β	S-Klotho 95% CI	P value
Age	-2.48	(-3.18, -1.78)	<0.01
Gender (female)			
Male	-39.71	(-55.20, -24.22)	<0.01
Race (White)			
Mexican	15.33	(-6.61, 37.28)	0.17
Other	31.35	(8.97, 53.73)	0.01
Black	80.97	(54.32, 107.62)	<0.01
Marital status (no married)			
Yes	-10.74	(-27.29, 5.80)	0.20
Poverty	1.09	(-4.07, 6.26)	0.67
Education (grade or less)			
High school	-21.39	(-46.51, 3.72)	0.09
Some college	-2.60	(-26.37, 21.16)	0.83
College or more	22.35	(-3.73, 48.42)	0.09
Smoke (no)			
Former	-39.01	(-55.08, -22.94)	<0.01
Now	-54.92	(-75.46, -34.38)	<0.01
CDAI	1.35	(-0.14, 2.85)	0.08
Energy intake	-0.0039	(-0.0120, 0.0042)	0.36
BMI	-1.27	(-2.47, -0.08)	0.04
Waist circumference	-1.22	(-1.78, -0.66)	<0.01
Use of medication (yes)			
No	26.12	(8.79, 43.45)	<0.01

CDAI: composite dietary antioxidant index; BMI: body mass index.

Composite dietary antioxidant index (CDAI) is a measure of individual antioxidant profile based on a combination of dietary antioxidants, including manganese, selenium, zinc, and vitamins A, C, and E [31]. The CDAI was developed to evaluate and reflect the overall impact of dietary antioxidants on health. Previous studies found that high CDAI was related to a decreased risk of various types of cancer [32–34]. To our knowledge, the relationship between CDAI and plasma levels of Klotho has not been evaluated. Whether or not dietary antioxidants influence S-Klotho levels remains largely unknown. In the current study, based on National Health and Nutrition Examination Survey (NHANES), we explored and evaluated the relationship between CDAI and S-Klotho in the middle-aged population.

2. Method

2.1. Study Population. The NHANES, which is a series of cross-sectional surveys, represents noninstitutionalized US civilian population (https://www.cdc.gov/nchs/nhanes/index.htm). The NHANES dataset includes demographic, socioeconomic, dietary, and health-related questionnaire data, which was collected through in-person interviews, physical and physiological examinations, and extensive and laboratory testing. NHANES was approved by the National

Center for Health Statistical research ethics review committees and publicly available (https://wwwn.cdc.gov/nchs/nhanes/). We combined five NHANES cycles (NHANES 2007-2008, 2009-2010, 2011-2012, 2013-2014, and 2015-2016 cycle). The inclusion criteria were as follows: those who had complete data about age, gender, race, marital status, education, poverty, smoke status, energy intake, body measurement, waist circumference, use of medication, diabetes mellitus and dietary antioxidant intake, and S-Klotho level. Participants with missing or unknown data were excluded. During 2007-2008, 2009-2010, 2011-2012, and 2013-2014 study cycles, 13,760 individuals were selected to participate in the study. Individuals with missing information of composite dietary antioxidant index and serum S-Klotho level were excluded ($N = 2,157$). Besides, individuals with missing information of age, gender, race, marital status, education, poverty, smoke status, energy intake, body mass index (BMI), waist circumference, and medication use were also excluded ($N = 1,210$). Finally, 10,393 individuals with complete information were included in our analyses. All NHANES protocols were approved by the National Center for Health Statistics Research Ethics Review Board, and participants provided written informed consent. Since it used deidentified data without personally identifiable information, this study was exempted from Institutional Review Board review.

2.2. Calculation of CDAI. The calculation of CDAI was described previously and validated in another prospective cohort study [31]. In brief, six antioxidants (manganese, selenium, zinc, and vitamins A, C, and E) were standardized. The CDAI was based on the sum of these standardized consumptions. Each participant's food and nutrient intake in the NHANES dataset was recorded based on nonconsecutive two-day 24-hour dietary recalls, based on interviews. On the first day, the participants were interviewed at the NHANES Mobile Examination Center and then 3 to 10 days later via telephone. The Food and Nutrient Database for Dietary Studies of the United States Department of Agriculture was used to calculate the intake of antioxidants, micronutrients, and total energy [35]. Based on the questionnaire interview, we determined the intake of dietary supplements during the past month, including dosage, frequency, and duration of consumption [36].

2.3. Measurement of S-Klotho Levels. According to the description available on the NHANES website [19], the levels of S-Klotho of each participate were quantified using commercially available ELISA (IBL International, Japan) of frozen serum specimens. These frozen serum specimens were stored at −80°C at the Centers for Disease Control and Prevention. IBL ELISA for measurement of Klotho concentration in human samples had been extensively validated prior to the start of the study. Available serum samples of Klotho concentration were obtained from 40- to 79-year-old participants in NHANES. In summary, standard curves and relative signals of calibrator concentrations consistently met the manufacturer's criteria. The linearity of the assay was evaluated using two samples with very high and high

Table 3: Multivariate analysis of association between CDAI and S-Klotho plasma levels.

Characteristic	Model I	P value	Model II	P value
CDAI	2.95 (1.47, 4.42)	<0.001	2.56 (0.65, 4.47)	<0.01
Vitamin A	7.56 (3.44, 11.69)	<0.01	6.87 (2.89, 10.86)	<0.001
Vitamin C	10.33 (2.40, 18.26)	0.01	7.29 (-1.41, 15.99)	0.10
Vitamin E	2.92 (-4.12, 9.95)	0.41	1.75 (-6.59, 10.10)	0.68
Mg	3.82 (-3.10, 10.74)	0.28	5.47 (-2.80, 13.74)	0.19
Zinc	0.53 (-5.99, 7.06)	0.87	5.98 (-1.80, 13.77)	0.13
Se	-1.39 (-9.44, 6.65)	0.73	6.24 (-3.56, 16.05)	0.21
Stratified by CDAI (quartile)				
Q1	5.22 (-5.92, 16.37)	0.35	1.04 (-12.05, 14.14)	0.87
Q2	-3.40 (-23.20, 16.40)	0.73	-4.49 (-24.18, 15.20)	0.65
Q3	-3.04 (-18.83, -12.76)	0.70	-3.45 (-19.34, 12.45)	0.67
Q4	2.66 (0.05, 5.26)	0.04	2.78 (0.50, 5.07)	0.02
Stratified by age (years)				
<60	2.58 (0.66, 4.49)	<0.01	1.19 (-1.45, 3.83)	0.37
≥60	3.61 (0.81, 6.41)	0.01	5.92 (2.05, 9.79)	<0.01
Stratified by gender				
Female	2.72 (0.12, 5.32)	0.04	-0.09 (-3.65, 3.48)	0.96
Male	3.06 (1.26, 4.85)	<0.01	3.94 (1.93, 5.95)	<0.01
Stratified by smoke				
Never	3.53 (1.43, 5.63)	<0.01	3.34 (0.62, 6.06)	0.02
Former	0.39 (-2.69, 3.48)	0.80	1.10 (-2.68, 4.89)	0.56
Now	1.44 (-1.80, 4.67)	0.38	1.16 (-4.02, 6.35)	0.66

CDAI: composite dietary antioxidant index; BMI: body mass index. Model I: age, sex, and race were adjusted. Model II: age, sex, marital status, race, poverty, education, energy intake, BMI, waist circumference, smoke status, and medication use were adjusted.
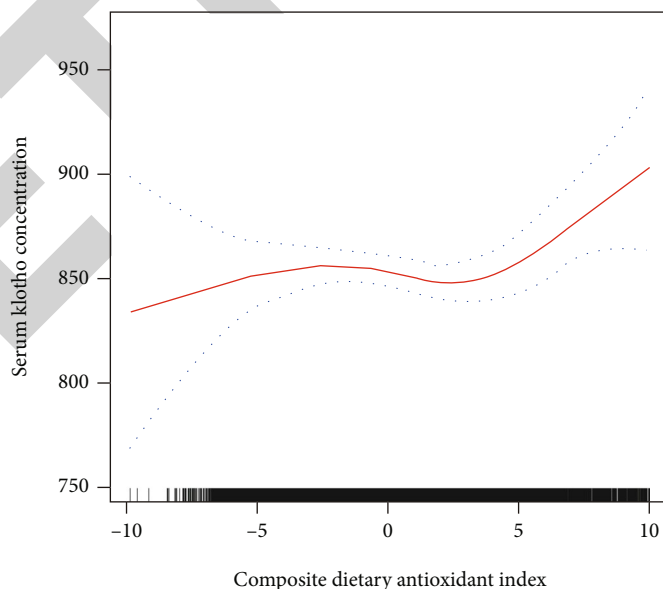
Figure 1: Association of composite dietary antioxidant index with S-Klotho plasma levels.

Klotho concentrations. The intra-assay precision was obtained from two Klotho samples, and the reference ranges of Klotho concentration were evaluated in 114 healthy donors. In accordance with the manufacturer's protocol, all samples were analyzed in duplicate, and the final value was calculated based on the average of the two values. All results of analyses automatically transmitted to the laboratory Oracle Management System and evaluated by the area

supervisor. Samples with greater than 10% duplicate findings were highlighted for repeated analysis. All the results were examined to ensure that they met the laboratory's routine acceptance standards before release.

2.4. Assessment of Covariates. To assess the influence of potential confounding factors, we selected several important covariates, including individual age (years), gender (male/female), race (White, non-Hispanic White/Black, non-Hispanic Black/Mexican, Mexican American/other, other Hispanic, other Race—including multiracial), marital status (no married/married), education level (grade or less/high school/some college/college or more), poverty (income-to-poverty ratio), smoking status (never/former/now smoker), total energy intake (Kcal/day), BMI, waist circumference, and use of medication.

2.5. Statistical Analysis. We gathered data from NHANES project via nhanesR. In order to illustrate the complexity of survey design, we incorporated clustering and stratification across analyses to reduce the probability of unequal selection and oversampling. For the categorical variables, the weighted chi-square test was used, and for the continuous variables, weighted linear regression model was adopted. To evaluate the relationship between CDAI and the level of S-Klotho, two models of linear regression were adopted. Model 1 was adjusted for age, gender, and race. Model 2 was adjusted for age, gender, and race, marital status, poverty, education, energy intake, BMI, waist circumference, smoke status, and medication use. The potential nonlinear association was investigated using a generalized additive model. A two-stage linear regression model was also used to determine the inflection point. All statistical analyses were performed using R packages and EmpowerStats. A *P* value < 0.05 was considered as statistically significant.

3. Results

The current study included 10,393 participants in the final analysis based on inclusion and exclusion criteria. The baseline features of included population were summarized in Table 1. Within the S-Klotho quartiles, significant differences were observed regarding age, gender, race, education status, smoking status, waist circumference, medication use, and CDAI. The individuals with higher levels of S-Klotho were younger, Black, had higher education, had never smoked, had a smaller waistline, no medication use, and had higher CDAI scores. There was no difference regarding marital status, poverty, BMI, and energy intake.

Further univariate analysis of associations between S-Klotho levels and various characteristics revealed that age, gender, smoke status, BMI, and waistline were inversely associated with levels of S-Klotho (Table 2). The Black and no medication use were positively associated with levels of S-Klotho (Table 2). There was a positive relationship between CDAI and serum levels of S-Klotho, although the relationship was not statistically significant (Table 2). After adjusting for age, gender, and race confounders, CDAI was significantly associated with S-Klotho levels (Table 3). In

Table 4: Threshold effect analysis of CDAI on S-Klotho by the two-piecewise linear regression.

Characteristic	Adjusted β (95% CI)	*P* value
Fitting by the standard linear model	2.56 (0.65, 4.47)	<0.01
Fitting by the two-piecewise linear model		
Inflection point		
CDAI < 1.5	0.46 (-1.9, 3.70)	0.78
CDAI > 1.5	3.38 (1.49, 5.27)	<0.01

Age, sex, marital status, race, poverty, education, energy intake, BMI, waist circumference, smoke status, and medication use were adjusted.

subgroup analysis, the positive association was more apparent in individuals with the highest quartiles of CDAI, all age groups, all gender groups, and never-smokers. Higher antioxidant intakes of vitamins A and C were significantly associated with higher levels of S-Klotho (Table 3). After controlling for additional confounders, such as marital status, poverty, education, energy intake, BMI, waist circumference, smoke status, and use of medication, CDAI was still significantly associated with S-Klotho levels (Table 3). In subgroup analysis, this positive association remained significant in individuals who had the highest quartiles of CDAI, older than 60 years, male gender, and who never smoked. Higher intake of vitamin A was significantly associated with higher levels of S-Klotho. With this relationship in mind, we further performed a threshold effect analysis using a nonlinear model. As Figure 1 and Table 4 shown, the serum level of S-Klotho increased by 3.38 pg/ml when the CDAI increased by one unit (CDAI > 1.5).

4. Discussion

In the current study, we demonstrated that overall antioxidant intakes, indicated by the CDAI, were positively and significantly associated with plasma levels of S-Klotho after adjusting for multiple covariates in the middle-aged population based on NHANES. In the aged, male, and never-smoking population, this positive association was more apparent. In the subgroup analysis of individual antioxidant components, a higher intake of vitamin A was significantly related to higher plasma levels of S-Klotho. Our results suggested that overall dietary antioxidants might influence serum levels of antiaging protein, S-Klotho.

The concentrations of RONS overwhelmingly contribute to oxidative stress, which leads to cell and tissue damage [37]. To maintain a steady state of biological redox, antioxidants may scavenge oxidants, which protects against oxidative stress. As a result, dietary antioxidants mitigate the damaging effects of oxidative stress and contribute to health [38]. CDAI represents comprehensive measurement of total antioxidant levels in the diet and is widely used in many studies. Proinflammatory cytokines, such as interleukin-1b and tumor necrosis factor-alpha, were inversely correlated with CDAI [39]. Several epidemiological studies showed that higher CDAI levels were

significantly associated with reduced risk of various types of cancer. Wright et al. first showed that the combination of dietary antioxidants reduced the risk of lung cancer among male smokers [31]. Paragomi et al. showed that the overall levels of dietary antioxidants decreased the risk of pancreatic cancer [34]. Yu et al. reported an inverse relationship between CDAI and the risk of colorectal cancer, suggesting that antioxidants might reduce the incidence of colorectal cancer in the population [32]. Besides, dietary antioxidants were also reported to be associated with mortality, although not consistently. Wang et al. observed that higher intakes of antioxidants were associated with reduced mortality risk from all causes and cardiovascular disease in diabetic adults [40]. According to other studies, higher intakes of magnesium, zinc, selenium, and vitamins A, C, and E were inversely related to reduced mortality risk [41–43]. However, Genkinger et al. reported that no significant relationships existed between dietary intakes of vitamins C, E, and overall mortality [44].

However, evidence is limited to suggest any relationship between dietary antioxidants and levels of S-Klotho. Klotho was originally identified by Kuro-o et al. in 1997 as a potential an antiaging gene [15]. Mice deficient in Klotho had shortened life spans and multiple disorders resembling premature aging in humans, while mice with overexpression of Klotho could extend life span and slow down the aging process [16–18]. S-Klotho was cleaved by secretases from transmembrane Klotho and entered the circulatory system. In the circulation, S-Klotho served as the main functional form [16, 45]. Increasing evidence had suggested that Klotho could exert vasculo-protective effects and was critical for vascular health. Semba et al. showed that higher plasma levels of Klotho were independently associated with a reduced risk of cardiovascular disease in the community-based cohort [46]. Navarro-Gonzalez et al. found that lower serum Klotho concentrations were negatively associated with the presence and severity of coronary artery disease [47]. Recently, Pan et al. also showed that reduced baseline levels of circulating Klotho were associated with an increased risk of coronary artery disease in a prospective study [48]. Besides, a growing body of evidence also indicated that Klotho played a crucial anti-inflammation, antiaging, insulin resistance role, and prevention of age-related diseases. Serum levels of Klotho were reported to be associated with the proinflammatory status and well-recognized inflammatory biomarkers in the cohort [27]. The S-Klotho modulated the degree of insulin/insulin-like growth factor-1 signaling and Wnt pathway, in combating aging and tumor growth [49]. Kurosu et al. found that antiaging properties of Klotho were partly through the induction of insulin resistance. They observed that Klotho could inhibit insulin and IGF1 signaling to induce insulin resistance [16]. In addition, Klotho also suppressed cellular apoptosis and protected against hypoxia, oxidative stress, and cytotoxic drugs. Lim et al. reported that Klotho inhibited the phosphatidyl-inositol 3-kinase/serine-threonine kinase pathway, thereby enhancing manganese superoxide dismutase expression via FoxO3a in response to Tac-induced oxidative stress [30]. Consequently, Klotho interfered with insulin-like growth factor 1 signaling and increased resistance to oxidative stress. However, no study investigated whether dietary antioxidant intakes affected S-Klotho levels. The findings of the present study indicated that dietary antioxidants were positively associated with serum levels of S-Klotho after adjusting for covariates, especially for vitamin A. Previously, Azimzadeh et al. reported that vitamin D supplementation prevented the reduction in plasma Klotho in the elderly among a randomized, double-blinded, placebo-controlled clinical trial [50]. The underlying mechanism might be related to the presence of a vitamin D response element in the Klotho gene both in humans and mice [15, 51]. The expression of Klotho was upregulated by the binding of 1,25-dihydroxyvitamin D to the vitamin D receptor on the Klotho gene [15, 51]. However, whether vitamin A influenced the expression of Klotho required further investigations.

To the best of our knowledge, this is the first study to investigate the relationship between overall dietary antioxidants and plasma levels of S-Klotho in a population-based cohort, as well as its originality, a large sample size, representing of the noninstitutionalized U.S. population, and standardized methods of data collection are major strengths, which minimized any measurement bias. Our results indicated that CDAI was significantly associated with S-Klotho levels. Serum levels of S-Klotho increased more when CDAI score was greater than 1.5. Our findings provided some novel insights and clinical significances that increased dietary antioxidant intakes might positively modulate higher serum levels of S-Klotho, which could protect against age-related diseases. Nevertheless, the current study has some limitations. First, this study could not construct or confirm any causal inference due to its retrospective design. Second, despite adjusting for potential confounding, residual confounding may still exist, which might influence the relationship between CDAI and the level of S-Klotho. Third, it is unclear whether our findings based on the middle-aged population can be extended to younger population. Further studies are needed to determine if the benefit of dietary antioxidants can be extended to different populations.

In summary, our study demonstrated that CDAI was significantly associated with S-Klotho levels in middle-aged population after adjusting for multiple variables. The positive relationship was mainly observed in males, aged participants, and never smokers. Further studies are needed before the results can be generalized to other populations and establish the causal relationship between CDAI and S-Klotho levels based on investigation into the underlying mechanisms.

Abbreviations

CDAI:	Component dietary antioxidant index
S-Klotho:	Soluble Klotho
BMI:	Body mass index
NHANES:	National Health and Nutrition Examination Surveys
ELISA:	Enzyme-linked immunosorbent assay

RONS: Reactive oxygen and nitrogen species.

Data Availability

The dataset was based on NHANES, which was publicly available and could be found below: https://www.cdc.gov/nchs/nhanes/.

Conflicts of Interest

All authors declare that there are no conflicts of interest.

Authors' Contributions

Xingkang He, Xiaoli Chen, and Ning Dai designed the study. Xingkang He, Xin Chen, Huiqin He, Da Miao, Hongxia Zhang, Yu Wang, and Xiaoli Chen conducted data extraction, interpreted the study results, and wrote the first draft of the manuscript parts. Xingkang He revised the manuscript. Huiqin He and Xin Chen contributed equally to this work.

Acknowledgments

References

[1] H. Haghi Aminjan, S. R. Abtahi, E. Hazrati, M. Chamanara, M. Jalili, and B. Paknejad, "Targeting of oxidative stress and inflammation through ROS/NF-kappaB pathway in phosphine-induced hepatotoxicity mitigation," *Life Sciences*, vol. 232, p. 116607, 2019.

[2] O. Firuzi, R. Miri, M. Tavakkoli, and L. Saso, "Antioxidant therapy: current status and future prospects," *Current Medicinal Chemistry*, vol. 18, no. 25, pp. 3871–3888, 2011.

[3] M. Sharifi-Rad, N. V. Anil Kumar, P. Zucca et al., "Lifestyle, oxidative stress, and antioxidants: back and forth in the pathophysiology of chronic diseases," *Frontiers in Physiology*, vol. 11, p. 694, 2020.

[4] Y. A. Hajam, R. Rani, S. Y. Ganie et al., "Oxidative stress in human pathology and aging: molecular mechanisms and perspectives," *Cell*, vol. 11, no. 3, 2022.

[5] M. Genestra, "Oxyl radicals, redox-sensitive signalling cascades and antioxidants," *Cellular Signalling*, vol. 19, no. 9, pp. 1807–1819, 2007.

[6] S. I. Dikalov and R. R. Nazarewicz, "Angiotensin II-induced production of mitochondrial reactive oxygen species: potential mechanisms and relevance for cardiovascular disease," *Antioxidants & Redox Signaling*, vol. 19, no. 10, pp. 1085–1094, 2013.

[7] I. Liguori, G. Russo, F. Curcio et al., "Oxidative stress, aging, and diseases," *Clinical Interventions in Aging*, vol. 13, pp. 757–772, 2018.

[8] R. Buffenstein, Y. H. Edrey, T. Yang, and J. Mele, "The oxidative stress theory of aging: embattled or invincible? Insights from non-traditional model organisms," *Age*, vol. 30, no. 2-3, pp. 99–109, 2008.

[9] G. Gavia-Garcia, J. Rosado-Perez, T. L. Arista-Ugalde, I. Aguiniga-Sanchez, E. Santiago-Osorio, and V. M. Mendoza-Nunez, "Telomere length and oxidative stress and its relation with metabolic syndrome components in the aging," *Biology*, vol. 10, no. 4, p. 253, 2021.

[10] S. Reichert and A. Stier, "Does oxidative stress shorten telomeres in vivo? A review," *Biology Letters*, vol. 13, no. 12, 2017.

[11] W. Ahmed and J. Lingner, "Impact of oxidative stress on telomere biology," *Differentiation*, vol. 99, pp. 21–27, 2018.

[12] A. M. Pisoschi and A. Pop, "The role of antioxidants in the chemistry of oxidative stress: a review," *European Journal of Medicinal Chemistry*, vol. 97, pp. 55–74, 2015.

[13] J. M. Lu, P. H. Lin, Q. Yao, and C. Chen, "Chemical and molecular mechanisms of antioxidants: experimental approaches and model systems," *Journal of Cellular and Molecular Medicine*, vol. 14, no. 4, pp. 840–860, 2010.

[14] J. Luo, K. Mills, S. le Cessie, R. Noordam, and D. van Heemst, "Ageing, age-related diseases and oxidative stress: what to do next?," *Ageing Research Reviews*, vol. 57, p. 100982, 2020.

[15] Y. Xu and Z. Sun, "Molecular basis of Klotho: from gene to function in aging," *Endocrine Reviews*, vol. 36, no. 2, pp. 174–193, 2015.

[16] H. Kurosu, M. Yamamoto, J. D. Clark et al., "Suppression of aging in mice by the hormone Klotho," *Science*, vol. 309, no. 5742, pp. 1829–1833, 2005.

[17] M. Kuro-o, Y. Matsumura, H. Aizawa et al., "Mutation of the mouse Klotho gene leads to a syndrome resembling ageing," *Nature*, vol. 390, no. 6655, pp. 45–51, 1997.

[18] H. Masuda, H. Chikuda, T. Suga, H. Kawaguchi, and M. Kuro-o, "Regulation of multiple ageing-like phenotypes by inducible Klotho gene expression in Klotho mutant mice," *Mechanisms of Ageing and Development*, vol. 126, no. 12, pp. 1274–1283, 2005.

[19] Y. Yamazaki, A. Imura, I. Urakawa et al., "Establishment of sandwich ELISA for soluble alpha-Klotho measurement: age-dependent change of soluble alpha-Klotho levels in healthy subjects," *Biochemical and Biophysical Research Communications*, vol. 398, no. 3, pp. 513–518, 2010.

[20] T. Siahanidou, M. Garatzioti, C. Lazaropoulou et al., "Plasma soluble α-Klotho protein levels in premature and term neonates: correlations with growth and metabolic parameters," *European Journal of Endocrinology*, vol. 167, no. 3, pp. 433–440, 2012.

[21] A. Espuch-Oliver, H. Vazquez-Lorente, L. Jurado-Fasoli et al., "References values of soluble alpha-Klotho serum levels using an enzyme-linked immunosorbent assay in healthy adults aged 18-85 years," *Journal of Clinical Medicine*, vol. 11, no. 9, 2022.

[22] Y. Matsumura, H. Aizawa, T. Shiraki-Iida, R. Nagai, M. Kuro-o, and Y. Nabeshima, "Identification of the human Klotho gene and its two transcripts encoding membrane and secreted Klotho protein," *Biochemical and Biophysical Research Communications*, vol. 242, no. 3, pp. 626–630, 1998.

[23] O. M. Kuro, "The Klotho proteins in health and disease," *Nature Reviews. Nephrology*, vol. 15, no. 1, pp. 27–44, 2019.

[24] J. H. Kim, K. H. Hwang, K. S. Park, I. D. Kong, and S. K. Cha, "Biological role of anti-aging protein Klotho," *Journal of Lifestyle Medicine*, vol. 5, no. 1, pp. 1–6, 2015.

Retraction

Retracted: si-PDGFRβ-Loaded Exosomes Suppress the Progression of Glioma by Inhibiting the Oxidative Associated PI3K/Akt/EZH2 Signaling Pathway

Oxidative Medicine and Cellular Longevity

This article has been retracted by Hindawi following an investigation undertaken by the publisher [1]. This investigation has uncovered evidence of one or more of the following indicators of systematic manipulation of the publication process:

(1) Discrepancies in scope

(2) Discrepancies in the description of the research reported

(3) Discrepancies between the availability of data and the research described

(4) Inappropriate citations

(5) Incoherent, meaningless and/or irrelevant content included in the article

(6) Manipulated or compromised peer review

The presence of these indicators undermines our confidence in the integrity of the article's content and we cannot, therefore, vouch for its reliability. Please note that this notice is intended solely to alert readers that the content of this article is unreliable. We have not investigated whether authors were aware of or involved in the systematic manipulation of the publication process.

Wiley and Hindawi regrets that the usual quality checks did not identify these issues before publication and have since put additional measures in place to safeguard research integrity.

We wish to credit our own Research Integrity and Research Publishing teams and anonymous and named external researchers and research integrity experts for contributing to this investigation.

The corresponding author, as the representative of all authors, has been given the opportunity to register their agreement or disagreement to this retraction. We have kept a record of any response received.

References

[1] Y. Li, H. Yu, Q. Ma et al., "si-PDGFRβ-Loaded Exosomes Suppress the Progression of Glioma by Inhibiting the Oxidative Associated PI3K/Akt/EZH2 Signaling Pathway," *Oxidative Medicine and Cellular Longevity*, vol. 2022, Article ID 5081439, 15 pages, 2022.

Hindawi

Research Article

si-PDGFRβ-Loaded Exosomes Suppress the Progression of Glioma by Inhibiting the Oxidative Associated PI3K/Akt/EZH2 Signaling Pathway

Yuping Li [iD],[1,2] **Hailong Yu** [iD],[1] **Qiang Ma** [iD],[1] **Min Wei** [iD],[2] **Xiaoguang Liu** [iD],[1] **Yajie Qi** [iD],[1] **Chen Li** [iD],[3] **Lun Dong** [iD],[1] and **Hengzhu Zhang** [iD][2]

[1]*Neuro Intensive Care Unit, Clinical Medical College, Yangzhou University, Yangzhou, China*
[2]*Department of Neurosurgery, Clinical Medical College, Yangzhou University, Yangzhou, China*
[3]*Department of Neurosurgery, Changzhou No. 2 People's Hospital, Changzhou, Jiangsu, China*

Correspondence should be addressed to Yuping Li; yupingli@yzu.edu.cn and Hengzhu Zhang; zhanghengzhu@sina.com

This study investigated the possibility of exosomes loaded with si-PDGFRβ ability to suppress the progression of glioma. Common gliomas develop from neuroglial progenitor cells. Many variables affect the survival rate and occurrence of gliomas. Understanding oxidative stress processes and creating new, efficient treatments are crucial because oxidative stress is linked to the development of brain tumors. For this purpose, selected clinical samples were subjected to various tests like quantitative real-time PCR, Cignal Finder RTK signaling 7-pathway reporter array analysis, CCK-8 analysis, flow cytometry, and immunoblotting. Here, we demonstrated that PDGFRβ expression was increased in glioma patients. Following that, cell-derived exosomes were extracted and collected and traced *in vivo*, and selected tissue samples were subjected to immunohistochemical analysis. The results indicated that the knockdown of PDGFRβ (si-PDGFRβ) inhibited the proliferation of glioma cells. Besides this, si-PDGFRβ-loaded exosomes induced a similar antitumor effect in glioma cells. The anticancer effect of si-PDGFRβ-loaded exosomes was mediated by the inactivation of the PI3K/Akt/EZH2 pathway. Finally, we verified that this exosome delivery system, si-PDGFRβ-loaded exosomes, had robust targeting and no associated toxicity. In conclusion, the study confirmed that si-PDGFRβ-loaded exosomes inhibit glioma progression via inactivating the PI3K/Akt/EZH2 signaling pathway.

1. Introduction

As the most common central nervous system (CNS) tumor, glioma accounts for over 26.6% of all CNS tumors, among which glioblastoma (GBM, WHO grade IV) with a low five-year survival rate (about 5.5%) occupies approximately 56.1% of all gliomas [1, 2]. The imbalance between oxidative and antioxidant activity in the body is referred to as oxidative stress. As part of regular metabolism, oxygen is reduced by electrons, creating numerous reactive oxygen species (ROS). The main contributors to oxidative stress are ROS, which can be directly detected and quantified. In addition to having defensive mechanisms that aid in the elimination of bacteria and pathogens, oxidative stress has the potential

to damage host cells through increased ROS accumulation. One of the most prevalent malignant tumors of the central nervous system is glioma, distinguished by redox state alterations. Even low-grade glioma with a good prognosis (including LGG, WHO grade I or II) inevitably relapses and develops into high-grade glioma (such as HGG, WHO grade III or IV) [3]. The abnormal proliferation, high invasion ability, high tolerance to hypoxia, existence of cancer stem cells, and immune escape from the microenvironment in GBM tumors cause therapeutic failure and adverse prognosis. For patients with GBM, the median overall survival time is only 14.5 to 16.6 months, even with aggressive surgical treatment combined with postoperative chemoradiotherapy [4]. Consequently, it is important to search for

biomarkers of diagnosis and prognosis for the early diagnosis and progression detection of glioma and to improve the treatment efficiency.

The PDGF family's five subtypes regulate various cellular functions, such as proliferation, differentiation, and activation of signal transduction, by binding to two specific receptors (PDGFR-α and PDGFR-β) [5]. PDGFR-β is an essential promoter of cell division and a vital polypeptide growth factor [6]. Several studies have confirmed that PDGFR-β can preferentially bind with PDGF-BB and have a strong promoting effect on the proliferation and differentiation of cancer cells [7]. For example, missense mutations in the exon of the PDGFR-β gene are associated with tumorigenesis and cell proliferation [8]. Furthermore, studies have shown that PDGF-BB and PDGFR-β knockout mice have severe cardiovascular and renal dysplasia, accompanied by aortic dilatation and bleeding. It suggests that PDGFR-β stimulates tumor angiogenesis by activating adjacent tissue cells and releasing vascular endothelial growth factors [9]. Many inhibitors and proangiogenesis factors determine the formation of tumor angiogenesis, among which PDGF family members are one of the essential factors in tumor angiogenesis [10]. Therefore, antitumor treatment strategies for PDGFR targets are getting more and more attention.

Modulating oxidative stress is considered to be an important method of treating cancer. Many kinds of oxidative medicine have been reported, including small molecule compounds, natural products, and nucleic acid drugs. In recent years, with the gradual deepening of exosome research, it has been gradually found that exosomes also play an important role in regulating cell oxidative damage and ROS. Exosomes are vesicles with a diameter of 30-100 nm [11]. They are secreted by all kinds of cells, including proteins, nucleic acids, and other components, and have been shown to modify the formation of an immunosuppressive tumor microenvironment [12, 13]. Studies have shown that exosomes carry long noncoding RNAs (lncRNAs), mRNAs, and microRNAs (miRNAs) and regulate the biological behavior of target cells by delivering these RNAs to target cells [14]. Therefore, exosomes play a crucial role in material and information exchange between cells. Exosomes are thought to be the carrier of many oncogenic factors and participate in developing glioma. In glioblastoma (GBM), the epidermal growth factor receptor (EGFR) variant III (EGFRv III) and other carcinogenic components are transferred to the microenvironment through exosomes and spread invasiveness [15]. It has been reported that VEGF was transported by glioma-derived exosomes (GEXs) to promote the formation of glioma blood vessels [16]. Exosomes, as a kind of vesicle secreted by cells, have good application potential in drug delivery. Compared to other nanodelivery systems such as lipids, polymers, and gold, live cell-derived exosomes have low immunogenicity. They are highly biocompatible nanocarriers and exhibit greater flexibility and very low cytotoxicity in loading the required antigens for efficient delivery [17, 18].

Moreover, exosomes do not have the problem of adsorbing proteins to produce protein crowns, which can achieve stable drug transport in the blood. The PI3K/Akt/mTOR signaling pathway is a significant pathway in regulating oxidative stress. Here, we show that exosomes loaded with si-PDGFRβ derived from pericytes exhibit antitumor properties through retarding the activation of the PI3K/Akt/mTOR signaling pathway in glioma.

2. Materials and Method

2.1. Clinical Samples. Fifty-nine patients with glioma were randomly selected for this study who were hospitalized in the Neurosurgery Department of Clinical Medical College of Yangzhou University and underwent surgical treatment from Jan 2020 to May 2021. Pathological types were based on WHO neuroepithelial tumor classification criteria. They were divided into the low-grade group (31 cases with WHO grade I-II, 15 males and 16 females) and high-grade group (28 cases with WHO grade III-IV, 16 males and 12 females), and 12 brain tissue resections from traumatic brain injury patients were selected as the control group. The Ethics Committee approved the experiments for the Clinical Medical College of Yangzhou University.

2.2. Quantitative Real-Time PCR (qRT-PCR). Total RNA extraction was performed with TRIzol reagent (AM1912, Thermo Scientific) and evaluated the quantity and purity of RNA with NanoDrop ND-1000 spectrophotometer (Thermo Scientific). Complementary DNAs were synthesized using an invalidated transcription kit (RR037A, Takara) and implemented as models for PCR assay. The Primer Premier 5.0 software was used to create the following primers for this study: PDGFRβ forward: 5$'$-ACTGCCCAG ACCTAGCAGTG-3$'$ and reverse: 5$'$-CAGGGAAGTAA GGTGCCAAC-3$'$ and GAPDH, forward: 5$'$-CAG GAGG CATTGCTGATGAT-3$'$ and reverse: 5$'$-GAAGGCTGGGG CTCATTT-3$'$. These primers were synthesized by Sangon Biotech (Shanghai, China).

2.3. Cignal Finder RTK Signaling 7-Pathway Reporter Array. To ascertain the critical downstream pathways regulated by PDGFRβ, Cignal Finder RTK signaling 7-Pathway Reporter array was performed. Subsequently, the pathway-specific transcription factor or control constructs were transfected into U251 cells. The relative activity of each signal pathway was driven by Dual-Luciferase® Reporter Assay System from Promega (Promega, Beijing, China).

2.4. Cell Counting Kit-8 (CCK-8) Assay. U251 cells (1×10^4 per well) were seeded into 96-well plates. At 0, 24 h, 48 h, and 72 h, 10 μL CCK-8 solution was added to each well and incubated with U251 cells at 37°C for 3 hours. U251 cells' absorbance (450 nm) was measured to determine their level of vitality.

2.5. Flow Cytometric Analysis (FACS). Induction of apoptosis in U251 cells was evaluated by PI and Annexin V-EGFP kit (KeyGen Biotech Co., Ltd., Nanjing, China). Briefly, U251 cells (5×10^6 cells/well) were seeded into 6-well plates and collected after transfection with the different

TABLE 1: Antibody information of immunoblot.

Antibodies	Dilution rates	Product codes	Manufacturers
β-Actin	1 : 1000	PA5-35201	Invitrogen
PDGFR beta	1 : 2000	Ab69506	Abcam
EZH2	1 : 1000	Ab283270	Abcam
p-Akt	1 : 1000	Ab38449	Abcam
Akt	1 : 1000	Ab8805	Abcam
p-PI3K	1 : 1000	Ab278545	Abcam
PI3K	1 : 1000	20584-1-AP	Protein Tech
CD63	1 : 1000	Ab134045	Abcam
TSG101	1 : 1000	Ab125011	Abcam
Bax	1 : 2000	PA5-17216	Invitrogen
Bcl-2	1 : 10000	AM4302	Invitrogen
Cleaved caspase-3	1 : 1000	ab155938	Abcam
Goat anti-mouse IgG H&L (HRP)	1 : 10000	ab6728	Abcam
Goat anti-rabbit IgG H&L (HRP)	1 : 10000	ab6721	Abcam

plasmids for 48 hours. Finally, these cells were washed with cold PBS at 4°C and analyzed through a flow cytometer.

2.6. Immunoblotting. Glioma tissues and cell line (U251) were rinsed with PBS and lysed with RIPA buffer (4693116001, Roche) with a protease inhibitor; the concentrations were examined through a BCA protein assay kit (23227, Thermo Scientific). The total protein sample (30 μg) was separated on 12.5% SDS-PAGE gels and next transferred onto 0.45 μm thin PVDF membranes (Merck Millipore). Blocking with 5% bovine serum albumin at room temperature for 1 hour, membranes were incubated with primary antibodies (as shown in Table 1) at 4°C overnight. After washing, membranes were incubated with secondary antibodies for 1 hour at room temperature. Finally, these protein bands were imaged, contrasted, and analyzed with an ECL assay kit (P0018FS; Beyotime Biotechnology), a ChemiDoc XRS imaging system, and Image Lab software (both Bio-Rad Laboratories, Inc., Hercules, CA, USA), respectively.

2.7. Cell Exosome Collection. Conditioned cell culture medium from 1×10^7 pericytes cells cultured for 24 h was collected. The culture media were centrifuged at 800 g for 5 minutes; the supernatant was centrifuged at $2000 \times g$, 4°C, 10 min. Next, the supernatant medium was collected, filtered into a 0.22 μm microporous membrane, and centrifuged at $100,000 \times g$, 4°C for 2 hours. After centrifugation, discard the supernatant, resuspend the tube wall pellet with PBS, and continue to centrifuge for 2 hours at $100,000 \times g$ at 4°C. Lastly, after abandoning the supernatant, the exosomal pellet was resuspended in 100 μL PBS and stored at -80°C for subsequent experiments.

2.8. In Vivo Exosome Tracing. Exosomes were treated with PKH26 fluorescent dye (2×10^6 M) at room temperature for 20 minutes. This reaction was stopped by 5% bovine serum albumin, resuspended in PBS, and centrifuged

($1,500 \times g$, 30 minutes) to separate exosomes. After that, fluorescent-labeled exosomes were injected into rats via tail vein, and perfusion samples were taken after 24 hours of modeling. The exosomes were observed in the tissue sections under a fluorescence microscope to see whether they reached the damaged area. Labeled exosomes were added to pericyte cultures to observe endocytosis under the fluorescence microscope.

2.9. Immunohistochemical (IHC) Analysis. For IHC, following deparaffining with xylene and hydration with gradient ethanol, the paraffin-embedded tissue sections were treated with citrate buffer at pH = 6 for 20 min and immersed in a humidified chamber with 3% H_2O_2 for 10 min. After washing and blocking, sections were incubated overnight with rabbit PI3K, AKT, and EZH2 antibodies (Table 1) in a humidified chamber at 4°C. Five randomly selected fields were captured using a bright-field microscope (Olympus, Tokyo, Japan) (magnification 200x) and analyzed by Image-Pro Plus v6.2 software (Media Cybernetics, Silver Spring, MD).

2.10. Statistical Analysis. Three duplicates of each experiment were carried out. SPSS (version 24; SPSS (IBM) Inc., Illinois, USA) was used for analysis. The classification variants were distributed in numerical numbers. Mean ± standard represented data deviation. Unpaired Student's t-test was evaluated for two sets of data comparison, and one-way ANOVA was used for multiple groups. The statistical meaning was determined when $P < 0.05$.

3. Results

3.1. PDGFRβ and PDL1 Are Upregulated in the GBM. To interrogate the differential expression of PDGFRβ in GBM and normal tissues, we integrated GBM data from TCGA and corresponding data of normal brain tissue from the GTEX database. We found that PDGFRβ in GBM was
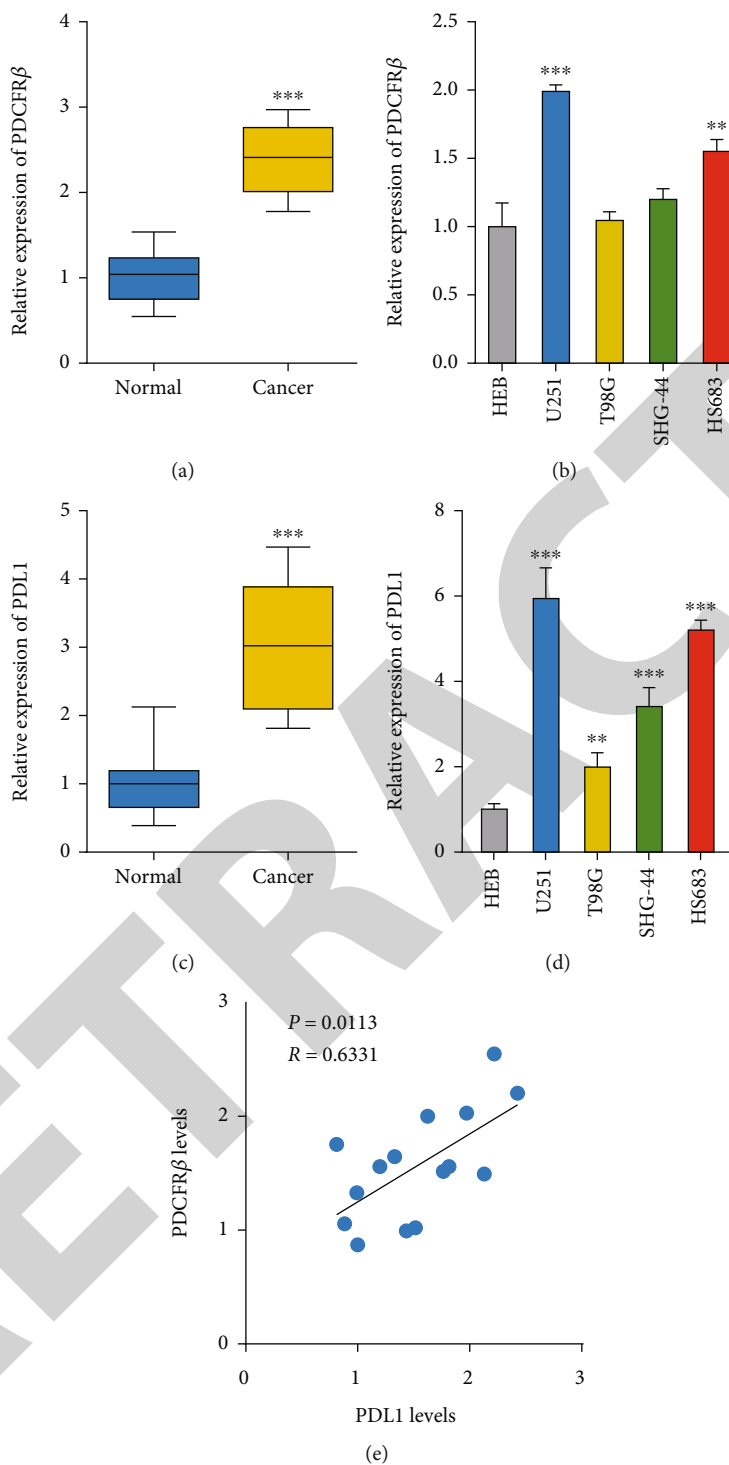
Figure 1: Differential expression of PDGFRβ in the clinical tissue samples and glioma cell lines. (a) Relative mRNA level of PDGFRβ in glioma patients (**$P < 0.01$ vs. normal group). (b) Relative mRNA level of PDGFRβ in glioma cells (**$P < 0.01$ vs. HEB cell group). (c) Relative mRNA level of PDL1 in glioma patients (**$P < 0.01$ vs. normal group). (d) Relative mRNA level of PDL1 in glioma cells (**$P < 0.01$ vs. HEB cell group). (e) The relationship between PDGFRβ and PDL1.

virtually higher than that in normal brain tissue (Figure S1A). IHC was employed and showed that the expression of PDGFRβ was higher in GBM than in the adjacent normal tissues (Figure S1B). Then, qrt-PCR results also showed that PDGFRβ was significantly

upregulated in the GBM tissues compared to the normal group (Figure 1(a)). We then compared the mRNA relative expression of PDGFRβ in glial cells of the human brain (HEB) and four different glioma cell lines (T98G, SHG-44, U251, and HS683) and found that the expression of

(a)

(b)

(c)

(d)

(e)
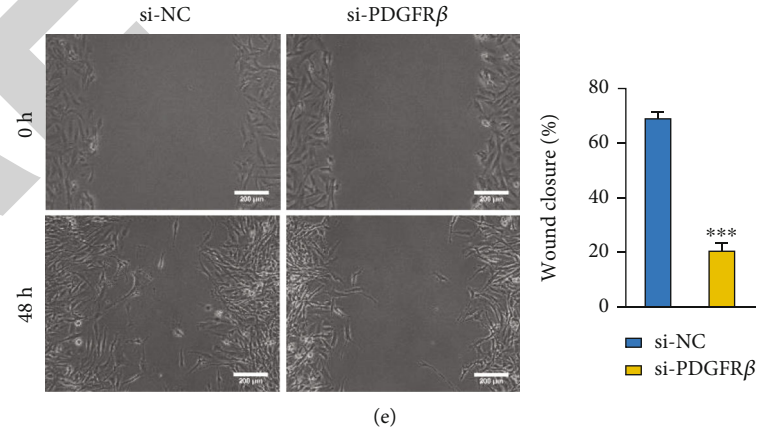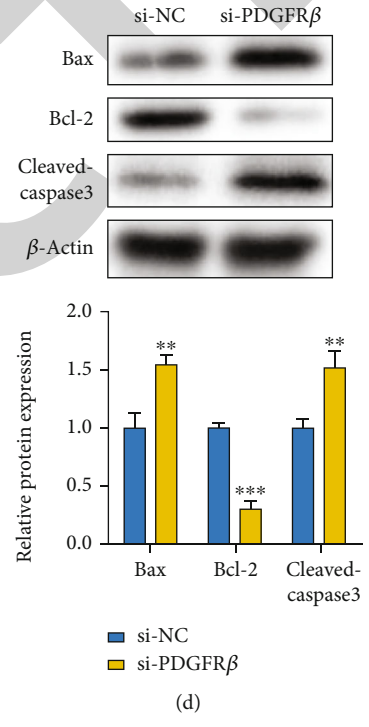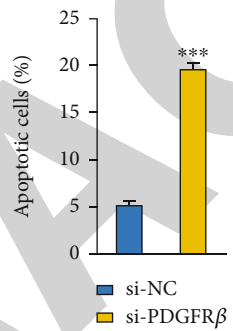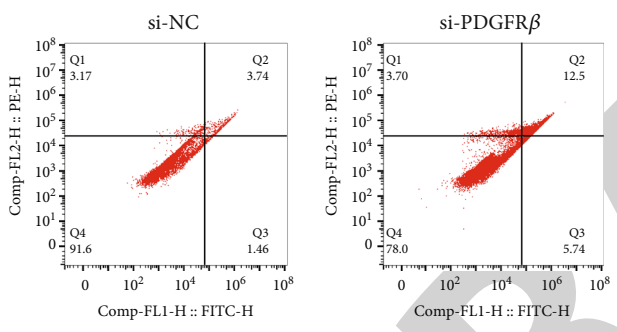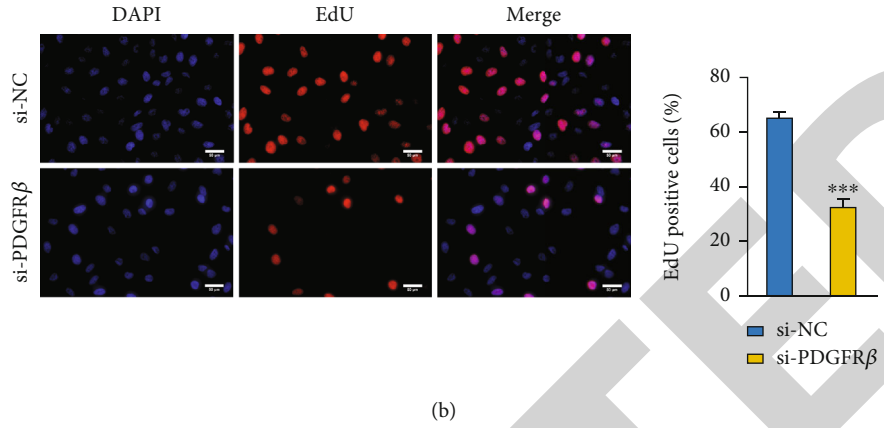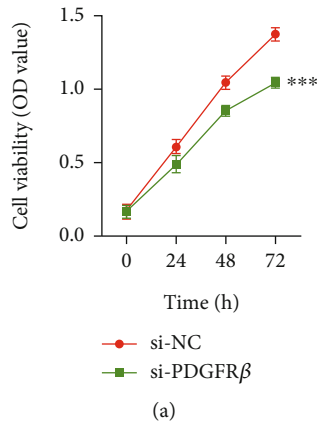
FIGURE 2: Continued.

(f)

(g)
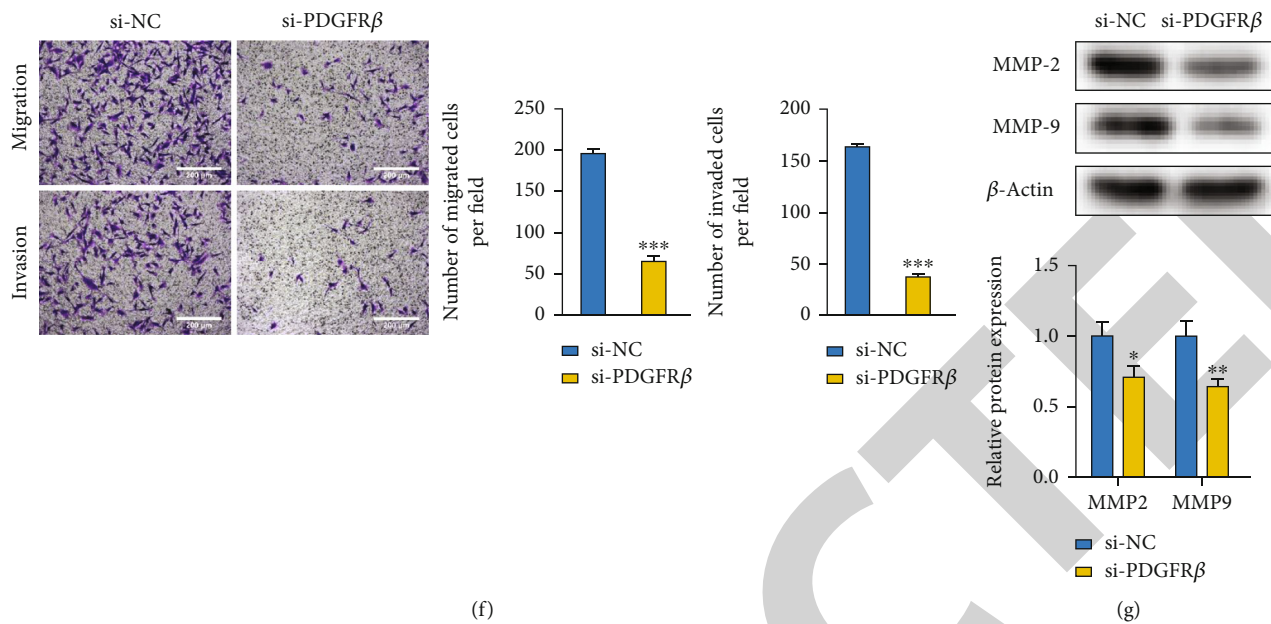
Figure 2: The effects of silencing PDGFRβ on tumor inhibition of U251 cells. (a) U251 cell viability was measured by CCK-8 after transfecting with si-NC or si-PDGFRβ at 0, 24 h, 48 h, and 72 h. (b) EdU detection showed that si-PDGFRβ induced apoptosis. (c) FACS analysis showed that si-PDGFRβ induced apoptosis. (d) Immunoblot analysis showed the levels of the proapoptotic protein of Bax and cleaved caspase-3 and antiapoptotic protein of Bcl-2. (e) Wound healing test showed that si-PDGFRβ inhibited the migration of glioma cells. (f) Transwell assay results showed that downregulation of PDGFR revealed caspase-cell migration and invasion in glioma. (g) There are indications that si-PDGFRβ lowered MMP2 and MMP9, the hall marker protein of tumor invasion and metastasis by immunoblot analysis (*$P < 0.05$, **$P < 0.01$, and ***$P < 0.001$ vs. si-NC group).

PDGFRβ was the highest in U251 cells (Figure 1(b)). According to the qPCR results, PDL1 was also significantly upregulated in the GBM tissues (Figure 1(c)). The expression of PDL1 was notably higher in U251 when compared to HEB cells (Figure 1(d)). Correlation analysis indicated positive results for PDGFRβ and PDL1 (Figure 1(e)).

3.2. Knockdown of PDGFRβ Forbids the Proliferation of Glioma Cells. Next, we checked the function of PDGFRβ on glioma cells naturally. CCK-8 analysis revealed that the cell viability of U251 was virtually diminished by the down-expression of PDGFRβ (si-PDGFRβ) (Figure 2(a)). Furthermore, EdU assay results showed that glioma cell proliferation ability was virtually reduced by si-PDGFRβ (Figure 2(b)). Finally, we tried to analyze whether downregulation of PDGFRβ could induce apoptosis in the U251 cell line. FACS analysis demonstrated that silencing of PDGFRβ induced apoptosis in the U251 cell line (Figure 2(c)). Further, immunoblot analysis showed that down-expression of PDGFRβ significantly boosted the levels of the proapoptotic protein of Bax and cleaved caspase-3 but lowered the level of antiapoptotic protein of Bcl-2 (Figure 2(d)). The above results showed that PDGFRβ knockdown restrained glioma cell proliferation and induced cell apoptosis.

We then examined the effects of si-PDGFRβ on glioma cell migration and invasion ability. Wound-healing assay (Figure 2(e)) and transwell assay (Figure 2(f)) showed that PDGFRβ downregulation inhibited the migration and invasion of glioma cells. Furthermore, down-expression of

PDGFRβ significantly decreased MMP2 and MMP9, the hall marker protein of tumor invasion and metastasis (Figure 2(g)). The above experimental data confirmed that si-PDGFRβ inhibited glioma cell migration and invasion ability.

3.3. Interference with PDGFRβ Downregulates PI3K/AKT/EZH2 Signal Transduction. We used the Cignal Finder RTK Signaling 7-Pathway Reporter Array to determine which pathways PDGFRβ regulates to cause downstream gene changes. Overexpression of PDGFRβ activated the PI3K/AKT pathway, and the knockdown of PDGFRβ inhibited it (Figure 3(a)). The P85 subunit of phosphoinositide 3-kinase (PI3K) has been reported to bind to phosphorylated PDGFR through the SH2 domain, and serine-threonine protein kinase (Akt) reactivates the downstream molecule. We examined the relationship between PDGFRβ and PI3K/AKT signaling pathway at the protein level; according to immunoblot analysis, si-PDGFRβ indeed lowered the levels of p-PI3K and p-AKT proteins (Figure 3(b)). It has been reported that EZH2 promotes tumor occurrence via governing AKT expression [19], and our test results suggested that si-PDGFRβ significantly downregulated the protein levels of EZH2 (Figure 3(b)). The pattern of PDL1 was also dramatically downregulated by si-PDGFRβ transfection.

3.4. Identification and Tracing of Exosomes. Transmission electron microscopy (TEM) results showed that the negatively stained exosomes were in the shape of saucers with a diameter of about 100 nm (Figure 4(a)). The particle sizes

(a)

(b)
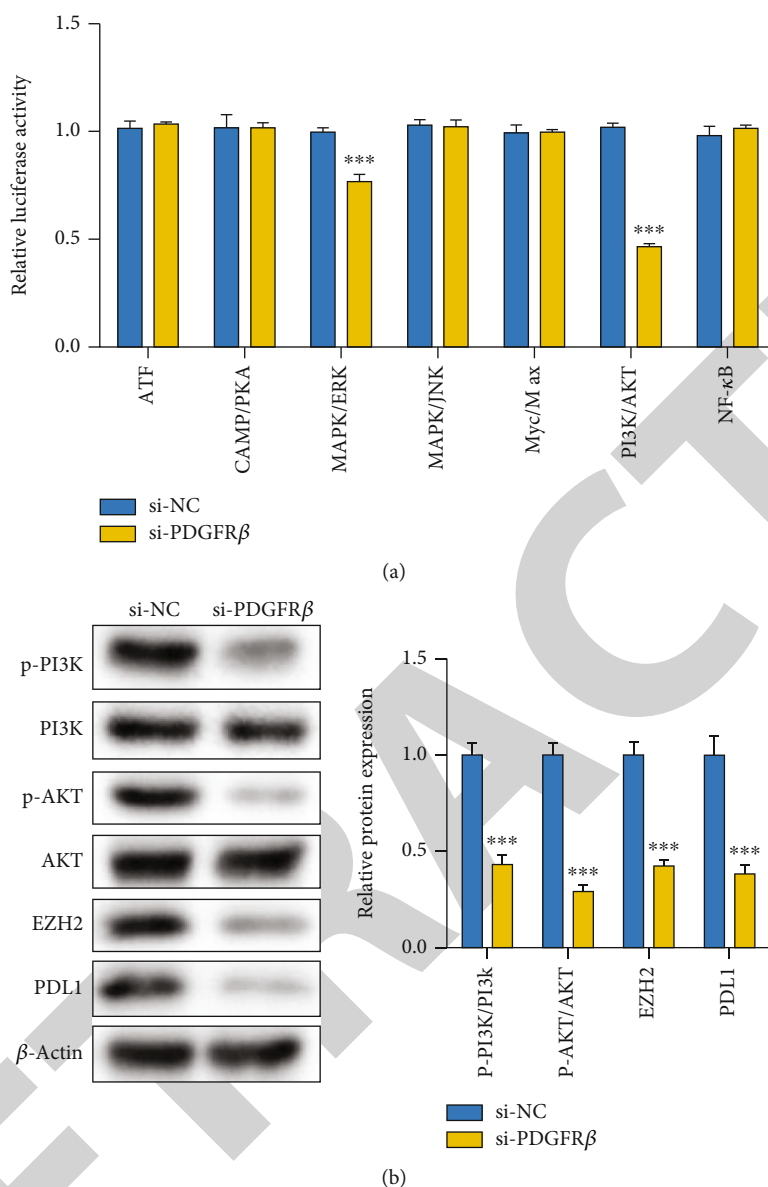
FIGURE 3: The antitumor effects are mediated by knocking down of si-PDGFR-β via downregulating PI3K/AKT/EZH2 signaling pathway. (a) The Cignal Finder RTK Signaling 10-Pathway Reporter Array demonstrated that the up-expression of PDGFRβ activated, and the knockdown of PDGFRβ downregulated the PI3K/AKT signaling pathway. (b) Immunoblot analysis displayed that down-expression of PDGFRβ decreased the p-PI3K, p-AKT, EZH2, and PDL1 protein levels (***$P < 0.001$ vs. si-NC group).

of exosomes derived from pericytes were concentrated in the range of 80-200 nm, consistent with the consensus of exosome diameter of 30-150 nm (Figure 4(b)). Immunoblot was used to identify exosome molecular markers. The results showed that exosomes derived from pericytes specifically expressed CD63 and TSG101, while the culture medium after exosome extraction did not express such molecules (Figure 4(c)). Exosomes labeled with PKH26 were cocultured with U251 cells, and red fluorescent was observed under a fluorescence microscope as exosomes, indicating that the exosomes could be uptaken by U251 cells (Figure 4(d)). Immunoblots have been applied to identify PDGFRβ protein expression. The results showed that when exosomes loaded with si-PDGFRβ were extracted, the pro-

tein level of PDGFRβ in cells decreased significantly (Figure 4(e)).

3.5. The Exosomes Loaded with si-PDGFRβ Resists the Proliferation, Invasion, and Migration of Glioma Cells. Next, we tested whether the exosomes loaded with si-PDGFRβ exerted tumor inhibition effects in glioma cell lines. The results of the CCK-8 and EdU assays stated clearly that si-PDGFRβ-loaded exosomes significantly reduced the cell viability of U251 (Figures 5(a) and 5(b)). In addition, FACS analysis revealed that exosomes loaded with si-PDGFRβ enhanced apoptosis in the U251 cell line (Figure 5(c)). Furthermore, wound healing and transwell assay findings

(a)

(b)

(c)

(d)

(e)
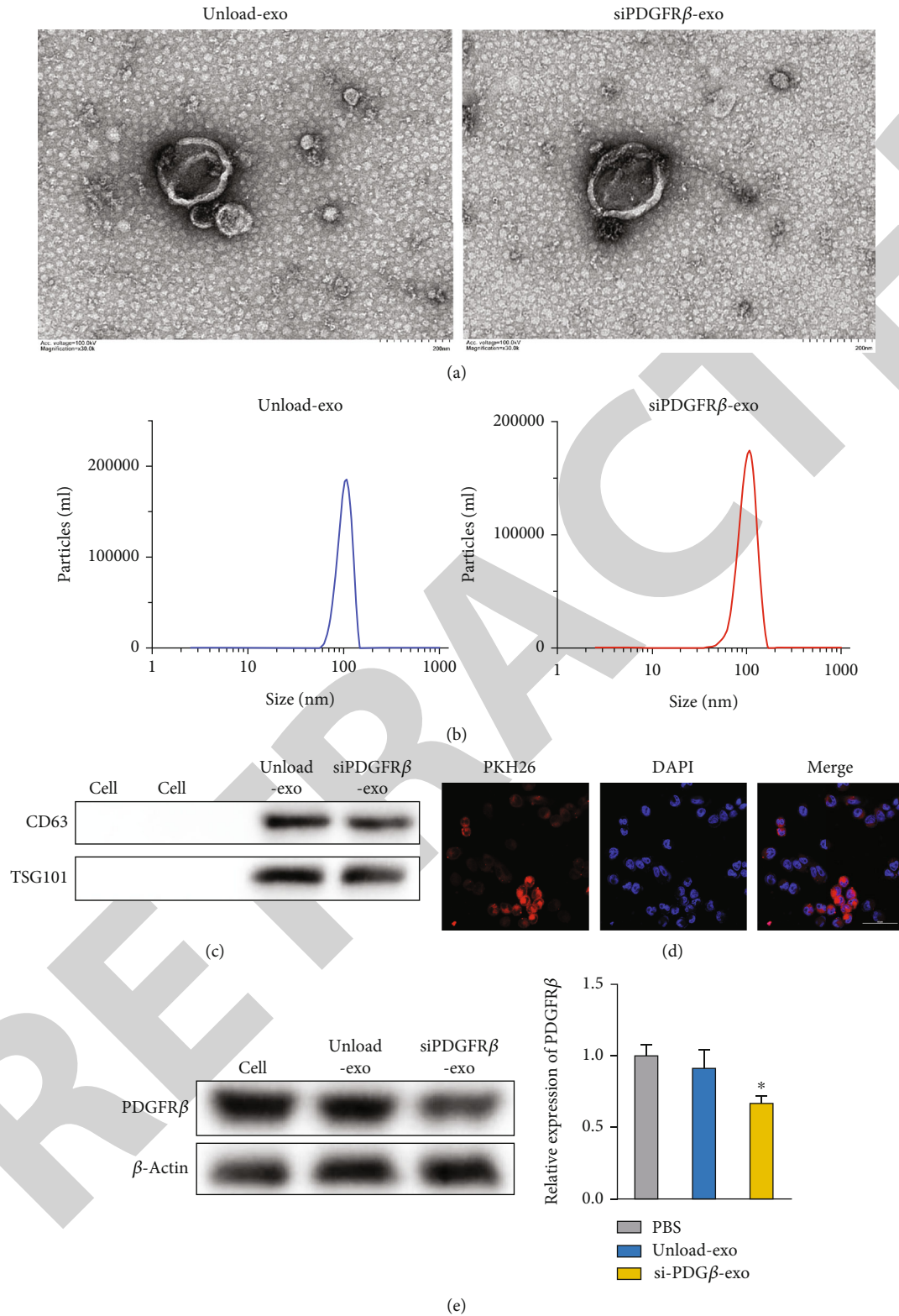
Figure 4: Identification of exosomes derived from pericyte. (a) Transmission electron microscopy (TEM) results showed that the negatively stained exosomes were in the shape of saucers with a diameter of about 100 nm. (b) The particle sizes of exosomes derived from pericytes were at about 100 nm according to nanoparticle size analysis. (c) Immunoblot results showed that exosomes derived from pericytes specifically expressed CD63 and TSG101, while the culture medium did not express such molecules after exosome extraction. (d) Red fluorescent was observed under a fluorescence microscope in U251 cells cocultured with PKH26 labeled exosomes. (e) Immunoblot results showed that when exosomes loaded with si-PDGFRβ were extracted, the protein level of PDGFRβ in cells decreased significantly ($^*P < 0.05$ vs. PBS or Unloaded-Exo group).

(a)

(b)

(c)

(d)
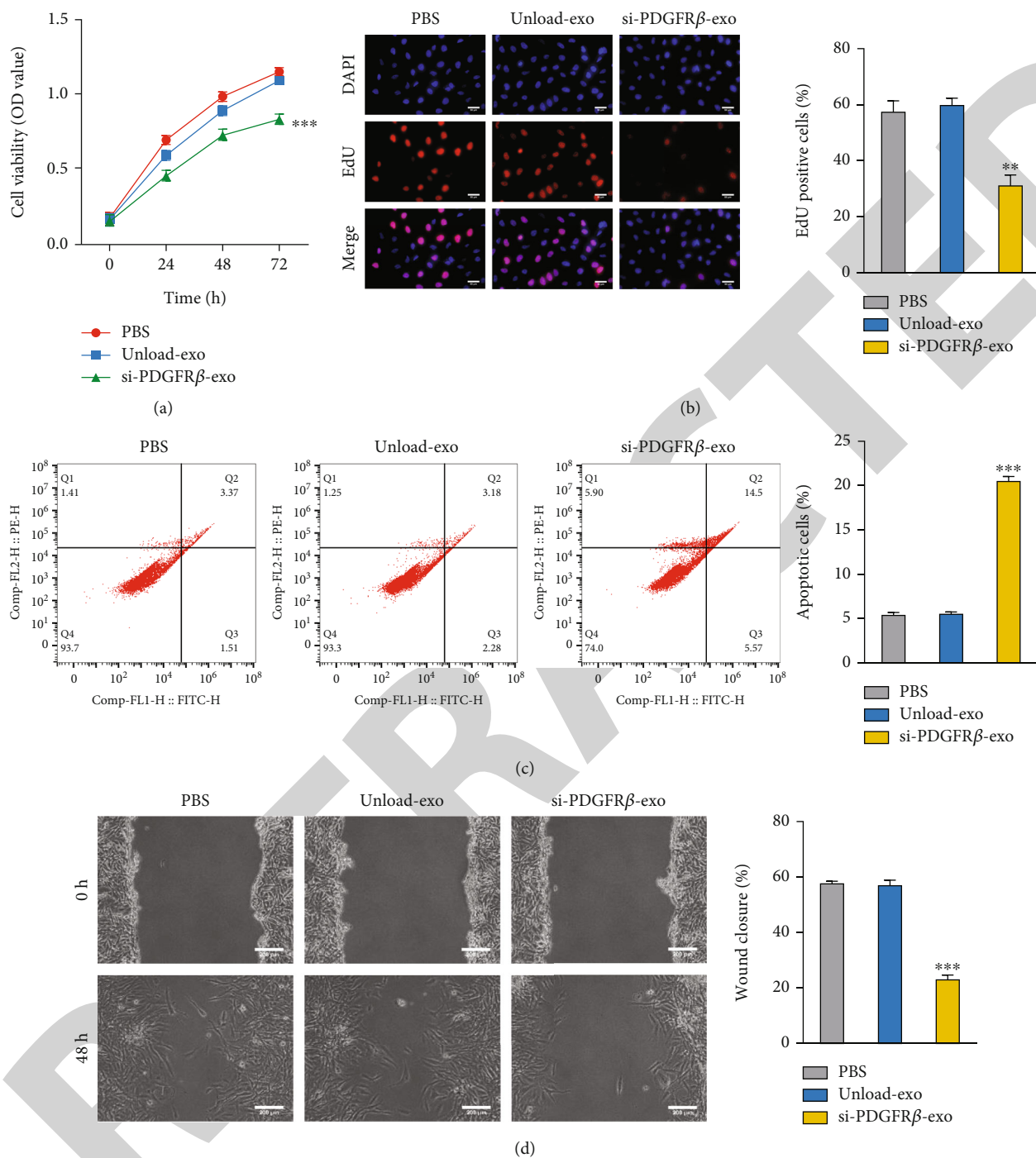
Figure 5: Continued.
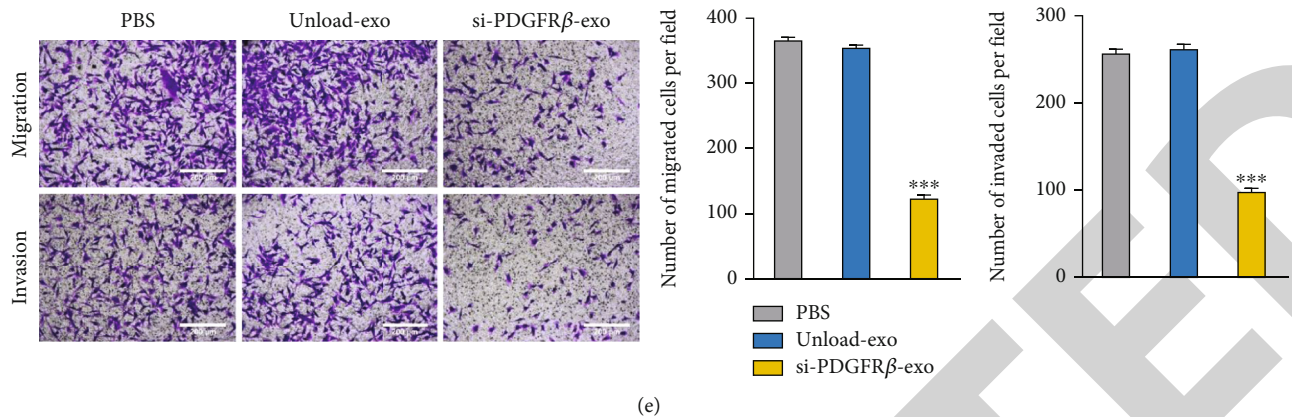
(e)

FIGURE 5: Exosomes loaded with si-PDGFRβ resists the proliferation, invasion, and migration of glioma cells. (a) U251 cell viability was measured by CCK-8 analysis after transfected with exosomes loaded with si-PDGFRβ (si-PDGFRβ-Exo) at 0, 24 h, 48 h, and 72 h. (b) EdU assay indicated that proliferation ability of glioma cells was significantly reduced by exosomes loaded with si-PDGFRβ. (c) FACS assay analysis demonstrated that exosomes loaded with si-PDGFRβ induced more apoptotic cells in the U251 cell line. (d) Wound healing test showed that cell migration of glioma of the si-PDGFRβ-Exo group was significantly inhibited. (e) Transwell assay results showed that si-PDGFRβ-Exo inhibited migration and invasion of glioma cells ($^{**}P < 0.01$ and $^{***}P < 0.001$ vs. PBS or Unloaded-Exo group).

showed that si-PDGFRβ-loaded exosomes suppressed the invasion and migration of U251 cells (Figures 5(d) and 5(e)).

3.6. The Exosomes Loaded with si-PDGFRβ Exerted Tumor Inhibition Effects on Glioma In Vivo.
We then explored whether exosomes loaded with si-PDGFRβ had the same effect in vivo. One week after in situ implantation of glioma cells, PBS, Unloaded-Exo, and si-PDGFRβ-Exo were injected into tumor-bearing mice via tail vein. Brain MRI was performed on the treated mice after four-week treatment to measure the volume of the transplanted tumor. The results showed that the exosomes loaded with si-PDGFRβ significantly inhibited the growth of gliomas (Figure 6(a)). We then tested the targeting ability of exosomes loaded with si-PDGFRβ. We observed that exosomes injected into the tail vein were mainly concentrated at the tumor site through in vivo imaging, suggesting that exosomes loaded with si-PDGFRβ had relatively high targeting ability (Figure 6(b)). H&E staining indicated that the si-PDGFRβ-Exo-treated group induced more necrotic cells than the PBS and Unload-Exo groups (Figure 6(c)). TUNEL assay indicated that si-PDGFRβ-Exo induced more apoptotic cells (Figure 6(c)). The tumor tissue in situ was collected for immunoblot detection. We found that si-PDGFRβ-Exo significantly decreased p-PI3K, p-AKT, EZH2, and PDL1 proteins, which was consistent with in vitro test results (Figure 6(d)).

3.7. In Vivo Exosome Treatment Is Safe.
We also evaluated the safety of exosome therapy. The body weight was statistically insignificant between the Unload-Exo and si-PDGFRβ-Exo groups compared with the PBS group (Figure 7(a)). In addition, visceral functional (such as heart, liver, spleen, lung, and kidney) tests showed no statistical difference among these three groups (Figure 7(b)). Also, the biochemical blood test had no remarkable diversities in the liver function of the three groups (Figure 7(c)). Based on the

above experimental results, it was suggested that the exosome was safe for treating glioma.

4. Discussion

Glioma is a common primary intracranial tumor belonging to the neuroepithelial tumor, which accounts for 44% of intracranial tumors, among which glioblastoma (GBM) with the highest malignant degree, accounts for 22.3% [20]. GBM has the characteristics of strong invasion ability and high malignant degree, and its overall survival rate is still short, even through surgical resection, radiotherapy, and chemotherapy. Oxidative stress is strongly related to the proliferation of cancer cells and is also important in glioma development. Studies have found that GBM is due to the mutation or deletion of tumor suppressor genes and the overexpression of oncogenes, causing cancer cell proliferation and invasion, which are not constrained by normal regulatory mechanisms. Finally, malignant pathological changes occur [21, 22]. Both PDGFR subtypes, PDGFRα and PDGFRβ, are transmembrane glycoproteins whose extracellular N-terminal binding with its ligand activates autophosphorylation of tyrosine residues in the intracellular domain of PDGFR and also activates specific target proteins to promote tyrosine residues phosphorylation, thus transferring the signal into the cell [23]. During embryonic development, PDGFR plays a significant part in physiological activities such as the maturation of the cardiovascular system, connective tissue, central nervous system, gonads, and lungs [5]. PDGFR and its ligands have been proved to be overexpressed in glioma, sarcoma, leukemia, epithelial cell carcinoma, and other malignant tumors and affect the malignant proliferation, vascular hyperplasia, and metastasis of tumor cells. There is a statistically significant positive correlation between PDGFR expression and pathological tumor grade of glioma [24]. Kim et al. have reported that the expression levels of the two receptors were different in
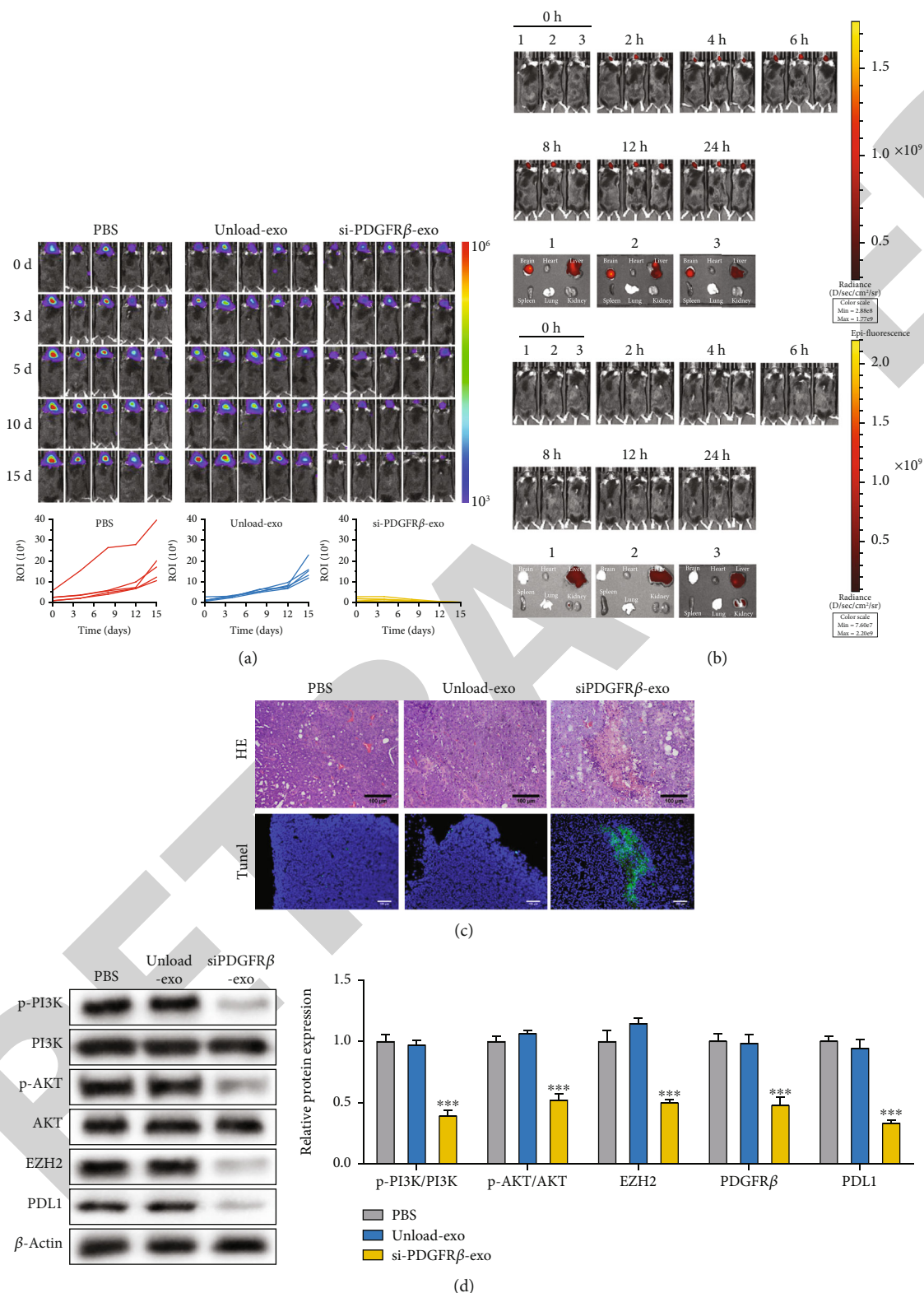
Figure 6: The exosomes loaded with si-PDGFRβ exerted tumor inhibition effects on glioma *in vivo*. (a) Brain MRI was performed on the treated mice after four-week treatment to measure the volume of the transplanted tumor. The results showed that the exosomes loaded with si-PDGFRβ significantly inhibited the growth of gliomas. (b) *In vivo* bioluminescence, imaging showed that exosomes loaded with si-PDGFRβ had relatively high targeting ability. (c) H&E staining indicated that the si-PDGFRβ-Exo-treated group induced more necrotic cells than the PBS and Unload-Exo groups. TUNEL assay indicated that si-PDGFRβ-Exo induced apoptosis. (d) Immunoblot detection demonstrated that si-PDGFRβ-Exo significantly decreased p-PI3K, p-AKT, EZH2, and PDL1 proteins (***$P < 0.001$ vs. PBS or Unloaded-Exo group).

(a)

(b)

(c)
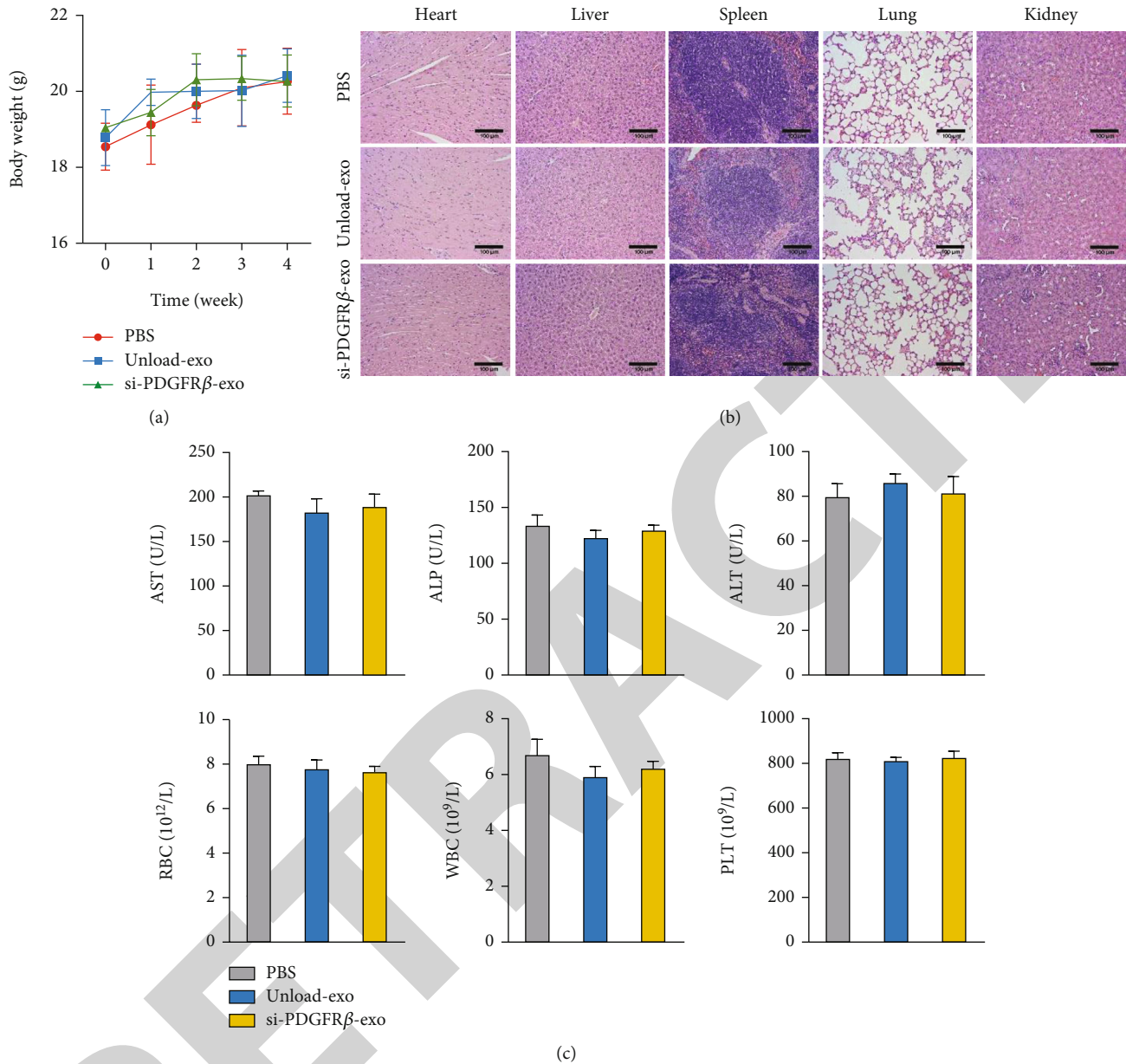
FIGURE 7: The evaluation of exosome treatment. (a) Body weight had no statistically difference between Unload-Exo, si-PDGFRβ-Exo, and PBS groups. (b) The liver, spleen, heart, lung, and kidney functional tests showed no remarkable diversities among three groups. (c) Liver function of the mice in three groups by biochemical blood test showed no significant differences.

glioma. PDGFRα was only expressed in a part of GBM patients, while PDGFRβ expression was more common in GBM patients.

Moreover, gene therapy targeting PDGFRβ weakens GBM stem cells' self-renewal and inhibits tumors' proliferation and invasion [25]. In this research, PDGFRβ expression was remarkably increased in the clinical samples from GBM patients and the U251 cell line. Moreover, consistent with previous studies, knockdown of PDGFRβ inhibits the metastasis of glioma cells. Moreover, this tumor inhibition was caused by the inhibition of PI3K/AKT/EZH2 signal transduction. Furthermore, we extracted exosomes derived from pericytes and found that exosomes loaded with si-PDGFRβ have the same tumor inhibition effect. In addition, we have

confirmed that this exosome has good safety and targeting properties through experiments and found that si-PDGFRβ-loaded exosomes inhibited the glioma progression through PI3K/Akt/EZH2 signaling pathway. Besides, PI3K/Akt/EZH2 signaling pathway was upregulated in glioma patients. Collectively, si-PDGFRβ-loaded exosomes derived from pericytes inhibit glioma's progression via downregulation of the PI3K/AKT/EZH2 signaling pathway.

Exosomes are bioactive nanoscale vesicles secreted by cells and are cup-shaped vesicles with a diameter of 40-140 nm and a lipid bilayer structure [26, 27]. There are many applications for exosomes at present. In the field of diagnosis, Goldie et al. found that among all small RNAs, miRNAs account for a higher proportion in exosomes than in the cells

from which they originate [28]. Serum lncRNA HOTAIR can be used as a novel diagnostic and prognostic marker of GBM [29]. The blood-brain barrier (BBB) is one of the significant hurdles in glioma chemotherapeutics. The majority of glioma chemotherapeutic drugs have poor utilization because of their low solubility in blood and short half-life [30]. One of the current technologies used to deliver drugs efficiently and highly targeted to the tumor site is encapsulating drugs in nanocarriers, which often contain targeting factors that facilitate entry into the tumor region [31]. However, the artificial nature of nanocarrier systems leads to problems related to toxicity in vivo. Exosomes, as extensive endogenous carriers, have many favorable drug delivery characteristics: small size, immune escape, the long half-life, and subtypes that target tumor cells [31]. More importantly, exosomes can load hydrophilic and hydrophobic drugs effectively. In this study, exosomes extracted from mouse pericellular cells were observed by TEM to be round or like a tea holder/cup structure, with dark surrounding color and a light center with an obvious three-dimensional sense. The diameter was about 100 nm, and the peak particle size was about 100 nm. The concentration of distribution was high at one time, showing no difference with the characteristics of exosomes previously reported in the literature [12].

The electroporation method is a mature method to load drugs into isolated exosomes. Its principle is to expose suspensions of exosomes and therapeutic drugs to an electric field, and the exosome membrane will generate numerous holes under a short high-pressure pulse, through which small drug molecules penetrate exosomes [17]. The siRNA is a promising therapeutic solution as a posttranscriptional gene regulation process for various pathological conditions and regulating cellular longevity. Wahlgren et al. measured the loading efficiency with fluorescently labeled siRNA, and the loading efficiency reached 25% [32]. In this paper, si-PDGFRβ was also transferred into exosomes by electroporation, and exosomes loaded with si-PDGFRβ had the same tumor inhibition effect as si-PDGFRβ. Pericytes secrete excessive transmembrane receptors, CD248, and other signal molecules to promote the angiogenesis of gliomas but also guide endothelial cells to secrete vascular endothelial growth factor (VEGF) through the PDGFRβ signaling pathway synergistically promoting tumor angiogenesis. In addition, endothelial cells secrete more VEGF in high-grade gliomas [33]. We confirmed that the exosomes loaded with si-PDGFRβ exerted tumor inhibition effects on glioma in vivo and were more robust in targeting low immunogenicity.

PI3K/Akt plays an essential part in the occurrence and progression of malignant tumors and has proven to be one of the therapeutic targets of malignant tumors [34]. Phillips et al. reported that myricetin promoted cell apoptosis in pancreatic cancer by inhibiting the PI3K/Akt signaling pathway [35]. As a polycomb-repressive complex-2 (PRC-2) component, the knockdown of EZH2 gene expression was found to induce cell arrest in the G2-M phase to inhibit cell proliferation [36]. Choi et al. found that EZH2 expression increased in 60.6% of gastric cancer patients but only 6.7% of nonneoplastic patients [37]. The Akt signaling pathway inhibits trimethylation of H3K27 through phosphonate EZH2 and disrupts gene silencing, leading to carcinogenesis [38]. We revealed that exosomes loaded with si-PDGFRβ, which targeted ZEB1, inhibited glioma cells' invasion, proliferation, and migration via inhibiting the PI3K/Akt/EZH2 pathway. More importantly, in vivo experiments revealed that exosomes loaded with si-PDGFRβ effectively and safely inhibit glioma development.

5. Conclusions

Increased free radical levels and diminished antioxidant defense responses are associated with the development of gliomas. Since oxidative stress plays a significant role in the aetiology of gliomas, antioxidant treatment may be effective in treating tumors. Therapeutic regimens still face numerous difficulties and problems. However, many kinds of oxidative medicine include small molecule compounds, natural products, nucleic acid drugs, and protein drugs. Exosomes, as a favorable carrier for various medicine, including oxidative medicine, could exert their antitumor properties by regulating oxidative stress, which enables their therapeutic effects in inhibiting proliferation and invasion. In summary, in vivo and in vitro experiments in this study showed that si-PDGFRβ-loaded exosomes may protect against glioma progression by preventing the activity of the PI3K/Akt/EZH2 signaling pathway. Moreover, evaluate the potential value of exosomes loaded with si-PDGFRβ as a treatment strategy for glioma.

Data Availability

The datasets for this study are available from the corresponding author upon reasonable request.

Ethical Approval

The Medical College approved the animal study of Yangzhou University, China. This study was reviewed and approved by the Research Ethics Committee of the Clinical Medical College of Yangzhou University, China.

Consent

All the patients provided their written informed consent to participate in this study.

Conflicts of Interest

The authors state that there is no conflict of interest.

Authors' Contributions

Y L and HL Y performed most experiments, analyzed data, and wrote the manuscript. QM and MW participated in the animal experiments. CL, XG L, and YJ Q participated in cell culture assays. HZ Z and LD collected glioma tissue samples. YP L and HZ Z designed the overall study, supervised the experiments, and write the paper. All authors contributed to the article and approved the submitted version.

Supplementary Materials

Figure S1: PDGFRβ was activated in clinical GBM samples. Both bioinformatic analysis and IHC results revealed that PDGFRβ was up-expressed in tumor tissues of GBM. (Supplementary Materials)

References

[1] L. Arko, I. Katsyv, G. E. Park, W. P. Luan, and J. K. Park, "Experimental approaches for the treatment of malignant gliomas," *Pharmacology & Therapeutics*, vol. 128, no. 1, pp. 1–36, 2010.

[2] M. L. Goodenberger and R. B. Jenkins, "Genetics of adult glioma," *Cancer Genetics*, vol. 205, no. 12, pp. 613–621, 2012.

[3] A. A. Stavrovskaya, S. S. Shushanov, and E. Y. Rybalkina, "Problems of glioblastoma multiforme drug resistance," *Biochemistry (Mosc)*, vol. 81, no. 2, pp. 91–100, 2016.

[4] R. Stupp, P. Dietrich, S. O. Kraljevic et al., "Promising survival for patients with newly diagnosed glioblastoma multiforme treated with concomitant radiation plus temozolomide followed by adjuvant temozolomide," *Journal of Clinical Oncology*, vol. 20, no. 5, pp. 1375–1382, 2002.

[5] J. Andrae, R. Gallini, and C. Betsholtz, "Role of platelet-derived growth factors in physiology and medicine," *Genes & Development*, vol. 22, no. 10, pp. 1276–1312, 2008.

[6] C. H. Heldin and B. Westermark, "Mechanism of action and in vivo role of platelet-derived growth factor," *Physiological Reviews*, vol. 79, no. 4, pp. 1283–1316, 1999.

[7] D. G. Gilbertson, M. E. Duff, J. W. West et al., "Platelet-derived growth factor C (PDGF-C), a novel growth factor that binds to PDGF alpha and beta receptor," *The Journal of Biological Chemistry*, vol. 276, no. 29, pp. 27406–27414, 2001.

[8] C. D'Sa-Eipper, J. R. Leonard, G. Putcha et al., "DNA damage-induced neural precursor cell apoptosis requires p53 and caspase 9 but neither Bax nor caspase 3," *Development*, vol. 128, no. 1, pp. 137–146, 2001.

[9] P. Levéen, M. Pekny, S. Gebre-Medhin, B. Swolin, E. Larsson, and C. Betsholtz, "Mice deficient for PDGF B show renal, cardiovascular, and hematological abnormalities," *Genes & Development*, vol. 8, no. 16, pp. 1875–1887, 1994.

[10] E. Bergsten, M. Uutela, X. Li et al., "PDGF-D is a specific, protease-activated ligand for the PDGF β-receptor," *Nature Cell Biology*, vol. 3, no. 5, pp. 512–516, 2001.

[11] R. Rana, S. Joon, K. Chauhan et al., "Role of extracellular vesicles in glioma progression: deciphering cellular biological processes to clinical applications," *Current Topics in Medicinal Chemistry*, vol. 21, no. 8, pp. 696–704, 2021.

[12] C. Théry, S. Amigorena, G. Raposo, and A. Clayton, "Isolation and characterization of exosomes from cell culture supernatants and biological fluids," *Current Protocols in Cell Biology*, vol. 30, no. 1, 2006.

[13] A. V. Vlassov, S. Magdaleno, R. Setterquist, and R. Conrad, "Exosomes: current knowledge of their composition, biological functions, and diagnostic and therapeutic potentials," *Biochimica et Biophysica Acta*, vol. 1820, no. 7, pp. 940–948, 2012.

[14] T. B. Steinbichler, J. Dudas, H. Riechelmann, and I. I. Skvortsova, "The role of exosomes in cancer metastasis," *Seminars in Cancer Biology*, vol. 44, pp. 170–181, 2017.

[15] X. Guo, W. Qiu, J. Wang et al., "Glioma exosomes mediate the expansion and function of myeloid-derived suppressor cells through micro RNA-29a/Hbp1 and microRNA-92a/Prkar1a pathways," *International Journal of Cancer*, vol. 144, no. 12, pp. 3111–3126, 2019.

[16] S. Yang, K. Guo, J. Li, and Z. Feng, "Framework formation of financial data classification standard in the era of the big data," *Procedia Computer Science*, vol. 30, pp. 88–96, 2014.

[17] L. Alvarez-Erviti, Y. Seow, H. Yin, C. Betts, S. Lakhal, and M. J. A. Wood, "Delivery of siRNA to the mouse brain by systemic injection of targeted exosomes," *Nature Biotechnology*, vol. 29, no. 4, pp. 341–345, 2011.

[18] S. Kamerkar, V. S. LeBleu, H. Sugimoto et al., "Exosomes facilitate therapeutic targeting of oncogenic KRAS in pancreatic cancer," *Nature*, vol. 546, no. 7659, pp. 498–503, 2017.

[19] X. Liu, X. Lu, F. Zhen et al., "LINC00665 induces acquired resistance to gefitinib through recruiting EZH2 and activating PI3K/AKT pathway in NSCLC," *Molecular Therapy-Nucleic Acids*, vol. 16, pp. 155–161, 2019.

[20] D. G. Brachman, S. L. Pugh, L. S. Ashby et al., "Phase 1/2 trials of temozolomide, motexafin gadolinium, and 60-Gy fractionated radiation for newly diagnosed supratentorial glioblastoma multiforme: final results of RTOG 0513," *International Journal of Radiation Oncology • Biology • Physics*, vol. 91, no. 5, pp. 961–967, 2015.

[21] X. Li, C. Wu, N. Chen et al., "PI3K/Akt/mTOR signaling pathway and targeted therapy for glioblastoma," *Oncotarget*, vol. 7, no. 22, pp. 33440–33450, 2016.

[22] C. Talarico, V. Dattilo, L. D'Antona et al., "SI113, a SGK1 inhibitor, potentiates the effects of radiotherapy, modulates the response to oxidative stress and induces cytotoxic autophagy in human glioblastoma multiforme cells," *Oncotarget*, vol. 7, no. 13, pp. 15868–15884, 2016.

[23] C. H. Heldin and A. Ostman, "Signal transduction via platelet-derived growth factor receptors," *Biochimica et Biophysica Acta*, vol. 1378, no. 1, pp. F79–113, 1998.

[24] O. Martinho, A. Longatto-Filho, M. B. Lambros et al., "Expression, mutation and copy number analysis of platelet-derived growth factor receptor A (PDGFRA) and its ligand PDGFA in gliomas," *British Journal of Cancer*, vol. 101, no. 6, pp. 973–982, 2009.

[25] Y. Kim, E. Kim, Q. Wu et al., "Platelet-derived growth factor receptors differentially inform intertumoral and intratumoral heterogeneity," *Genes & Development*, vol. 26, no. 11, pp. 1247–1262, 2012.

[26] E. H. Koritzinsky, J. M. Street, R. A. Star, and P. S. T. Yuen, "Quantification of exosomes," *Journal of Cellular Physiology*, vol. 232, no. 7, pp. 1587–1590, 2017.

[27] C. Théry, M. Ostrowski, and E. Segura, "Membrane vesicles as conveyors of immune responses," *Nature Reviews. Immunology*, vol. 9, no. 8, pp. 581–593, 2009.

Retraction

Retracted: Metoprolol Mitigates Ischemic Heart Remodeling and Fibrosis by Increasing the Expression of AKAP5 in Ischemic Heart

Oxidative Medicine and Cellular Longevity

Received 26 September 2023; Accepted 26 September 2023; Published 27 September 2023

This article has been retracted by Hindawi following an investigation undertaken by the publisher [1]. This investigation has uncovered evidence of one or more of the following indicators of systematic manipulation of the publication process:

(1) Discrepancies in scope

(2) Discrepancies in the description of the research reported

(3) Discrepancies between the availability of data and the research described

(4) Inappropriate citations

(5) Incoherent, meaningless and/or irrelevant content included in the article

(6) Peer-review manipulation

The presence of these indicators undermines our confidence in the integrity of the article's content and we cannot, therefore, vouch for its reliability. Please note that this notice is intended solely to alert readers that the content of this article is unreliable. We have not investigated whether authors were aware of or involved in the systematic manipulation of the publication process.

Wiley and Hindawi regrets that the usual quality checks did not identify these issues before publication and have since put additional measures in place to safeguard research integrity.

We wish to credit our own Research Integrity and Research Publishing teams and anonymous and named external researchers and research integrity experts for contributing to this investigation.

The corresponding author, as the representative of all authors, has been given the opportunity to register their agreement or disagreement to this retraction. We have kept a record of any response received.

References

[1] F. Zhu, Q. Wang, Z. Wang, X. Zhang, B. Zhang, and H. Wang, "Metoprolol Mitigates Ischemic Heart Remodeling and Fibrosis by Increasing the Expression of AKAP5 in Ischemic Heart," *Oxidative Medicine and Cellular Longevity*, vol. 2022, Article ID 5993459, 8 pages, 2022.

Research Article

Metoprolol Mitigates Ischemic Heart Remodeling and Fibrosis by Increasing the Expression of AKAP5 in Ischemic Heart

Feng Zhu, Qiushu Wang, Zhi Wang, Xu Zhang, Benkai Zhang, and Hegui Wang ⓘ

Department of Cardiology, Yijishan Hospital of Wannan Medical College, Wuhu, China

Correspondence should be addressed to Hegui Wang; wanghegui@wnmc.edu.cn

The harm of heart failure mainly causes patients to develop dyspnea, fatigue, fluid retention, and other symptoms, which impair patients' activity tolerance and lead to a dramatic decrease in patients' quality of life. The purpose of this study was to verify whether metoprolol regulates AKAP5 expression and test the role of AKAP5 postinjury in mitigating cardiac infarction-associated tissue remodeling and fibrosis. Sprague-Dawley (SD) rats underwent coronary artery ligation (CAL), which was followed immediately with metoprolol daily. And western blot and coimmunoprecipitation experiments were performed to detect the expression of related proteins in the sham-operated group, model group, and drug-treated group. HW/BW ratio and cardiac expression of COL1 and COL3 were increased in rats following CAL compared with shams. Treatment with metoprolol postinjury was associated with a decrease in HW/BW ratio and COL1/COL3 expression compared to uncontrolled rats. CAL resulted in decreased cardiac AKAP5 expression compared to the control group, while metoprolol treatment restored levels compared to baseline shams. Cardiac expression levels of NFATc3/p-NFATc3 and GATA4 were modest at baseline and increased with injury, whereas metoprolol suppressed gene expression to below injury-associated changes. Immunoprecipitation indicated that AKAP5 could bind and regulate PP2B. In summary, we know that metoprolol alleviates ischemic cardiac remodeling and fibrosis, and the mechanism of alleviating remodeling may improve cardiac AKAP5 expression and AKAP5-PP2B interaction.

1. Introduction

Patients with heart failure have severely diminished systolic as well as diastolic function and diminished cardiac pumping. Heart failure (HF) has many hazards that can affect the quality of life, affect organ function, and be life-threatening. Recent results from epidemiological surveys of HF in China show a weighted HF prevalence of 1.3%, or approximately 13.7 million HF patients, among our population of residents aged ≥35 years. The incidence of HF continues to rise as the population ages [1, 2]. Unfortunately, HF is minimally symptomatic even with real cardiac structural changes such as left ventricular (LV) hypertrophy, LV systolic or diastolic dysfunction, and valvular disease. The prognosis for advanced HF is poor. Therefore, early intervention is likely to be more impactful in reducing morbidity and mortality.

LV remodeling (LVR) is common after ischemic myocardial injury and manifests as changes in ventricular thickness and size. This compensation mechanism initially minimizes cardiac dysfunction but, over time, proves inadequate at maintaining cardiac function [3]. Postischemic cardiac remodeling is worsened by chronic activation of the neuroendocrine system and unrestrained extracellular matrix deposition. Several cytokines and hormones promote this process, including hyperactive beta-adrenocortical hormones, and are found to increase in animal models and people with cardiac remodeling [4]. Ventricular remodeling is caused by a complex series of cellular and molecular mechanisms leading to progressive changes in ventricular weight, volume, and morphology of cardiomyocytes and the myocardial matrix, characterized by progressive dilation of the primary Mi region and LV volume. It begins in the early stage of AMI and is a response of the myocardium to

myocardial injury and cardiac overload. Recent studies have shown that changes in the structure and composition of the extracellular matrix of cardiac muscle are an early event in the progression of left ventricular myocardial remodeling and cardiac pump dysfunction and have an important role in myocardial remodeling [5].

Chronic heart failure is a slow process, often taking over a decade for symptoms to develop. In this process, the heart is engaged in a constant interplay with the organism, with the impact of the neuroendocrine system being most pronounced. This is mainly manifested in the remodeling of the myocardium. Any single organ and tissue of an organism have a certain structure-activity relationship, and what structure determines what function it performs. In turn, because an organism requires such a function, an organ or tissue evolves progressively into its present-day shape. Thus, an organ lesion, although not necessarily one in which a structural change occurs, must illustrate that the organ has developed the lesion. Structural alterations are accumulated in response to a variety of humoral and cellular factors as well as various receptors for prolonged periods [6]. For myocardial remodeling, because the myocardium is nonrenewable, hypertrophy, apoptosis, and remodeling of the glial network outside the cardiomyocyte can be used as entry points to explain myocardial remodeling. In the RAS system, β Adrenergic system, the role of the sympathetic system in promoting ventricular remodeling has been demonstrated several times. The ECM plays an important role in maintaining the structural and functional integrity of the heart, and disruption of the dynamic balance between myocardial interstitial fibrillar collagen synthesis and degradation damages the microenvironment of the heart, which has also been confirmed to be associated with the ventricular remodeling in recent years and is gaining increasing attention [7].

AKAP5, also known as akap79/150, includes a variety of proteins of different genera encoded by the homologous gene AKAP5, including bovine akap75, human akap79, and rat and mouse AKAP150 [8]. Under normal physiological conditions, akap79/150 can affect cardiac myocytes. The signal transduction and sensitize recycling of adrenaline receptors [9], regulation of the cardiac hypertrophy signal [10], and the coupling of excitation-contraction, relaxation, and intracellular calcium circulation [10–12] in cardiac cells are involved in ensuring the normal function and morphology of the heart. In arrhythmia, AKAP150 acts in two ways: it intensifies arrhythmia caused by calcium channel-related gene mutation [13], and it may have a therapeutic effect on arrhythmia caused by potassium channel-related gene mutation [14, 15].

β1-adrenergic receptor (β-AR) stimulation *in vitro* and *in vivo* increased the expression and activity of matrix metalloproteinases 2 and 9 (MMP-2 and MMP-9) in cardiac myocytes [16]; it also induced cardiomyocyte apoptosis [7, 17, 18]. In addition, β1-AR–mediated increase in cyclic adenosine monophosphate was greater in AKAP5 null myocytes [19]. There are few studies on the role of AKAP5 in cardiac function, especially there are few studies on the role of AKAP5 to regulate myocardial remodeling and fibrosis after myocardial infarction. The focus of this article is on whether β-AR blockers regulate the expression of AKAP5 and the downstream signal protein after myocardial infarction.

However, how or if AKAP5 participates in the regulation of β1-ARs in ischemic cardiac remodeling is minimally studied. Herein, we tested the hypothesis that therapy with selective β1-AR blocker metoprolol can ameliorate ischemic cardiac remodeling by alerting AKAP5 levels.

2. Materials and Methods

2.1. Animals. Adult male Sprague-Dawley (SD) rats (~200 g/animal) were obtained from the Zhejiang Experimental Animal Center of Zhejiang University (Hangzhou, China; License No. [SCXK (Zhen) 20140001]). The animals were raised in the Central Laboratory Animal Room of the Rocky Mountain Hospital of Wannan Medical College (Wuhu, China). All animal experimental protocols used in this study were approved by the Ethics Committee of Yanjishan Hospital of Wannan Medical College and met the guidelines for the use of live animals.

2.2. Reagents and Equipment. Bicinchoninic Acid (BCA) protein quantification kits were from the Bey time Institute of Biotechnology (Nanjing, China). Antibodies to AKAP5, NFATc3, p-NFATc3, and GATA4 were from Santa Cruz Biotechnology (Dallas, Texas, US). Antibody to PP2B was from Cell Signaling Technology (CST; Beverly, Massachusetts, US), and COL1 and COL3 were from Abcam (Cambridge, UK). The chemiluminescence imager was from Tanon Science & Technology Co., Ltd. (Shanghai, China), and the microplate reader was from Bio-Rad Laboratories, Inc. (Hercules, California, US).

2.3. Myocardial Infarction Model. 50 adult male Sprague-Dawley (SD) rats were anesthetized by intraperitoneal injection of 10% chloral hydrate (0.3 mL/100 g) and connected to an RM6240 Multi-path Physio meter (Chengdu Instrument Factory, Chengdu, China). After tracheal intubation, animals were mechanically ventilated (Beijing Zhoushan Electronic Technology Co., Ltd., Beijing, China). Using sterile techniques, the thoracic cavity was opened between the third and fourth ribs on the left margin of the sternum, and a ligature was placed on the root of the left anterior descending coronary artery. Wounds were closed in layers. Sham animals underwent all procedures except coronary ligature. Animals were observed until fully recovered. Finally, five rats survived in each group. Of note, the rats should be housed in a single cage after surgery. Although rats themselves have a relatively strong anti-infection ability, prevention of infection is beneficial to promote postoperative recovery, and good postoperative care can improve the survival rate of animal models. Therefore, all surgical instruments used preoperatively were sterilized by 75% alcohol immersion. After surgery, 800000 U of penicillin was injected intraperitoneally. After the rat is anesthetized and awake, it is associated with sugar water and feeding without fasting. An appropriate amount of energy supplementation is available postoperatively. Winter should pay attention to education.

2.4. Study Design. The study groups with interventions were as follows. Overall, 50 rats were randomly divided into three groups for follow-up experiments, (1) a sham-operated control group (sham group) fed normal rat chow; (2) an injury group that underwent coronary artery ligation; (3) the third group was the metoprolol treatment group. The rats were treated with metoprolol (20 mg/kg/d) for 8 weeks. The sham and model groups were garaged the same amount of saline vehicle for 8 weeks. The rats were given intraperitoneal injections of appropriate amounts of pentobarbital sodium for sedation and analgesia for three consecutive days after the operation. The rats were euthanized by intravenous injection of 100 mg/kg of phenobarbital.

2.5. Western Blot. On study completion, animals were humanely euthanized, and their hearts were excised. Tissue was homogenized in lysis buffer, agitated on wet ice for 30 mins, centrifuged at 12000 rpm, and then the supernatant was reserved. Measurement of total protein concentration was conducted using the BCA method. To detect protein concentration, we performed gel electrophoresis by loading equivalent amounts of protein in each group. After protein transfer, blots were incubated in bovine serum albumin at room temperature for 2 h. Following PBS washing, the corresponding primary antibodies (dilution, 1: 1000; Cell Signaling Technology, Inc., Danvers, MA, USA) were added and kept at 4°C for 14 h. After washing, blots were incubated with the secondary antibody at room temperature for 1 h, washed, and exposed to a chemiluminescence agent. ImageJ software (National Institutes of Health, Bethesda, Maryland, US) was employed to quantitate protein band expression.

2.6. Coimmunoprecipitation. The cardiac lysate was incubated with AKAP5 antibody (dilution, 1: 1000; Cell Signaling Technology, Inc., Danvers, MA, USA) or rabbit antimouse immunoglobulin G (1 : 3,000, Abcam, Cambridge, MA, USA) and incubated at 4°C for 14 h. Protein A/G agarose beads were added to the mixtures and incubated at 4°C for 4 h followed by centrifugation at 3000 rpm for 3 min. The supernatant was discarded, and beads were washed and boiled in water for 5 min. Samples were then subjected to western blot as detailed above.

2.7. Statistical Analysis. SPSS version 18.0 was used for statistical analysis. Statistical differences among groups were assessed using a two-tailed Student's t-test (two experimental groups) or ANOVA (three or more groups). $p < 0.05$ was considered statistically significant. The results have expressed the means ± SD, n ≥ 3.

3. Results

3.1. Characterization of the Ischemic Cardiac Model. Gross observation found that before coronary ligature, hearts appeared bright red in color, and electrocardiogram waveforms were normal, as shown in Figure 1(a). After ligature, blanching of the cardiac wall was observed in the distribution of the left anterior descending coronary. Marked changes were also seen in the ECG. Specifically, the J point of lead II and the ST-T segment were uniformly elevated, as shown in Figure 1(b). These later results are consistent with ischemic myocardial infarction.

3.2. Ischemia-Mediated Increase in Cardiac Weight Is Ameliorated by Metoprolol. The ratios of heart weight to body weight (HW/BW) were determined by weighing heart samples from each group of rats and comparing them with the weight of the rats before sacrifice. Coronary ligation resulted in a significant increase in HW/BW ratio; this was attenuated in animals treated with metoprolol ($P < 0.05$, $n = 5$), as shown in Figure 2.

3.3. Metoprolol Attenuates Matrix Protein Expression in Ischemic Hearts. Protein expression levels of matric genes COL1 and COL3 were greater in ischemia hearts compared to sham hearts. Metoprolol treatment was associated with a decrease in matrix protein expression in ischemic hearts ($P < 0.05$, $n = 5$), as shown in Figure 3.

3.4. Metoprolol Corrects Ischemia-Driven Changes in Cardiac AKAP5, P-NFATc3/NFATc3 and GATA4. Ischemia was associated with a decrease in cardiac AKAP5 compared to sham, which was attenuated by metoprolol attenuated ($P < 0.05$, $n = 5$), as shown in Figure 4(a) and Figure 4(b). In contrast, ischemia was associated with decreased cardiac p-NFATc3/NFATc3 and increased GATA4 compared to sham, and metoprolol suppressed these changes ($P < 0.05$, $n = 5$), as shown in Figure 4(c) to Figure 4(f).

3.5. Cardiac AKAP5 and PP2B Immunoprecipitated in Heart Tissue. Adrenergic receptors control cardiac function and size. In turn, AKAPs, and specifically AKAP5, regulate β-AR activity. PP2B is widely expressed in the heart and elsewhere and is reported to be complex with various AKAPs [20]. Consistent with this, AKAP5 and PP2B were colocalized by immunoprecipitation in cardiac samples, and this relationship appeared to change under ischemia and metoprolol treatment, as shown in Figure 5(a). Western blots of protein levels were found in samples employed in AKAP5, as shown in Figure 5(b).

4. Discussion

In preclinical models, heart injury and subsequent cardiac remodeling are commonly induced models via several techniques such as aortic-arch constriction [21], ischemia [22], toxic agents [23], and hypertension. Ischemic cardiac remodeling is characterized by organ hypertrophy, fibrosis, and functional deterioration [24]. Ischemic cardiac hemodynamic changes can induce heart failure via systolic dysfunction [25]. This process is potentiated by reflex sympathetic-nerve activation and the release of catecholamines such as norepinephrine and epinephrine [26]. While initially supporting ventricular contractility and heart rate to maintain cardiac output [27] long-term sympathetic-nerve activation is detrimental [28, 29]. The pathological mechanisms involved in creating animal models of congestive heart failure include pressure overload, volume overload, and decreased cardiac contractility. Myocardial ischemia causes a reduction in the number of cardiomyocytes and a decrease

(a)   (b)
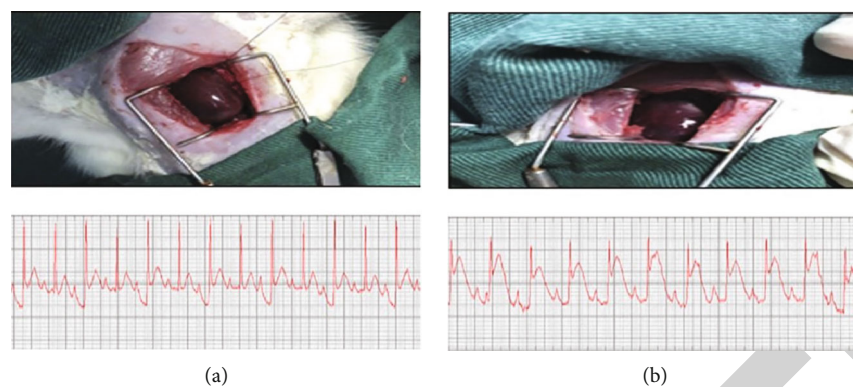
Figure 1: Ligation of the anterior descending coronary induces ischemia. Whole heart images showing heart color and ECG tracings before (a) and after myocardial infarction (b). Representative hearts and tracing are shown from a total of four animals.

(a)   (b)
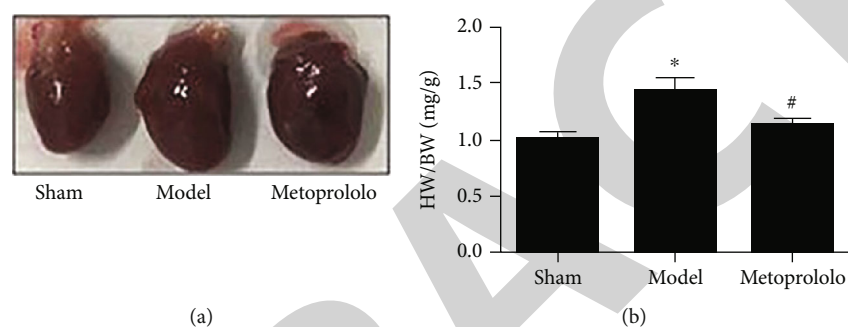
Figure 2: Ischemia-mediated increase in cardiac weight is ameliorated by metoprolol. Rats were subject to ischemia ± metoprolol, and HW/BW ratios were determined. (a) Morphologic appearance of rat hearts in each group. (b) Calculated HW/BW ratios in each group of rats. $^*P < 0.05$ indicates comparison with the sham group; $^#P < 0.05$ indicates comparison with the metoprolol-treated group.

(a)   (b)

(c)   (d)
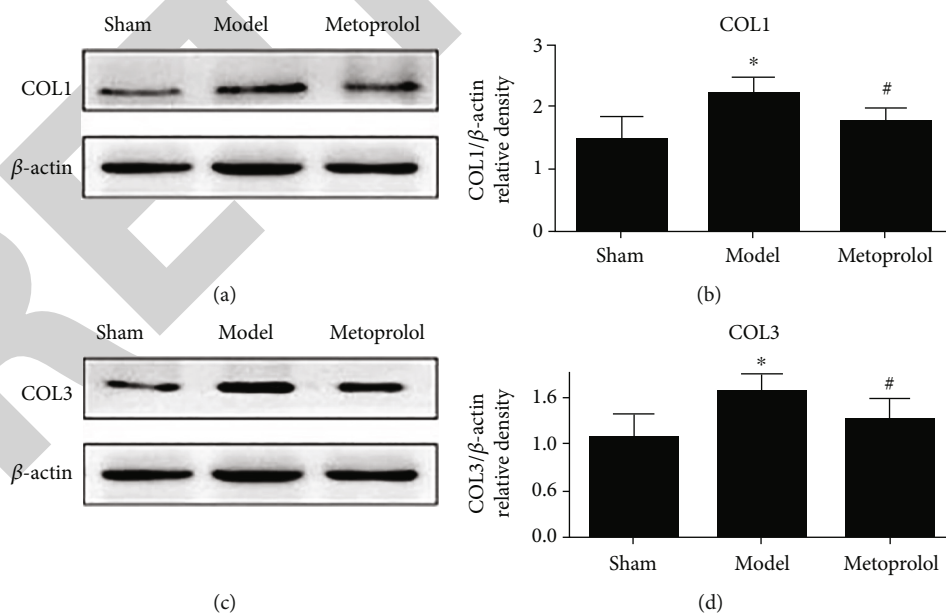
Figure 3: Metoprolol attenuates matrix protein expression in ischemic hearts. Changes in expression levels of COL1 and COL3 proteins. (a and c) Western blot expression of COL1 and COL3 and respective densitometry. (b and d) $^*P < 0.05$ indicates comparison with the sham group; $^#P < 0.05$ indicates comparison with the metoprolol-treated group.
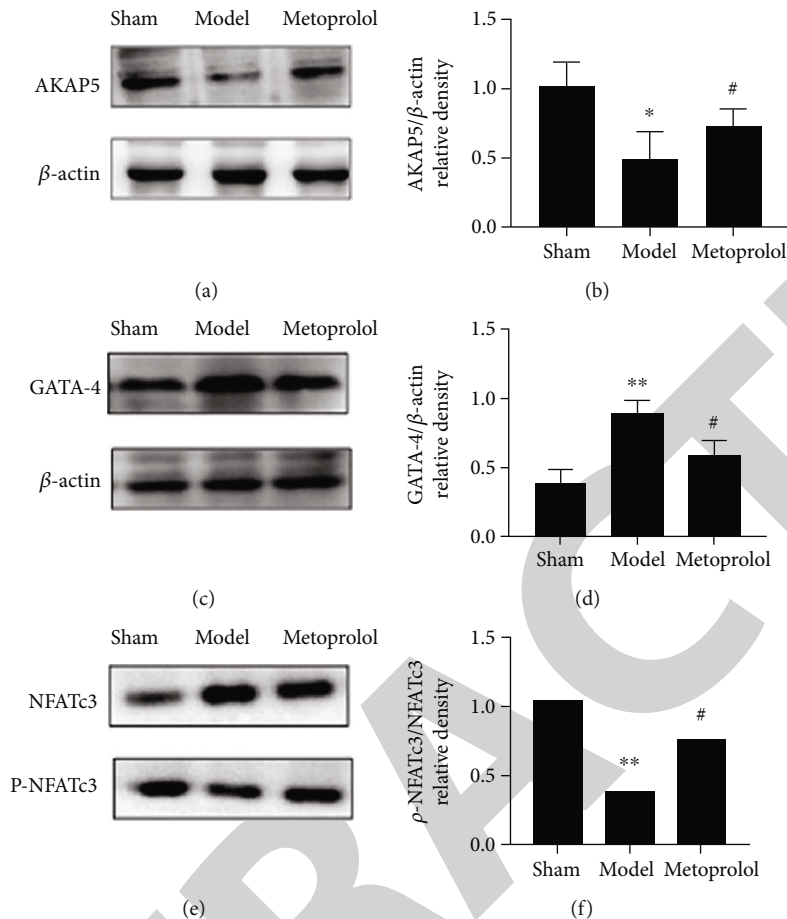
Figure 4: Metoprolol corrects ischemia-driven changes in cardiac AKAP5, NFATc3, and GATA4 changes in AKAP5, NFATc3, and GATA4 expression during myocardial remodeling. (a, c, and e) Protein expression of AKAP5, NFATc3, and GATA4 was detected by western blot. (b, d, and f) Densitometry analysis of respective blots. $^{**}P < 0.01$ indicates comparison with the sham group; $^{#}P < 0.05$ indicates comparison with the metoprolol-treated group.

in cardiac contractility, and animal models are mainly used for experimental studies of pathophysiological changes and novel therapeutic approaches after myocardial ischemia. Many kinds of animals can be used for model making, easy to operate and observe, but they are expensive, so many researchers prefer to choose individual rats which are moderate and relatively inexpensive, and Sprague-Dawley rats and Wistar rats, which are a common choice. Coronary artery ligation and liquid nitrogen freezing of the left ventricle are commonly used methods in animal models of rats, and both can cause ischemia and necrosis of the left ventricular myocardium, and the former is mainly through stenosis or occlusion of the coronary artery to cause myocardial ischemia and infarction, and to cause heart failure by decreasing myocardial contractility; the greatest advantage is clinical relevance, but it is affected by many factors; the area of the infarct area is not easy to control, and the location often changes. The variation between animal models is large, and assays of cardiac function are prone to variability; However, the location of scar tissue caused by infarction in the frostbite model is relatively fixed, and the area size of the scar is also relatively constant, with little animal variation when cardiac function is measured, but with poor clin-

ical relevance. The former was chosen given the advantages and disadvantages of each of the two models, and our experimental study design of stem cell transgenic therapy for CHD focused on maximizing clinical simulation.

Metoprolol belongs to class 2A, that is, partially activated β 1-receptor blockers, which can slow down the rate of atrioventricular conduction, inhibit muscle contraction, and reduce dirty rhythmicity. After taking metoprolol, the drug was evenly dispersed in the gastrointestinal tract, and the drug was released steadily and steadily, which made the drug concentration stable, the peak concentration lower, and reduced the adverse reactions to the drug. And for patients with chronic "insufficiency" combined with muscle infarction, improve the visceral function of patients, reduce the incidence of abnormal incidence, reduce the death of patients, and reduce the pain of patients with chronic "insufficiency" combined with muscle infarction.

Herein, we established a model of acute cardiac ischemia and tested the role of the adrenergic blockade to revert the morphologic and gene-associated changes. The present study demonstrates, for the first time, that metoprolol can restore cardiac expression levels of AKAP5 and suppress the levels of p-NFATc3/NFATc3 and GATA4 and enhance
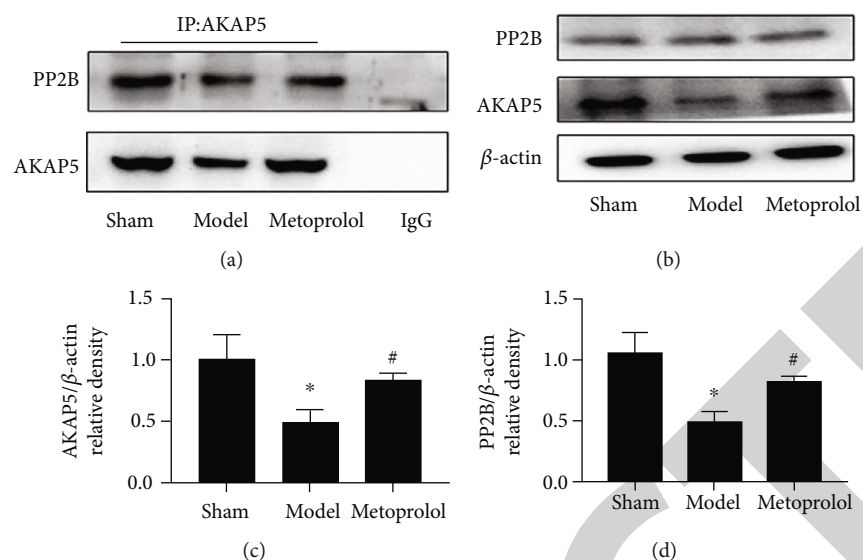
(a)

(b)

(c)

(d)

FIGURE 5: Cardiac AKAP5 and PP2B immunoprecipitated in heart tissue. Immunoprecipitation pulldown displaying association of AKAP5 and PP2B. (a) In the AKAP5 coimmunoprecipitation experiment, the PP2B band was not noted in IgG control incubated samples. (b) Western blot showing the expression of AKAP5 and PP2B in samples employed in the coimmunoprecipitation experiment. AKAP5 was found to bind and regulate PP2B. $*P < 0.05$ indicates comparison to the sham group; $\#P < 0.05$ indicates comparison to the metoprolol-treated group.

cardiac AKAP5 and PP2B protein-protein interaction in rat chronic myocardial infarction model. The results indicate that treatment with metoprolol mitigates ischemic cardiac remodeling and fibrosis, which mechanism of mitigating remodeling likely to improve cardiac AKAP5 expression and AKAP5-PP2B interaction. Metoprolol can be a selectively antagonized β-1-adrenoceptor. Studies have shown that metoprolol can reduce the level of proinflammatory cytokine TNF-α and IL-1 [30, 31]. Similarly, metoprolol has a positive therapeutic effect on MI rats by inhibiting the expression of proto-oncogene protein [32, 33]. That is, β adrenergic blockade was tested against established cardiac changes. While the loss of adrenergic support may alter function to some degree, in this study, we found this treatment reverted or limited adverse cardiac remodeling and fibrosis. At the same time, changes in key genes involved in adrenergic signaling were improved. This included reversion of ischemia-mediated changes in cardiac AKAP5, p-NFATc3, and GATA4. Therefore, β adrenergic blockade may alter the interaction between AKAP5 and the general dephosphorylating enzyme PP2B (calcineurin). PP2B also altered NFAT activity [34] and is implicated in cardiac remodeling. Ventricular remodeling after myocardial infarction mainly includes hypertrophy and fibrosis of myocardial cells. The representative proteins of fibrosis are COL-1 and COL-3. In the experiment, protein expression of COL-1 and COL-3 was detected in the hearts of three groups of mice. COL-1 and COL-3 were significantly higher than in the control, and COL-1 and COL-3 were significantly higher than in the model group, indicating that metoprolol can slow myocardial fibrosis [35–37].

This study has several limitations. First, the characterization of the ischemic model was morphologic and not correlated with functional outcomes. It would be useful to have

also determined systolic and diastolic contractility, chamber volume, and cardiac output. Second, changes in gene protein levels do not equate with protein function. It will be useful to assess if target proteins had altered activity under the conditions of the model. Third, immunoprecipitation, while showing adherence, does not represent true molecular binding. Such interactions are further supported by advanced fluorescent microscopy.

In summary, the present study revealed that adrenergic blockade can resolve established ischemic cardiac remodeling and alter protein levels of key signaling intermediates, which mechanism of mitigating remodeling is likely to improve cardiac AKAP5 expression and AKAP5-PP2B interaction. Further research is needed to determine how and to what extent AKAP5 targets cardiomyocyte remodeling in the context of HF.

Data Availability

The simulation experiment data used to support the findings of this study are available from the corresponding author upon request.

Ethical Approval

All animal experimental protocols used in this study were approved by the Ethics Committee of Yanjishan Hospital of Wannan Medical College and met the guidelines for the use of live animals.

Conflicts of Interest

The authors declare that they have no competing interests.

Authors' Contributions

Acknowledgments

References

[1] M. F. Piepoli, M. Adamo, A. Barison et al., "Preventing heart failure: a position paper of the heart failure association in collaboration with the European Association of Preventive Cardiology," *European Journal of Preventive Cardiology*, vol. 29, no. 1, pp. 275–300, 2022.

[2] G. Savarese and L. H. Lund, "Global public health burden of heart failure," *Cardiac Failure Review*, vol. 3, no. 1, pp. 7–11, 2017.

[3] V. T. Hotta, D. D. C. Rassi, J. L. B. Pena et al., "Critical analysis and limitations of the diagnosis of heart failure with preserved ejection fraction (HFpEF)," *Arquivos Brasileiros de Cardiologia*, vol. 119, no. 3, pp. 470–479, 2022.

[4] S. Gautam, "Post-myocardial Infarction heart failure: a review on management of drug therapies," *Cureus*, vol. 14, article e25745, 2022.

[5] G. Wang, X. Liu, Z. Guo et al., "Effect of entresto on clinical symptoms, ventricular remodeling, rehabilitation, and hospitalization rate in patients with both acute myocardial infarction and acute heart failure," *Evidence-based Complementary and Alternative Medicine*, vol. 2022, Article ID 7650937, 7 pages, 2022.

[6] J. S. Kwon, E. W. Barr, J. K. Chuprun, and W. J. Koch, "In Vivo Stimulation of α- and β-Adrenoceptors in Mice Differentially Alters Small RNA Content of Circulating Extracellular Vesicles," *Cells*, vol. 10, no. 5, 2021.

[7] K. Singh, L. Xiao, A. Remondino, D. B. Sawyer, and W. S. Colucci, "Adrenergic regulation of cardiac myocyte apoptosis," *Journal of Cellular Physiology*, vol. 189, no. 3, pp. 257–265, 2001.

[8] D. Diviani, E. Reggi, M. Arambasic, S. Caso, and D. Maric, "Emerging roles of A-kinase anchoring proteins in cardiovascular pathophysiology," *Biochimica et Biophysica Acta*, vol. 1863, no. 7, pp. 1926–1936, 2016.

[9] M. M. Nooh, S. Mancarella, and S. W. Bahouth, "Novel paradigms governing β_1-Adrenergic receptor trafficking in primary adult rat cardiac myocytes," *Molecular Pharmacology*, vol. 94, no. 2, pp. 862–875, 2018.

[10] X. Li, S. M. Matta, R. D. Sullivan, and S. W. Bahouth, "Carvedilol reverses cardiac insufficiency in AKAP5 knockout mice by normalizing the activities of calcineurin and CaMKII," *Cardiovascular Research*, vol. 104, no. 2, pp. 270–279, 2014.

[11] C. B. Nichols, C. F. Rossow, M. F. Navedo et al., "Sympathetic stimulation of adult cardiomyocytes requires association of AKAP5 with a subpopulation of L-type calcium channels," *Circulation Research*, vol. 107, no. 6, pp. 747–756, 2010.

[12] L. Li, J. Li, B. M. Drum et al., "Loss of AKAP150 promotes pathological remodelling and heart failure propensity by disrupting calcium cycling and contractile reserve," *Cardiovascular Research*, vol. 113, no. 2, pp. 147–159, 2017.

[13] E. P. Cheng, C. Yuan, M. F. Navedo et al., "Restoration of normal L-type Ca2+ channel function during Timothy syndrome by ablation of an anchoring protein," *Circulation Research*, vol. 109, no. 3, pp. 255–261, 2011.

[14] D. P. Byrne, M. H. Omar, E. J. Kennedy, P. A. Eyers, and J. D. Scott, "Biochemical analysis of AKAP-anchored PKA signaling complexes," *Methods in Molecular Biology*, vol. 2483, pp. 297–317, 2022.

[15] T. Huang, B. Zhang, Z. Wang, Y. Wang, W. Li, and H. Wang, "AKAP5 anchors PKA to enhance regulation of the HERG channel," *The International Journal of Biochemistry & Cell Biology*, vol. 122, article 105741, 2020.

[16] P. Krishnamurthy, V. Subramanian, M. Singh, and K. Singh, "$\beta1$ integrins modulate beta-adrenergic receptor-stimulated cardiac myocyte apoptosis and myocardial remodeling," *Hypertension*, vol. 49, no. 4, pp. 865–872, 2007.

[17] R. Kumari, A. G. Ray, D. Mukherjee, D. Kar, A. Konar, and A. Bandyopadhyay, "Downregulation of PTEN Promotes autophagy via concurrent reduction in apoptosis in cardiac hypertrophy in PPAR α–/– mice," *Frontiers in Cardiovascular Medicine*, vol. 9, article 798639, 2022.

[18] Y. Shizukuda, P. M. Buttrick, D. L. Geenen, A. C. Borczuk, R. N. Kitsis, and E. H. Sonnenblick, "Beta-adrenergic stimulation causes cardiocyte apoptosis: influence of tachycardia and hypertrophy," *The American Journal of Physiology*, vol. 275, no. 3, pp. H961–H968, 1998.

[19] X. Li, M. M. Nooh, and S. W. Bahouth, "Role of AKAP79/150 protein in β_1-adrenergic receptor trafficking and signaling in mammalian cells," *The Journal of Biological Chemistry*, vol. 288, no. 47, pp. 33797–33812, 2013.

[20] J. Li, S. Aponte Paris, H. Thakur, M. S. Kapiloff, and K. L. Dodge-Kafka, "Muscle A-kinase-anchoring protein-β-bound calcineurin toggles active and repressive transcriptional complexes of myocyte enhancer factor 2D," *The Journal of Biological Chemistry*, vol. 294, no. 7, pp. 2543–2554, 2019.

[21] T. Thum, C. Gross, J. Fiedler et al., "MicroRNA-21 contributes to myocardial disease by stimulating MAP kinase signalling in fibroblasts," *Nature*, vol. 456, no. 7224, pp. 980–984, 2008.

[22] Y. Zhang, K. Köhler, J. Xu et al., "Inhibition of p53 after acute myocardial infarction: reduction of apoptosis is counteracted by disturbed scar formation and cardiac rupture," *Journal of Molecular and Cellular Cardiology*, vol. 50, no. 3, pp. 471–478, 2011.

[23] N. Potočnik, M. Perše, A. Cerar, R. Injac, and Ž. Finderle, "Cardiac autonomic modulation induced by doxorubicin in a rodent model of colorectal cancer and the influence of fullerenol pretreatment," *PLoS One*, vol. 12, no. 7, article e0181632, 2017.

[24] G. Heusch, P. Libby, B. Gersh et al., "Cardiovascular remodelling in coronary artery disease and heart failure," *The Lancet*, vol. 383, no. 9932, pp. 1933–1943, 2014.

[25] R. G. McKay, M. A. Pfeffer, R. C. Pasternak et al., "Left ventricular remodeling after myocardial infarction: a corollary to infarct expansion," *Circulation*, vol. 74, no. 4, pp. 693–702, 1986.

[26] H. S. Mueller and S. M. Ayres, "Propranolol decreases sympathetic nervous activity reflected by plasma catecholamines

Retraction

Retracted: Antioxidant Indexes and Immune Function of the Intestinal Flora of Compound Microecological Preparations

Oxidative Medicine and Cellular Longevity

This article has been retracted by Hindawi following an investigation undertaken by the publisher [1]. This investigation has uncovered evidence of one or more of the following indicators of systematic manipulation of the publication process:

(1) Discrepancies in scope

(2) Discrepancies in the description of the research reported

(3) Discrepancies between the availability of data and the research described

(4) Inappropriate citations

(5) Incoherent, meaningless and/or irrelevant content included in the article

(6) Manipulated or compromised peer review

The presence of these indicators undermines our confidence in the integrity of the article's content and we cannot, therefore, vouch for its reliability. Please note that this notice is intended solely to alert readers that the content of this article is unreliable. We have not investigated whether authors were aware of or involved in the systematic manipulation of the publication process.

Wiley and Hindawi regrets that the usual quality checks did not identify these issues before publication and have since put additional measures in place to safeguard research integrity.

We wish to credit our own Research Integrity and Research Publishing teams and anonymous and named external researchers and research integrity experts for contributing to this investigation.

The corresponding author, as the representative of all authors, has been given the opportunity to register their agreement or disagreement to this retraction. We have kept a record of any response received.

References

[1] W. Sun and L. Zhang, "Antioxidant Indexes and Immune Function of the Intestinal Flora of Compound Microecological Preparations," *Oxidative Medicine and Cellular Longevity*, vol. 2022, Article ID 5498514, 13 pages, 2022.

Research Article

Antioxidant Indexes and Immune Function of the Intestinal Flora of Compound Microecological Preparations

Wanzhen Sun[1] and Li Zhang [2]

[1]*Clinical Laboratory, Wuhan Mental Health Center, Wuhan, 430012 Hubei Province, China*
[2]*Clinical Laboratory, The Second Staff Hospital of Wuhan Iron and Steel (Group) Company, Wuhan, 430085 Hubei, China*

Correspondence should be addressed to Li Zhang; 3180100193@caa.edu.cn

Compound probiotics are biological products made by mixing and cultivating various probiotics according to appropriate composition and ratio. It can not only play the role of a variety of probiotics in composition but also the effect of the ratio is often greater than the effect of the single strain alone. These probiotics are good for the body's immune system in living organisms. They act as immune boosters in living organisms. They are considered the safest form of treatment. In this review, the effects of microecological agents on antioxidant indices and immune function of chicks were studied, and radial basis neural network (RBFNN) was described. Aiming at the deficiency of traditional RBFNN learning strategy, a three-layer RBFNN method based on immune mechanism was proposed. In this paper, the microecological evaluation preparation was added into chicken feed. The study showed that chickens fed with probiotics gained significant body weight at 6 weeks of age. Compared with the control group, the experimental group increased by 15.70%. In each feed/gain ratio, the feed/gain ratio of the experimental group was significantly decreased at 6 weeks of age, which was 30.37% lower than that of the control group. Compared with the control group, the spleen, bursa of Fabricius, and thymus of the experimental group were increased by 63.02%, 38.77%, and 26.82%, respectively, indicating that the compound probiotics could improve the immunity of chickens.

1. Introduction

Compound microecological preparations can help the body return to normal nutrition, growth, and health, and it is one of the more popular new feed additives in current research. Adding it to animal diets can achieve an effect similar to antibiotics to a certain extent. Because of its green, nontoxic, nondrug-resistant, safe, and efficient characteristics, it has been gradually used in the livestock breeding industry. For example, poultry farming plays an important role in developing China's animal husbandry and is the world's second-largest poultry producer and consumer. On the other hand, most microecological products currently on the market are composed of one or more lactic acid bacteria, bacilli, and yeasts of the same genus. While the microecological preparations composed of different genus microorganisms can play their respective advantages, they can also compensate for the insufficiency

of a single strain. Therefore, it has gradually become the trend of research and development of compound microecological preparations and has achieved good use effects and considerable economic benefits. Among living things, these probiotics are excellent for the immune system of the body. They strengthen the immune systems of living things. Therefore, they are regarded as the most secure form of therapy.

The growing number of studies investigating the use of review probiotics to improve patient health outcomes has prompted the need for a systematic review and summary of the relevant literature. Wang et al. summarized the origin and characteristics of Chinese medicine-probiotic mixed livestock and poultry microecological preparations (CPCMP) strain based on reviewing the literature on probiotics and traditional Chinese medicine microecological preparations in recent years [1]. Given the complex composition of traditional Chinese medicine compound preparations and the unclear

mechanism of action which restricts the development of traditional Chinese medicine, Jie et al. has achieved extensive and remarkable results [2]. Naito et al. used compound-specific stable isotope analysis of amino acids (CSIA) to study terrestrial mammals in a controlled feeding experiment of captive Asian black bears [3]. Guo et al. studied the etiology, characteristics, and relatively effective treatment methods of three common gastrointestinal diseases, including diarrhea, constipation, and irritable bowel syndrome, based on gut microbes. Taking diarrhea, constipation, and irritable bowel syndrome as examples, the role and mechanism of traditional Chinese medicine and microecological substances in gastrointestinal diseases were discussed to provide a reference for more reasonable and effective treatment of gastrointestinal diseases [4]. The Kokaeva et al. study aimed at developing a method to improve the ecological and consumption characteristics of dairy cows and their derived milk by rationally using antioxidant toxins and mold Zap in diets containing subtoxic doses of nitrate and aflatoxin B1 [5]. However, the impact of reviewing microecological preparations needs to be examined from multiple perspectives to be more comprehensive.

Artificial intelligence is an important technical tool to support the development of information fusion, among which RBFNN is another hot spot of intelligence research. For problems involving function approximation, radial basis function (RBF) networks are a popular variety of artificial neural networks. The universal approximation and quicker learning speed of radial basis function networks set them apart from other neural networks. Moreira et al. proposed the modeling, performance evaluation, and comparative analysis of an artificial neural network technique called Radial Basis Function Network (RBFNN network) to identify gestational diabetes cases that may lead to multiple risks to the mother and fetus [6]. Leema et al. discussed a classification framework for diagnosing diseases using a Quantum Behavioral Particle Swarm Optimization Neural Network (QPSONN) classifier, and the neural network used for classification is RBFNN [7]. Amin et al. proposed an ENRBFN that approximates the unmodeled dynamics of a hovering vehicle based on an adaptive trajectory tracking controller based on the Extended Normalized Radial Basis Function (ENRBF) [8]. Mohapatra and Mohanty described how the demand for hospital services is increasing daily, and intelligent services for patients are critical to calculating mortality rates. A method for detecting arrhythmias using wavelet transform and data mining techniques was adopted [9]. Pomprapa et al. proposed the application of backstepping control in the oxygenation of the cardiopulmonary system. Without prior knowledge of the underlying system dynamics, an RBF network was integrated into a closed-loop subsystem and trained to recognize unknown nonlinear functions [10]. These algorithms achieve the research goals to a certain extent, but the rationality of the calculation process can be further improved. The compound probiotic microecological preparation was applied to the chicks. By measuring the weight gain, feed-to-weight ratio and immune organs, and other indices of the chickens, it was found that the compound probiotic microecological preparation promoted growth and had a positive effect on the immune function of chickens. The

innovation of this paper is that through the experimental study of chicken activity, compound probiotics are added to chicken feed to improve chicken growth performance, feed utilization rate, and immunity. In every capsule of the probiotic complex, there are 6 billion friendly bacteria. These bacteria include Lactobacillus acidophilus, which typically colonizes the upper intestine, and Bifidobacterium bifidum, which typically colonizes the lower intestine. The ability of these bacteria to produce lactic acid as a byproduct of glucose metabolism distinguishes them from other bacteria. Gram-positive bacteria, such as Lactobacillus, are defined as having a thick peptidoglycan cell wall.

The rest of the paper is organized as section 2 gives RBFNN method based on the immune system, section 3 gives an experiment on the effect of compound microecological preparation on chicks, section 4 gives us results, and the conclusion is given in section 5.

2. RBFNN Method Based on Immune System

In this section, we will discuss the biological immune system, RBF network learning strategy, and design of RBF NN based on the immune system in detail.

2.1. Biological Immune System. The immune system protects the body from pathogens through a multilayered defense structure, and as the defense layer increases, its specificity for pathogens increases layer by layer. An organism that infects its host with the disease is referred to as a pathogen, and the severity of the disease symptoms is referred to as virulence. Pathogens include viruses, bacteria, unicellular, and multicellular eukaryotes, as well as other taxonomically diverse organisms. Briefly, this hierarchical structure is divided into three lines of defense, which can be classified into two categories: innate immunity and specific immunity [11, 12], as shown in Figure 1.

This part mainly introduces the biological immune system mechanism related to the proposed algorithm, and readers can refer to other aspects of the mechanism. The biological immune system is composed of many complex cells, molecules, and organs. These tissues can cope with foreign virus infection to achieve the function of protecting the health and stability of the body. The biological immune system includes two related subsystems, innate immunity, and adaptive immunity. The organic combination of these two subsystems can recognize and eliminate foreign viruses, bacteria, etc., to achieve the function of defense [13]. These infectious agents are hereinafter collectively referred to as antigens.

Figure 2 is a schematic diagram of the mechanism of interaction between innate and adaptive immunity. When Ag invades the body, a specific antigen-presenting cell in the innate immune system can quickly recognize the invading Ag and absorb and decompose it into many gene segments. These decomposed gene segments are adsorbed to the cell's major histocompatibility complex (MHC) to form MHC protein receptors. The MHC is a collection of genes that produce proteins found on the cell surfaces and aid the immune system in recognizing.
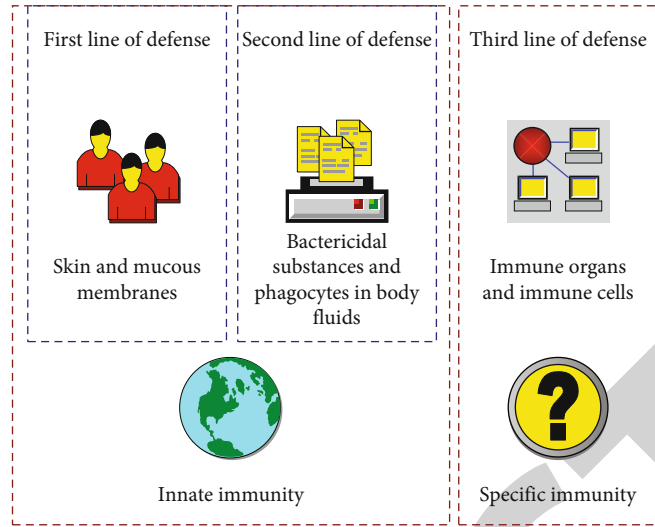
FIGURE 1: Immune hierarchy diagram.
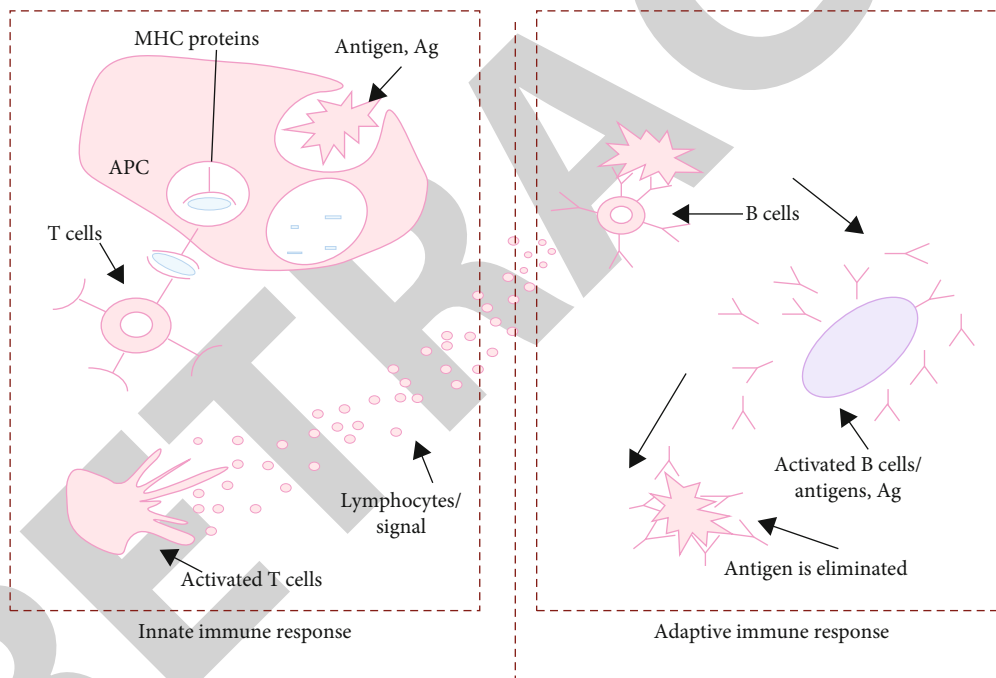
FIGURE 2: Mechanisms of innate and adaptive immune interactions.

Major Histocompatibility Complex (MHC) is a collection of genes that produce proteins found on the cell surfaces and aid in the immune system's ability to identify foreign objects. The higher vertebrates contain MHC proteins. The complex is also known as the human leukocyte antigen (HLA) system in humans. These receptors are presented on the surface of the MHC, and T cells in the immune system also have a receptor molecule on the surface that recognizes different MIHC complexes. Once T cells recognize the MHC complex, they are activated to secrete or differentiate into lymphocytes or other chemical signals. These cellular or chemical signals stimulate other elements of the immune system to facilitate the development of an adaptive immune response [14, 15].

Immune response, immune tolerance, and immune feedback are the three stages of the immune mechanism. After the antigen enters the body, the immune cells recognize the antigen molecule and undergo the corresponding process of cell activation, cell differentiation, and immune function, that is, an immune response. In the process of an immune response, several steps are included, such as specific recognition, antigen presentation, lymphocyte activation, antibody generation, an immune reaction between antibody and antigen, and the formation of immune memory [16]. One of the key features of the immune system is its capacity for learning and memory, which is demonstrated by the immune system's capacity to remember the antigenic structure it encounters for

the first time. Antigen specificity and long-lasting effects are features of immune memory. The primary distinction between humoral and cell-mediated immunity is the production of antigen-specific antibodies by humoral immunity as opposed to cell-mediated immunity. T lymphocytes, however, obliterate infected cells. Immune feedback has two corresponding feedback mechanisms for humoral immunity and cellular immunity, and the principle is shown in Figure 3.

In Layman's terms, immunity is a physiological reflection that aims at identifying self and nonself and, at the same time, remove nonself to ensure the integrity of the body. After a fight with a pathogen (antibody), the body would retain the ability to fight against the pathogen so that when the body encounters the same pathogen again, it can quickly and effectively make defenses to protect the body from damage. Compared with the specific immune system, the innate immune system is universal and memoryless, while the latter is specificity and memory [17, 18].

The ability to learn and remember is one of the main characteristics of the immune system, which is manifested in the ability of the immune system to learn and remember the antigenic structure it encounters for the first time. Immune memory is characterized by antigen specificity and durable effects [19]. Both T cells and B cells are involved in immune memory; that is, during the immune response, both memory B cells and memory T cells are present. The formation process of immune memory cells is shown in Figure 4.

2.2. RBF Network Learning Strategy. RBFNN is a typical local approximation network model [20]. Given the training samples, then, the learning strategy of RBFNN should solve the following problems: first, determining the structure of the network, that is, determining the number of hidden layer nodes h of the network; secondly, determining the data center v_o and width δ_o of each radial basis function; finally, determining the output of the network modifies the weights e_o and the bias q.

In RBFNN, the nonlinear activation function of the hidden layer and the linear parameters of the output layer are updated on different "time scales". Different layers play different roles, so different update strategies can be used. There are four commonly used learning methods for RBFNN, as shown in Figure 5.

In the fourth strategy, except that the number of network nodes j needs to be predetermined, the other free parameters of RBFNN are trained by performing a supervised learning process, so this learning strategy identifies the generalized form of RBFNN. This strategy is mostly implemented by the error-corrected gradient descent method (An optimization algorithm called gradient descent is frequently used to train neural networks and machine learning models. These models are trained using training data, and the cost function within gradient descent specifically serves as a barometer, gauging its accuracy with each new training set), whose form is similar to the back-propagation algorithm (BP algorithm) [21].

Let (c_m, a_m) represent the input data, and its corresponding expected output, and u_m represent the actual output of
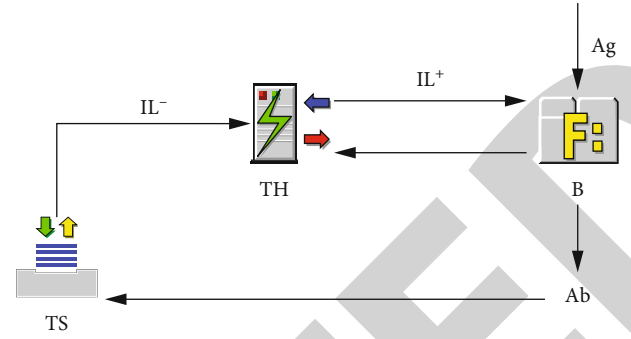

Figure 3: Principle of immune feedback.

the network, then the error r_m of the network at time m is

$$r_m = a_m - u_m. \tag{1}$$

For a parameter μ in a network, it is adjusted by the gradient training algorithm by

$$\mu_{m+1} = \mu_m - \lambda_\mu \frac{\partial r_m^2}{\partial \mu_m}. \tag{2}$$

In Formula (2), λ_μ is an adaptive coefficient. Specifically, in the RBF network, the gradient training algorithm obtains various network parameters according to

$$
\begin{aligned}
\Delta v_{o,m} &= v_{o,m+1} - v_{o,m} = \lambda_v r_m e_{o,m} \exp\left(-\frac{\|c_m - v_{o,m}\|^2}{2\delta_{o,m}^2}\right) \frac{\|c_m - v_{o,m}\|}{\delta_{o,m}^2}, \\
\Delta \delta_{o,m} &= \delta_{o,m+1} - \delta_{o,m} = \lambda_\delta r_m e_{o,m} \exp\left(-\frac{\|c_m - v_{o,m}\|^2}{2\delta_{o,m}^2}\right) \frac{\|c_m - v_{o,m}\|}{\delta_{o,m}^3}, \\
\Delta e_{o,m} &= e_{o,m+1} - e_{o,m} = \lambda_e r_m \exp\left(-\frac{\|c_m - v_{o,m}\|^2}{2\delta_{o,m}^2}\right), \\
\Delta q_m &= q_{m+1} - q_m = \lambda_q r_m.
\end{aligned}
\tag{3}
$$

The initial search of gradient training algorithms is usually performed from the parameter space, limiting the search region of the parameter space to a known useful region. In most cases, the gradient training method provides a convenient and feasible RBF network learning strategy.

The common disadvantage of the above methods is that the global RBF network parameters cannot be obtained by learning, and most of them need to predetermine the number h of network center points. In addition, except for the supervised center selection method, which obtains the remaining network parameters through the supervised learning process, the other methods focus on the training of the network center v_o. The network expansion constant δ_o is predesigned or determined by the distance between the data centers, and the global optimal value cannot be guaranteed. The expansion constant has an important impact on the performance of the RBF network: if its value is too large, it means that a large number of hidden nodes are needed to fit the function
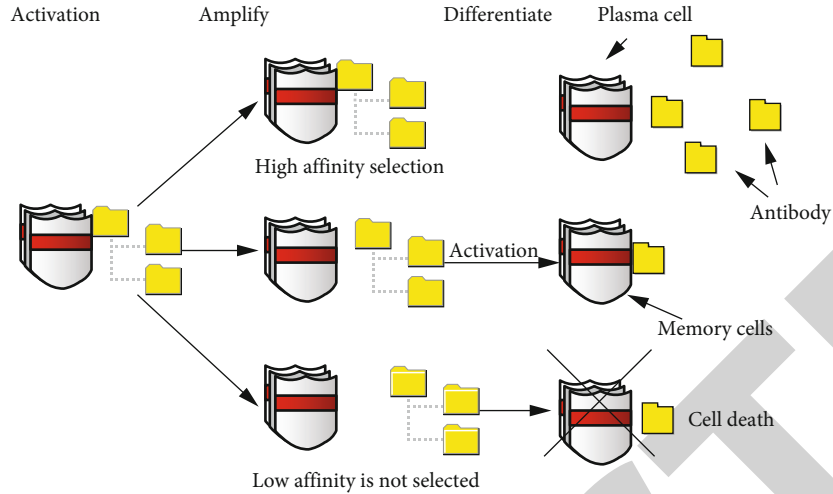
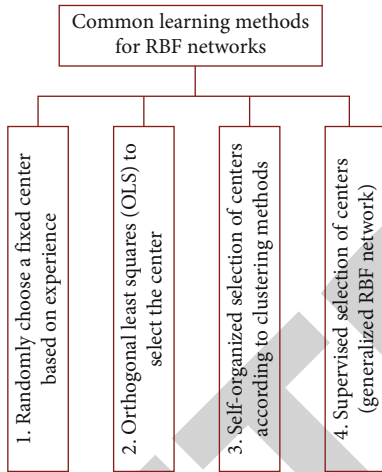Figure 4: The Process of immune memory cell formation.

Figure 5: Common learning methods for RBFNN.

with a fast-changing speed, and the basis function curve overlaps the response area more; and if its value is too small, a large number of hidden nodes are needed to fit the smoother function, which would lead to the degradation of the performance of the RBF network. Of course, there are also some learning strategies based on evolutionary methods to dynamically adjust the RBF network center, but most of them have problems like the above-mentioned problem that the optimal training value of the global network parameters cannot be obtained, which may lead to problems such as excessive algorithm complexity, long training time, and easy to fall into local minima [22, 23].

2.3. Design of RBFNN Based on Immune System. Because of the shortcomings and problems of the above existing RBFNN learning strategies, this paper proposes an immune system-based RBFNN design and training strategy, which introduces a unique immune system-specific vaccine extraction and inoculation mechanism, thereby simplifying the network training process and optimizing its performance.

The design goal of the RBFNN learning strategy is to determine the globally optimized RBF network parameters: $\omega = \{j, v_o, \delta_o, e_o, q\}$. The design parameter of the nonlinear neuron in the hidden layer of the network is $\{j, v_o, \delta_o\}$, and $\{e_o, q\}$ is the design parameter of the linear neuron in the output layer of the network ($o = 1, \cdots, j$).

When designing a learning strategy, it is unnecessary and highly efficient to design the global parameters ω in the same optimization space. The parameter is the key to the design of the hidden layer structure and even the entire RBF network topology. Determining this parameter first can greatly simplify the network training process. Since the network output layer is a linear neuron, therefore, as long as a reasonable hidden layer of the network is constructed and the parameter $\{v_o, \delta_o\}$ is determined, the output layer parameter $\{e_o, q\}$ can be determined by an efficient linear optimization method.

Because of the above two points, this paper proposes a three-level learning structure strategy of RBFNN based on the immune mechanism: dividing the global RBFNN parameter space ω into three subspaces. That is, design optimization is carried out for $\omega_1 = \{j\}$, $\omega_2 = \{v_o, \delta_o\}$, and $\omega_3 = \{e_o, q\}$, respectively. Figure 6 shows the three-level learning structure framework of the RBFNN: the first level calculates ω_1 to determine the topology of the entire RBF network, and this level is a process of extracting vaccines according to the problem to be solved; the second stage is postvaccination to determine ω_2 to identify neurons in the hidden layers of the network, and this stage is designed using an immune algorithm. The third stage uses the least squares estimation ω_3 to determine the output layer neurons of the network. After the three-level learning, the global RBF network parameter $\omega = \{\omega_1, \omega_2, \omega_3\}$ is determined, that is, a complete RBF network is constructed.

The first level: extracting the vaccine and determining the network structure.

The first level mainly calculates the number of neurons in the hidden layer of the network; that is, it calculates
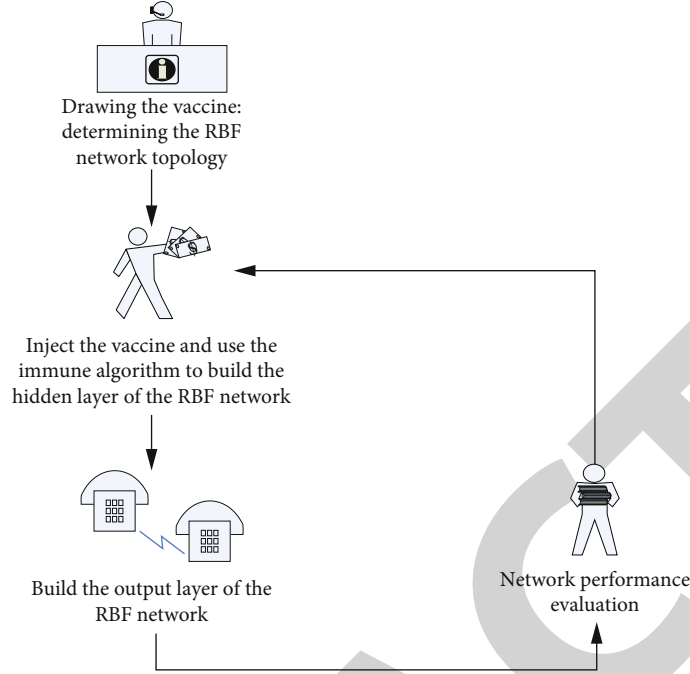
FIGURE 6: Three-level learning structure of RBFNN.

$\varpi_1 = \{j\}$. Let the maximum number of hidden layer nodes Maxh allowed by the currently constructed RBF network be the number of input training samples M. The minimum number of nodes is set to 1. Let $L = 1 : 1 :$ Maxh, that is, to search within the allowable range of the number of nodes with a step size of 1. When searching, one data is randomly selected in the input sample $c \in T^{m \times M}$ as the data center $\{v_1, v_2, v_3\}$, which satisfies the

$$v_o = c_{\text{Round}(1+\text{rand}*(M-1))}$$
$$\cdot \left(o = 1, 2, \cdots, l, c = [c_1, c_2, \cdots, c_m]^Y \in T^{m \times M}, l = 1 : \text{Maxh} \right) \tag{4}$$

In Formula (4), Round$(\cdot)$ is the rounding function, rand is a uniform random number in the interval $[0, 1]$, and m is the dimension of the input data. After determining the data center, the width of all hidden layer basis functions is set to be fixed, and the basis function expansion constant δ is selected according to Formula (5) to ensure that the basis functions are neither too sharp nor too smooth.

$$\delta = \frac{\max \left(\|v_o - v_k\| \right)}{\sqrt{2l}} \left(o, k = 1, 2, \cdots, l, l = 1 : \text{Maxh} \right). \tag{5}$$

After determining the center and expansion constant, the pseudo-inverse matrix method (The concept of the inverse of a square, the invertible matrix is generalized to arbitrary matrices by the pseudo-inverse of an m by n matrix A. Concerning A, the singular value decomposition (SVD) can be used to express the pseudo-inverse) is used to determine the

linear parameters of the output layer of the network as follows:

$$He + q = a \Rightarrow [e, q] = \left[H, O'_M \right]^+$$
$$\times q \left(e \in T^{l \times n}, q \in T^n \Rightarrow [e, q] \in T^{(l+1) \times n} \right), \tag{6}$$

$$H \in T^{M \times l}, O'_M \in T^{M \times 1} \Rightarrow \left[H, O'_M \right] \in T^{(l+1) \times n}, a \in T^{M \times n} \right). \tag{7}$$

In Formula (6), $a \in T^{M \times n}$ is the n-dimensional expected response vector of M training data sets; $\left[H, O'_M \right]^+$ is the pseudo-inverse matrix of matrix $[H, O'_M]$, of which $O'_M \in T^{M \times 1}$ is an M-dimensional column vector whose element is 1, and $H \in T^{M \times l}$ is defined.

After determining the center and expansion constant, the pseudo-inverse matrix method is used to determine the linear parameters of the output layer of the network as follows:

$$H = \left\{ h_{ok} = \exp \frac{\|c_k - v_o\|^2}{2\varsigma^2}, k = 1, 2, \cdots, M, o = 1, 2, \cdots, l \right\}. \tag{8}$$

In Formula (8), c_k is the k-th input vector of the input training data set, and M is the number of training samples. According to Formula (4) and Formula (8), the RBF network of this stage is constructed. Observing the output error ϑ of the network when l takes different values in the search space of $k = 1 :$ Maxh. The value of l when $\vartheta \leq \lambda\vartheta$ is the number k of hidden layer nodes of the network RBF determined at this stage, where $\lambda\vartheta$ is the specified upper limit of error.

The first stage is the process of extracting vaccines, and the output vaccine is the number of nodes $j = l$ in the hidden layer of the network.

Level 2: vaccination and using an immune algorithm to construct RBFNN hidden layers. An RBF network's hidden layer is nonlinear, while its output layer is linear. The Euclidean norm (distance) between the input vector and the center of the unit is computed by the argument of the activation function of each hidden unit in the RBF network.

The vaccine injected in the second stage is the vaccine h extracted in the first stage; that is, based on determining the network structure, the parameter $\varpi_2 = \{v_o, \delta_o\}$ of the nonlinear neuron in the hidden layer is determined by learning. The details are as follows:

Antigen: the objective function to be solved by the RBFNN.

Antibody: antibody population is $S = \{s_1, s_2, \cdots, s_N\}$, and N is the size of the antibody population. Any one of the antibodies is designed in the form of $s_o = [v, \delta]$, which corresponds to the hidden layer parameters of the RBF network. Among them, $v = \{v_1, v_2, \cdots, v_j\}$ corresponds to the data center of the hidden layer, and $\delta = \{\delta_1, \delta_2, \cdots, \delta_j\}$ corresponds to the hidden layer expansion constant. Antibodies are encoded in real numbers.

When initializing the antibody group, the vector v is generated by randomly selecting j data in the input sample $c \in T^{m \times M}$, and the vector δ is randomly generated within its value range $[f, i]$, as shown in

$$v_{1 \sim k} = c_{Round(1 + \text{rand} * (M-1))} \left(c = [c_1, c_2, \cdots, c_m]^Y \in T^{m \times M}, \quad (9) \right.$$

$$\delta_{1 \sim k} = f + \text{rand} * (i - f). \tag{10}$$

In Formula (9) and Formula (10), $\text{Round}(\cdot)$ and rand have the same meanings as Formula (4).

Antibody-antigen affinity: using the output error function of the constructed RBF network to evaluate the antibody-antigen affinity.

$$g = \sum_{y=1}^{M} \sum_{o=1}^{j} (U_o(y) - A_o(y))^2. \tag{11}$$

In Formula (11), $U_o(y)$ and $A_o(y)$ are the actual output and expected output of the o-th node in the y-th input pattern, respectively. M and j are the number of input samples and the number of hidden layer nodes, respectively.

Clonal selection: by using the clonal selection operator to generate a new generation of antibody populations, mainly including antibody cloning, mutation, and clonal selection process. When an antigen comes into contact with the immune system, its epitopes eventually only react with B-lymphocytes that have more-or-less compatible B-cell receptors on their surface, activating those B-lymphocytes. Clonal selection is the name given to this process. A single antibody is expanded into a subantibody population after cloning. The cloned subantibody group is subjected to mutation operation according to the mutation probability a_n. The vector v representing the center and the vector δ representing

the expansion constant in the antibody are mutated according to Formula (12), and Formula (14), respectively, wherein the same parameters have the same meaning as above. Clonal selection is based on affinity selection in the subantibody population after clonal mutation to retain the optimal antibody with the smallest affinity (i.e., the smallest error in the output of the hidden layer of the network).

$$v \longrightarrow v : v_o = \varepsilon_1 v_o + \varepsilon_2 c_{t1} + \varepsilon_3 c_{t2} a \le a_n, \tag{12}$$

$$o = Round(1 + \text{rand} * (j - 1)), t1, t2$$
$$= (1 + \text{rand} * (M - 1)), \varepsilon_{1 \sim 3} \in [0, 1], \tag{13}$$

$$\delta \longrightarrow \delta : \delta_{(Round(1+\text{rand}*(j-1)))} = f + \text{rand} * (i - f) a \le a_n \tag{14}$$

The output of the second stage is the optimal antibody in the previous generation ICSA antibody population, which is the learning process of the artificial immune algorithm after vaccination. The output is the center v_o and expansion constant δ_o of the hidden layer neurons of the RBFNN.

The third stage: the output layer of the RBFNN is constructed based on the ϖ_2 calculated by the first stage and the second stage, that is, based on the matrix equation

$$Fe + q = a \tag{15}$$

The network output parameters $\varpi_3 = \{e_o, q\}$ is estimated by using the least squares method. In Formula (15), the definition of $H \in T^{M \times j}$ is the same as that of Formula (8), and the meaning of $a \in T^{M \times n}$ is the same as that of Formula (8).

The basic flow of this three-stage learning algorithm for RBFNN is shown in Figure 7, where the stopping condition is set to evolve to the maximum algebra or satisfy the desired error criterion.

3. Experiment on the Effect of Compound Microecological Preparation on Chicks

In this section, we discuss the experimental setup in detail.

3.1. Experimental Design. Numerous studies have shown the emergence of antibiotic resistance and immunosuppression in farm animals and poultry. Reduced immunity is a condition known as immunosuppression. Cell immunity and/or humoral (antibodies) immunity may be compromised. Immunosuppression can be brought on by pathogens, an unbalanced diet (deficiencies), a lack of biosecurity, poor management (stress), or a combination of these factors. It can be seen that the use of compound microecological preparations instead of antibiotics, on the one hand, improves the economic benefits of animal husbandry. On the other hand, it prevents the toxic side effects caused by drugs and has unique social and economic benefits. Studies have shown that this preparation can increase the number of T cells in the immune organs of chicks and can improve daily weight gain and meat-to-feed ratio. The identification of foreign substances by various types of immunocompetent cells is the most complex aspect of the immune system seen in
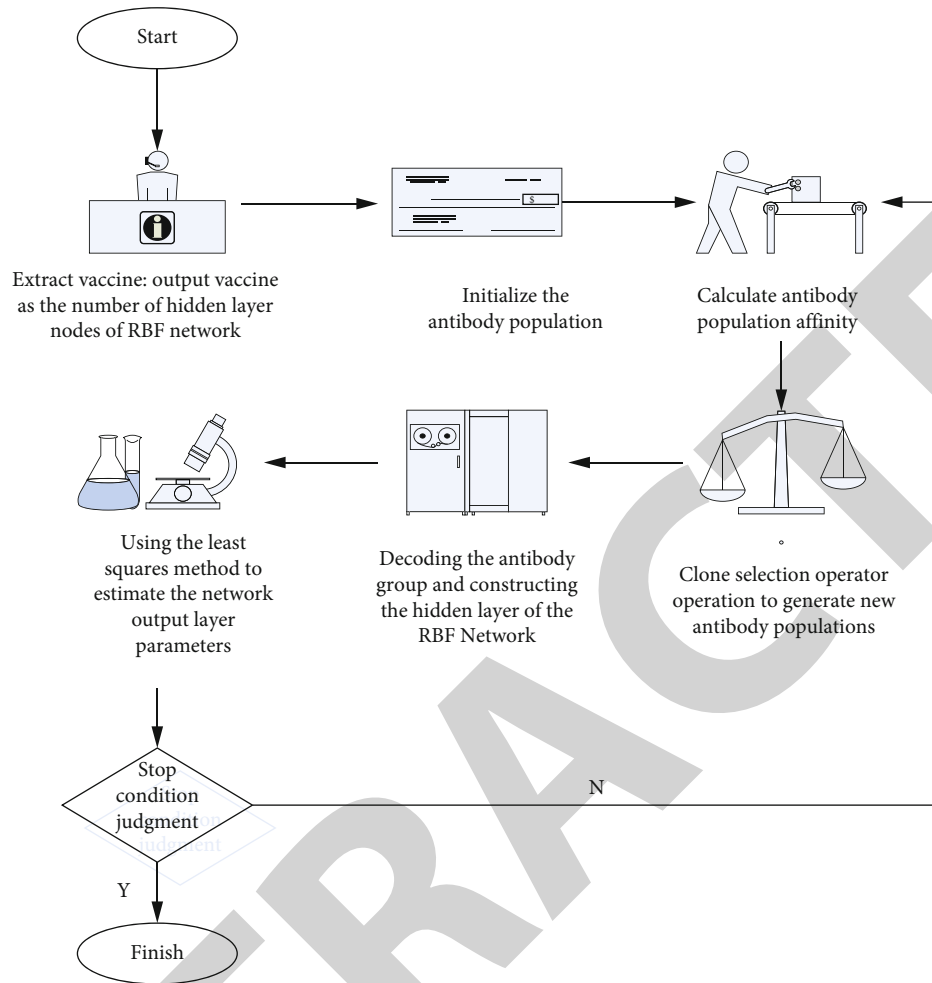
Figure 7: Three-level algorithm of RBFNN based on immune mechanism.

vertebrates. Birds are the first vertebrate species in which a distinct lymphoid system dichotomy has been identified as follows: (1) T lymphocytes from the thymus, which act as effector cells in cell-mediated immunity, and (2) bursa-derived (b) lymphocytes, which are the precursor cells of the plasma cell that synthesizes antibodies.

In this paper, microecological compound preparations were used to feed chickens to investigate their effects on the growth performance and immune function of chickens.

Selecting normally fed day-old chicks and observing for 3 days. After culling sick and weak chickens, 200 healthy chickens with similar body weights were randomly divided into the control group and experimental group, with 100 in each group (20 in each cage, 5 cages in total). All laying hens were fed and watered ad libitum during the week and vaccinated against avian influenza with eye and nose drops. A variety of other birds, including domestic poultry, can contract the viral infection known as avian influenza. Shorebirds and wild waterfowl are frequently asymptomatic carriers. Low pathogenicity strains commonly cause respiratory symptoms in poultry. The experiment lasted for 6 weeks, and other feeding methods strictly followed the feeding methods of chickens (0-6 weeks old).

The measurement indicators are as follows: Control group: basal diet; and experimental group: basal diet +200 mg/kg compound probiotics.

The specific data is shown in Table 1.

3.2. Growth Performance. All chickens were weighed on the morning of the first day of the test period at weeks 0, 1, 2, 3, 4, 5, and 6 to calculate weekly gain, feed consumption, and feed weight ratio.

3.3. Immune Organ Index. On the 3rd, 4th, and 6th week of the experiment, 6 chickens were randomly selected. The jugular vein was incised, the spleen, thymus, and bursa were separated, blood was collected, and fat was removed to measure fresh weight and calculate the immune organ index. Jugular veins are simple to spot because they are located just below the skin. Considering that they deliver oxygenated blood to the brain. The carotid arteries are frequently visible on the surface of the neck muscle, close to the head, in chickens, geese, and guinea fowl. The chicken spleen, which is the largest peripheral lymphoid organ, is important for both bacterial and viral immune responses to acquired antigens. The bursa of Fabricius is a chestnut-sized, sac-like

TABLE 1: Basal diet composition and nutritional standards.

Nutritional composition	0 ~ 3 weeks (%)	4 ~ 6 weeks (%)	Nutritional level	0 ~ 3 weeks (%)	4 ~ 6 weeks (%)
Corn	63.75	60.9	Metabolizable energy (MJ/kg)	12.90	12.80
Soybean meal	25.34	28.5	Crude protein (%)	9.00	21.20
Cottonseed meal	2.88	0	Arginine (%)	0.70	1.16
Corn protein flour	1.3	1.4	Methionine+ Optine (%)	0.80	0.90
Fish meal	1.2	2.8	Calcium (%)	0.68	0.43
Wheat flakes	0.3	1.1	Total phosphorus (%)	0.41	1.10
Stone powder	0	0.1	Available phosphorus	0.95	0.71
Calcium hydrogen phosphate	1.42	1.5			
Salt	0.24	0.9			
Choline chloride	0.12	0.1			
Sodium sulfate	0.12	0.14			
Methionine	0.06	0.9			
Lysine	0.13	0.12			
Soybean oil	1.9	0.04			
Vitamins	0.04	0.3			
Premix	1.2	1.2			
Total	100	100			

(a) Weekly weight gain

(b) Material consumption

(c) Material to weight ratio
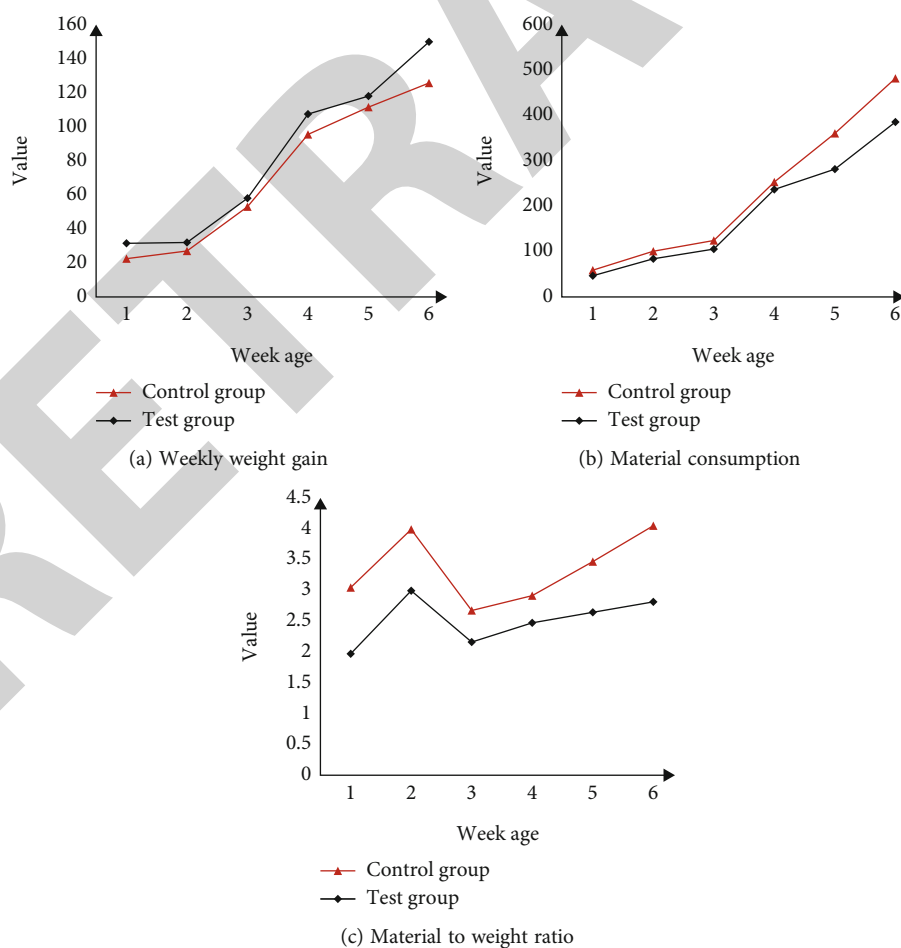
FIGURE 8: Mean weight gain, feed consumption, and feed-to-weight ratio (g) of chicks at different stages.

(a) Spleen

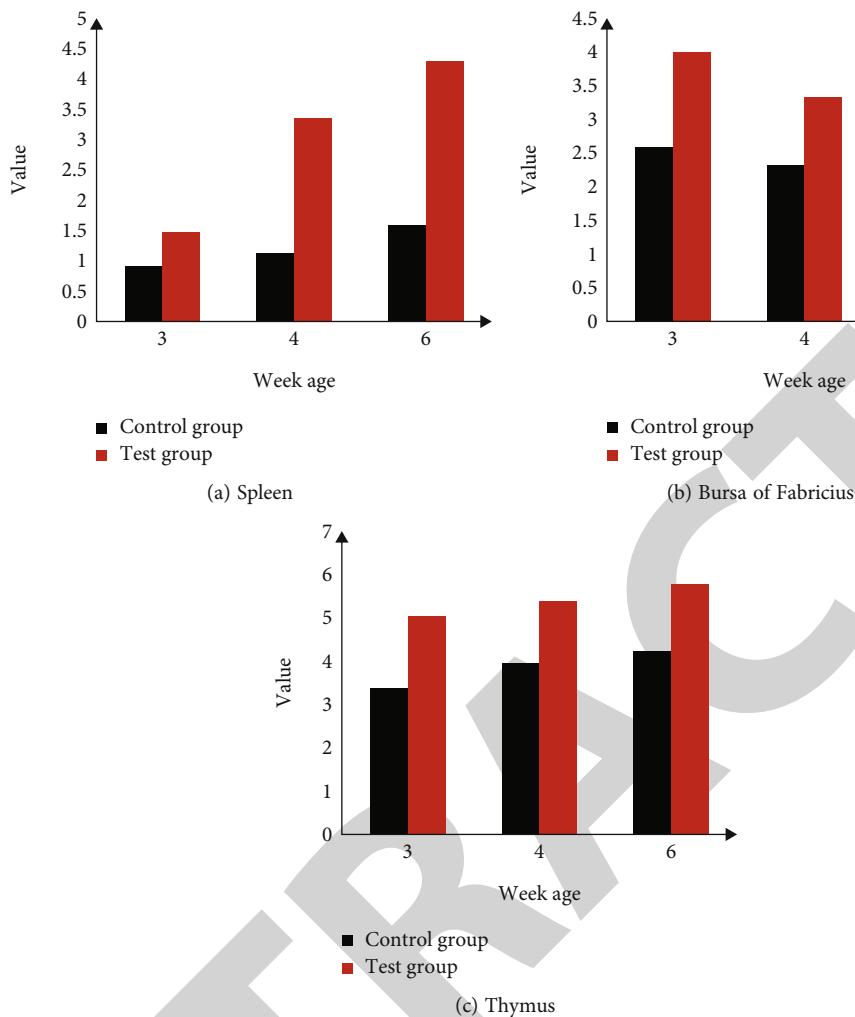(b) Bursa of Fabricius

(c) Thymus

FIGURE 9: Chicken immune organ index in each group (mg. g^{-1}).

organ in the chicken that is anterior to the sacrum, and dorsal to the rectum. It connects to the posterior part of the cloaca via a short duct. The chicken thymus is made up of several lobes that span almost the entire length of the neck above the jugular vein on either side. The thyroid is located right next to the posterior lobe.

3.4. Determination of Biochemical Blood Indicators. On the morning of the first day of the 3rd, 4th, and 6th week of the experiment, 10 chickens were randomly selected every day. The cardiac blood was collected to prepare heparin anticoagulation and sterile serum samples to determine the required values. Heparin is a drug and a naturally occurring glycosaminoglycan that is also referred to as unfractionated heparin. Heparins are classified as anticoagulants because they rely on the activity of antithrombin. It is specifically used to treat unstable angina and heart attacks.

3.5. The Number of Intestinal Flora. Three chickens of 2, 4, and 6 weeks of age were randomly selected, then fasted for 12 hours (without water) and weighed, and the chickens were euthanized by intracardiac air injection. Colony counts

were counted after 48 hours of anaerobic culture in a 37°C biochemical incubator, while E. coli was counted after 24 hours of aerobic culture in red methylene blue agar medium. Colony counts were expressed as the logarithm of the total number of bacterial colonies per gram of intestinal content [(1 gCFU)/g].

3.6. Plasma Total Antioxidant Capacity (T-AOC). 6 chickens of 2, 3, 4, and 5 weeks of age were randomly selected for each repetition, then fasted for 12 hours (without drinking water). The blood was collected from the fin vein, and the plasma was centrifuged at 3000 r/min for 10 minutes.

4. Results

In this section, we will discuss the influence on growth performance, the influence of the immune organ index, the influence of blood biochemical indicators, the influence of the number of chickens' cecal flora, and the influence of antioxidant capacity in detail.
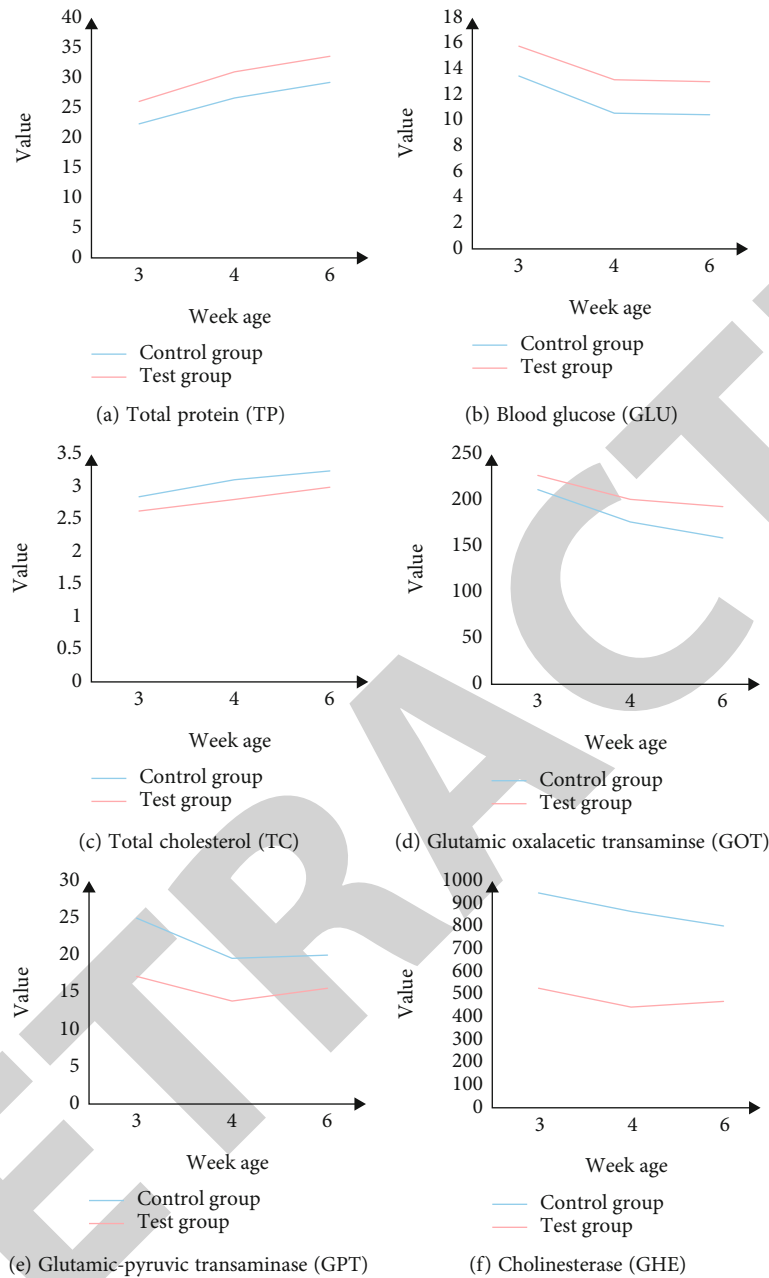
(a) Total protein (TP)

(b) Blood glucose (GLU)

(c) Total cholesterol (TC)

(d) Glutamic oxalacetic transaminse (GOT)

(e) Glutamic-pyruvic transaminase (GPT)

(f) Cholinesterase (GHE)

Figure 10: Effects of compound probiotic microecological additives on blood biochemical indexes of chicks.

4.1. Influence on Growth Performance. As can be seen from Figure 8, during the experimental period, the experimental group had a significant difference in weekly weight gain compared with the control group ($p < 0.05$) (Figure 8(a)). The weight gain of the experimental group added with the compound probiotics was significantly higher than that of the control group, and the experimental group was 15.70% higher than the control group at the age of 6 weeks. In terms of feed consumption, the ratio of the experimental group was lower than that of the control group, and the difference was significant ($p < 0.05$) (Figure 8(b)). In terms of feed-to-weight ratio, the ratio of the experimental group was lower than that of the control group, and the difference was significant ($p < 0.05$). The feed ratio of the 6-week-old experimen-

tal group was 30.37% lower than that of the control group (Figure 8(c)).

4.2. Influence of Immune Organ Index. It can be seen from Figure 9 that the indexes of the spleen (Figure 9(a)), bursa (Figure 9(b)), and thymus (Figure 9(c)) of the chickens in the test group were higher than those in the control group. At 6 weeks of age, the spleen, bursa, and thymus indexes of the chickens in the experimental group were 63.02%, 38.77%, and 26.82% higher, respectively, with significant differences ($p < 0.05$). The immune level of chickens is affected by the developmental status of immune organs. The increase in the relative weight of immune organs means that the immune level of the body also increases.

Table 2: Effects on the numbers of chicken cecum and *Escherichia coli*.

Project	Week age	Control group	Test group
Lactic acid bacteria	2	7.93	8.88
	4	8.57	8.95
	6	8.04	8.13
Escherichia coli	2	8.08	7.60
	4	8.17	7.84
	6	8.55	8.28

Table 3: Effects on total antioxidant capacity of chicken plasma.

Week age	Control group	Test group
2	23.01	24.91
3	14.98	19.55
4	17.06	20.39
5	17.39	22.02

4.3. Influence of Blood Biochemical Indicators. It can be seen from Figure 10 that the total protein value of the experimental group was higher than that of the control group, and the difference was significant ($p < 0.05$) (Figure 10(a)). Regarding the blood glucose value, the difference between the control group and the test group was not significant ($p > 0.05$) (Figure 10(b)). Compared with the control group, cholesterol in the experimental group was significantly decreased ($p < 0.05$) (Figure 10(c)). The glutamic oxalacetic transaminase was significantly increased ($p < 0.05$) (Figure 10(d)), and glutamic-pyruvic transaminase was significantly decreased ($p < 0.05$). 0.05) (Figure 10(e)), and cholinesterase was significantly increased ($p < 0.05$) (Figure 10(f)). The above indicators all indicate that the probiotic compound microecological preparation has a promoting effect on the immunity of the body.

4.4. Influence of the Number of Chicken Cecal Flora. Around 400 to 500 different species of bacteria from 190 different genera are found in the colon of a healthy adult, but only a few of these genera together make up the majority of the feces' cultivable flora. It can be seen from Table 2 that at 2, 4, and 6 weeks of age, the number of lactobacillus cecum in the test group was slightly higher than that in the control group, indicating that the addition of the compound probiotic (Living microorganisms known as probiotics may aid in the treatment and prevention of certain diseases when consumed. The gut microbiota, a bacterial colony, plays a role in digestion, immune health, and other processes. Microbes are a class of creatures made up of bacteria, fungi, viruses, and protozoa) and its adjuvant has the potential to promote the reproduction of lactobacillus caeca. The addition of microbial complex and its adjuvant did not improve the results, and there was no significant difference in the number of *Escherichia coli* (E. coli is present in all types of poultry. In the majority of animals, including poultry, the gut naturally contains the Escherichia bacteria. Other bacteria in the gut normally keep it in check, but if large colonies form, it can result in serious discomfort, illness, and even death) between the chicken groups ($p > 0.05$).

4.5. Influence of Antioxidant Capacity. As can be seen from Table 3, the total antioxidant capacity of chicken plasma in the experimental group was slightly higher than that in the control group during the entire experimental period. The addition of microbial complex and its adjuvant significantly improved the total antioxidant capacity (Total antioxidant capacity (TAC) is a commonly used analyte to evaluate the antioxidant status of biological samples and can assess the antioxidant defense against free radicals produced in a particular disease) of broiler plasma ($p < 0.05$), and the experimental group was significantly higher than the control group ($p < 0.05$). This means that the addition of complex probiotics and their auxiliary substances can effectively increase the level of antioxidants in the body.

5. Conclusion and Future Work

This paper provided a theoretical basis for the possibility of adding probiotic complexes to chicken diets by measuring the effects of probiotic complex probiotics on growth performance, immune function, cecal flora numbers, and antioxidant capacity. When chickens were fed the prepared probiotic complex probiotic, the number of activated T cells and serum erythrocyte immunomodulatory factor activity were significantly increased. This indicated that the complex probiotics support the growth and immune function of chickens. However, there are still deficiencies in the test. This test only discussed the effect of compound probiotics on the growth and immunity of chicks. However, the optimum amount of addition in production practice and the possible effects are still unknown. Therefore, the research should continue.

Data Availability

No data were used to support this study.

Conflicts of Interest

The authors have no conflicts of interest.

Acknowledgments

References

[1] R. Wang, W. Cai, X. Wang, J. Gao, and M. Huang, "Progress in Chinese medicine-probiotics compound microecological preparations for livestock and poultry," *Chinese Journal of Biotechnology*, vol. 35, no. 6, pp. 972–987, 2019.